Zurnadzhy V.I., Efremenko V.G., Petryshynets I.,
Chabak Yu.G., Efremenko A.V.

IMPROVEMENT OF MECHANICAL PROPERTIES OF STRUCTURAL STEELS BY MULTI-PHASE STRUCTURE FORMATION

PREMIER
Publishing
Premier Publishing s.r.o.

Praha 2022

Authors:
Zurnadzhy Vadym Ivanovych [1]
Efremenko Vasyl Georgijovych [1, 2]
Petryshynets Ivan [2]
Chabak Yuliia Gennadiivna [1, 2]
Efremenko Alexiy Vasilijovych [1]

[1] *Pryazovskyi State Technical University, Mariupol, Ukraine*
[2] *Institute of Materials Research of Slovak Academy of Sciences, Kosice, Slovakia*

Reviewer:
Zaichuk Natalia Petrivna (Lutsk National Technical University, Lutsk, Ukraine)

Improvement of mechanical properties of structural steels by multi-phase structure formation / Zurnadzhy V. I., Efremenko V. G., Petryshynets I., Chabak Yu. G., Efremenko A. V. – Praha: Premier Publishing s.r.o. 2022. – 142 p.

ISBN 978-80-908612-7-5

DOI:10.29013/ IMPSSMPSF.ZurnadzhyV.I.EfremenkoV.G.PetryshynetsI.ChabakYu.G.EfremenkoA.V.142.2022

The monograph is devoted to improving the mechanical and exploitation characteristics of Advanced High Strength Steels through the development of the heat treatment technology based on the "Quenching & Partitioning" (Q&P) principle. The experimental data presented in the monograph clearly reveal the advantages of Q&P technology over standard heat treatment technologies due to the formation of a multi-phase structure with advanced properties. Special attention is paid to the retention of austenite in the structure, its metastability to strain-induced martensite transformation, and the contribution of the TRIP effect to the steel behaviour under the load. The monograph is hoped to be of interest to researchers and engineers specializing in metallurgy and heat treatment of metals.

This monograph was published within the frame of:
(a) the project funded by the Ministry of Education and Science of Ukraine (0120U102087);
(b) Ukrainian-Slovak research project funded by the Ministry of Education and Science of Ukraine (0122U200119) and Slovak Research and Development Agency (APVV-SK-UA-21-0023).

Subscribe to print 11/03/2022. Format 60×84/16.
Offset Paper. Garnitura Minion Pro. Pec. liter. 11.
Typeset in Premier Publishing s.r.o. Praha, Czech Republic.

Printed by Premier Publishing s.r.o.
Praha 8 – Karlín, Lyčkovo nám. 508/7, PSČ 18600, Czech Republic
pub@ppublishing.org, ppublishing.org

ISBN 978-80-908612-7-5

Contents

Preface 5

Chapter 1. State-of-the-art in the improvement of mechanical properties of low-alloyed steels 6

1.1 Current trends in heat treatment of high-strength steel 6

1.2 The main directions in the development of the third generation high-strength steels 10

1.3 Q&P steel: chemical composition and heat treatment technology 13

Chapter 2. Mechanisms and kinetics of phase-structural transformations in medium-carbon Si-Mn-Cr-V steels . . 21

2.1 Materials and methods 21

2.2 The austenite transformation kinetics under isothermal conditions and morphology of transformation products 24

2.3 Determination of M_S temperature and kinetics of athermal martensitic transformation in 60Si2CrV and 55Si3Mn2CrVMoNb steels 28

2.4 Effect of athermic martensite on the bainitic transformation kinetics 34

2.5 The selection of quenching temperature for Q&P treatment based on the "Constrained ParaEquilibrium" concept 40

2.6 Dilatometric study of Q&P-treated steels 42

Chapter 3. Effect of Q&P treatment on the microstructure and mechanical properties of 60Si2CrV and 55Si3Mn2CrVMoNb steels 51

3.1 Microstructure and mechanical properties of 60Si2CrV steel subjected to Q&P treatment 51

3.2 Effect of low tempering on the microstructure and mechanical properties of Q & P-treated 60Si2CrV steel 63
3.3 Effect of heat treatment modes on microstructure and mechanical properties of 55Si3Mn2CrVMoNb steel 69
3.4 Q & P-integrated steel heat treatment modes and their effect on the mechanical properties of 55Si3Mn2CrVMoNb steel 88
3.5 Deformation stability of retained austenite in Q & P treated 55Si3Mn2CrVMoNb steel 92
3.6 Q & P-treated medium-carbon low alloyed steels as candidates in third generation AHSS 97

Chapter 4. Improvement of 0.7–0.8 wt.% C steel performance characteristics using Q & P heat treatment 100
4.1 Effect of Q & P treatment on abrasive wear resistance of 0.75 wt.% C low-alloyed steel 100
4.2 Improving the exploitation performance of steel grinding balls through Q & P-based heat treatment 107

References 123

Preface

The development of world metallurgical technology is focused on increasing the mechanical properties of metallic products. Among the urgent tasks is an improvement of mechanical properties of rolled structural steel which allows reducing the metal consumption in different structures (buildings, warehouses, aircraft hangars, metro stations, stadiums, bridges, etc.). The most challenging issues are connected with increasing the properties of low-alloyed steel pursuing the total cost reduction.

Heat treatment is a very effective technology to control the mechanical behaviour of rolled steel products. A new approach in this area is a heat treatment, based on the principle of "Quenching and Partitioning" (Q&P), proposed in the early 2000s. It can significantly increase the strength of low-alloyed steels while maintaining satisfactory ductility and toughness by creating a multiphase structure formed at different stages of processing. Despite the impressive research activity in this area, the most published work refers Q&P technology regarding low-carbon steels (up to 0.20 wt.% C). The data devoted to studying Q&P regarding medium-carbon and high-carbon steels are very limited, which narrows the possible applications of this technology. In this regard, the present effort aims to reveal the prospects for using Q&P technology for steels with higher carbon content in a wide range of applications.

Chapter 1 presents a literature overview on the topic of research. Chapter 2 describes the experimental methods and equipment used in the work. Also Chapter 2 outlines the results of studying the mechanism and kinetics of phase-structural transformations in medium-carbon Si-Mn-Cr-V steels. Chapter 3 is focused on the evolution of microstructure and mechanical properties in low-alloyed steels of 60Si2CrV grade and 55Si3Mn2CrVMoNb grade under the Q&P heat treatment. Chapter 4 is devoted to the development of Q&P-based technology of heat-strengthening rolled steel balls, aimed at improving their performance.

The authors hope that the results of the research presented in this monograph may be of interest to researchers and engineers specializing in metallurgy and heat treatment of metals, and may be useful in the educational process of preparing undergraduates for the specialty "Materials Science and Engineering".

Chapter 1. State-of-the-art in the improvement of mechanical properties of low-alloyed steels

1.1 Current trends in heat treatment of high-strength steel

The increasing strength of structural steel is one of the main directions of saving energy, materials, and financial resources in the machine building and construction industry. In this regard, the technologies of heat treatment aimed at improving a "strength/ductility" combination in low-alloyed structural steels are well adopted in the metallurgical industry [1–3].

The term "High Strength Steel" is interpreted differently. According to Goldstein's classification [4], high-strength steels include steels with an ultimate tensile strength (UTS) of at least 1500 MPa with a relative elongation of at least 15%. Such a set of mechanical properties is attributed to several classes of high-alloyed steels, namely: (a) martensite-aging steels (intermetallic phases precipitation from martensite during aging), (b) martensitic steels, alloyed by Cr, Mo, Ni, W, V, (c) dispersion-hardening steels alloyed by V and Mo (carbide precipitation at 550–650 °C), and (d) metastable austenitic steels susceptible for strain-induced martensitic transformation (SIMT) [4]. The chemical composition and mechanical properties of these steels are shown in Table 1.1. Despite their high mechanical properties, a significant disadvantage of these steels is the high cost associated with alloying by large amounts of costly alloying elements (Ni, Mo, V, W).

According to another classification, the term "High Strength Steel" is most often referred to low-carbon steel with a minimum yield tensile strength (YTS) of 210–550 MPa [5, 6]. When YTS > 550 MPa, the steel is classified as particularly strong and called AHSS (Advanced High Strength Steel); sometimes these steels are referred to UHSS (Ultra High Strength Steel) [5, 7]. HSS and AHSS differ not only in strength but also in the microstructure. HSS have ferrite or ferrite-pearlite structure while AHSS's microstructure contains two or more phase-structural constituents (bainite, martensite, ferrite, retained austenite (RA)). This is a natural composite combining strong (hard) and ductile phase components thus ensuring high strength with acceptable ductility and toughness. Due to the multiphase structure, AHSS exhibits a much higher set of mechanical

Table 1.1. The mechanica properties of high-strength steels of different grades [4]

Steel groupe	Steel grades	Content (wt.%):									Mechanical properties, not less than			
		C	*Si*	*Mn*	*Ni*	*Co*	*Mo*	*Ti*	*Cr*	*V*	*UTS*, MPa	*YTS*, MPa	*TEL*, %	*KCU*, J/cm^2
Maraging	Ni18Co9Mo5Ti	≤0.03	–	–	18.0	9.0	5.0	0.7	0.1*Al*		2200	1950	8	35
	Ni18Co12Mo5Ti2	≤0.03	–	–	18.0	12.0	4.0	1.7	0.2*Al*	–	2450	2350	7	–
	Cr12Ni2Co16Mo4	≤0.03	–	–	2.0	16.0	4.0	0.2	12	–	1550	1480	8	50
Martensitic	30CrMnSiNi2A	0.3	1.0	1.2	1.6	–	–	–	1.0	–	1850	1600	13	60
	40CrMnSiNi3BA	0.4	0.7	0.7	2.8	–	–	–	1.0	–	2000	1700	11	40
	En26	0.4	0.2	0.6	2.5	–	0.5	–	0.7	–	1860	1610	13	–
	High-Tough	0.3	1.5	1.3	1.8	–	0.4	–	0.3	–	1650	1400	14	–
Dispersion-hardened	40Cr5Mo2SiV	0.4	0.9	–	–	–	1.3	–	5.0	0.6	1720	–	12	37
	HST140	0.4	0.2	–	–	–	2.0	–	5.0	0.5	2250	1780	7	–
	Chromodi	0.3	1.0	–	–	–	1.5	–	5.0	1.0	1890	–	–	–
Austenitic	30Cr9Ni8Mo4Mn2Si2	0.3	2.0	2.0	8.5	–	4.0	–	9.0	–	1500	1430	50	–
	60Mn14Cr9Si2	0.6	2.0	14.0	–	–	–	–	9.0	–	1100			

properties as compared with HSS steels. Consumers of AHSS are the automotive industry, the military industry, construction, energetics, etc.

Figure 1.1 presents a diagram of "Tensile Strength-Elongation" correlations for different classes of HSS, namely: (a) steels with low carbon content (Interstitial Free – IF); (b) steels that are strengthened during drying of applied paint (BH – Bake Hardening); (c) low carbon manganese (C–Mn) alloy steels; (d) ferrite-bainite steels (FB); (e) high-strength low-alloyed steels (HSLA) with micro-alloying by Ti, V or Nb (which allows satisfactory ductility and cold-drawing capacity at strength up to 800 MPa). At present, HSS is increasingly replaced in the industry by AHSS due to the higher properties complex of the latter.

AHSS, in turn, are divided into three generations. The first generation is represented by dual-phase steels (DP), complex-phase steels (CP), TRIP-assisted steels, martensitic steels (MART), and steels for hot deformation (PHS – Press Hardening Steel). Dual-phase steels, as a rule, have a ferrite-martensitic structure [8, 10], in which the ferrite proportion significantly exceeds the martensite proportion, which allows for achieving a higher strength level while maintaining ductility at the HSLA level. In general, DP steels are characterized by UTS of 500–1200 MPa with a total elongation (TEL) of 10–30%. Some of the most common representatives of this class are DP800 and DP980 after heat treatment perform UTS not less than 800 MPa and 980 MPa with a minimum TEL of 17 and 9%, respectively [11].

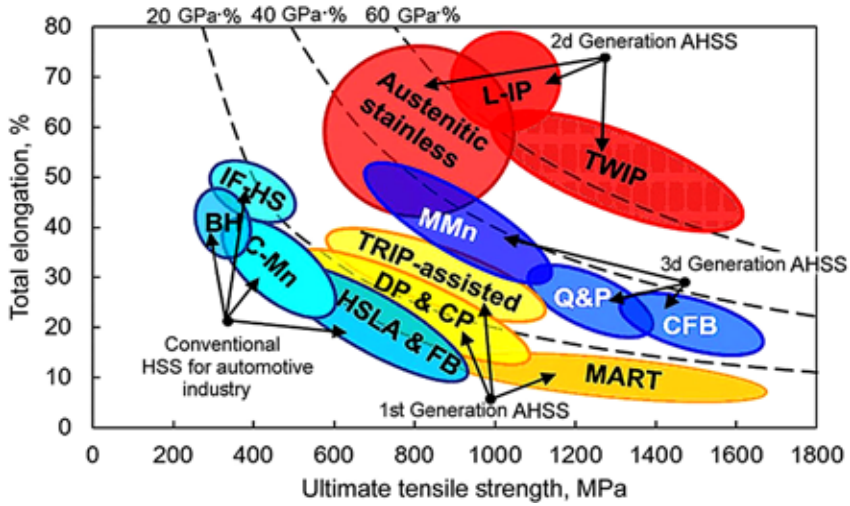

Figure 1.1. Mechanical properties of HSSs and AHSSs

Complex-phase steels (CP) have a tensile strength similar to dual-phase steels (800–1200 MPa) while their yield strength is higher due to the structure containing ferrite, martensite, and bainite. In addition, CP steels are customary microalloyed by V, Ti, and Nb for grain refinement to increase the mechanical properties [12]. Martensitic steels, by name, have a mostly martensitic structure, which allows them to achieve an increased strength level (UTS of 900–1800 MPa) but causes a rather low ductility. For example, MS1300 grade steel has UTS ≤ 1300 MPa with an elongation of only 2–3% [13].

The TRIP-assisted steels contain 5–15 vol.% of RA along with ferrite and martensite, which is unusual for low carbon low-alloyed steels [14]. During deformation, retained austenite undergoes a strain-induced martensite transformation. This provides the steel with a unique set of mechanical properties (including abnormally high plasticity) that is designated as a TRIP (Transformation Induced Plasticity) effect.

The influence of stresses on martensitic transformation was first investigated by Sheil in 1932. The scientific basis for the use of SIMT to enhance steel properties was laid in the 1960s by Ural metallurgists' pioneering research under the guidance of Bogachev [15]. This trend was further developed by Zackey and Parker [16] and other researchers including Ukrainian scientists L. Malinov, O. Chelyakh, V. Popov, M. Brykov, et al. [17–20]. Currently, the TRIP effect is one of the main directions of the development of high-strength steel. The strain-induced formation a'-martensite or e-martensite provides an increasing the work hardening coefficient, redistribution of the load under deformation, and external stress relaxation [22]. Due to SIMT, compressive stresses appear in front of the growing crack thus inhibiting its propagation [19]. Intense strengthening under SIMT prevents the localization of deformation; this delays the "necking" under the tension, causing the "running neck" effect, which leads to an abnormal increase in TEL [16, 18]. As a result, the steel containing metastable austenite may possess an improved combination of strength and ductility [18, 23–26]. Due to a SIMT, the TRIP-assisted steels (which have similar to CP and DP steels strength of 590–1180 MPa), as a rule, have a higher ductility. The representative of this class is a TRIP780 grade, which has UTS ≥ 780 MPa and a TEL of ≥ 24% [11].

TRIP-assisted steels are an example of using metastable austenite to improve the mechanical properties of low-alloyed steels. There are various techniques that allow to obtain retained austenite (in low carbon steels) or to increase its volume fraction in the structure (in medium- and high carbon

steels). In this direction (SIMT, TRIP effect) one can highlight the contribution of Malinov and Chelyakh (presenting Pryazovskyi State Technical University) to the field. They developed different original ways to obtain metastable austenite in the steels and cast irons of different alloying systems. In particular, they proposed to increase RA volume fraction by (a) using austempering for the steels 0.6CrSi, 0.6Si2, 0.45CrNi2MoV for automotive applications [27], (b) holding in the $(\alpha + \gamma)$ area for the redistribution of elements with enriching the austenite with carbon and austenite-forming elements (for the steels of 0.4CrNi, 0.4CrNi2Mo, 0.6Si2 grades, grey cast iron) [28, 29], (c) applying a chemical-thermal treatment with subsequent quenching from high temperature (for steels of 0.1Mn2VNb, 0.5Mn grades) [30, 31]; (d) using thermo-cycling treatment (for steel of 0.2Mn grade [32]), etc.

The second generation of AHSS is represented by three grades of steel, namely: TWIP steels (Twinning-Induced Plasticity), L–IP steels (Lightweight Steels with Induced Plasticity), and high-strength corrosion resistance austenitic steels. In contrast to the first-generation steels the second-generation ones fully austenitic structure. The most known steels of the 2nd generation are TWIP steels. The austenitic structure, in this case, is obtained due to alloying by 14–28 wt.% Mn. At present, the TWIP steel of 500/980 grade has been used, which, has a UTS/YTS not lower than 980/500 MPa, respectively, with total elongation of 50–60% [33]. L–IP steels are carbon-free TWIP steels containing aluminum to reduce (together with manganese) the weight of steel [34]. High-strength corrosion-resistant austenitic steels contain 14–18 wt.% Cr to stand with corrosion along with improved mechanical properties. As an example, CN1.07 steel has a YTS of 1075 MPa with a TEL of 74% [35].

The widespread use of second-generation steels is hampered by their high cost, and therefore the task is to develop third-generation high-strength steels. The latter should outperform the first-generation steels by the set of mechanical properties complex and at the same time, they should have lower costs as compared with the second-generation steels.

1.2 The main directions in the development of the third generation high-strength steels

Currently, there are three main approaches to achieving the third-generation AHSS requirements. They are connected with the development of: (a) TWIP steels with medium manganese content [36–38], (b) steel with carbide-free nanobainite [39–41], and (c) steels subjected to Q&P treatment [42–44].

Medium-Mn TWIP steels are a modified version of second-generation TWIP high-Mn steels. Medium-Mn TWIP steels contain a medium (4–10 wt.%) amount of manganese, which can significantly reduce the metal cost while maintaining a high strength/ductility combination. Thus, the steel containing 0.3 wt.% C, 6 wt.% Mn, 1.5 wt.% Si, and 3 wt.% Al possesses UTS of 1130 MPa and TEL of 58% [45]. Another advantage of these steels is the rather high hardenability, which allows the simple heat treatment with cooling in the air.

Medium-Mn steels are heat treated in two stages. The first stage is the quenching from the austenitic region, after which the steel's microstructure consists mainly of martensite and a minor fraction of retained austenite. The second stage is annealing in the intercritical temperature, where martensite partially "reverses" into austenite, and partially transforms into recrystallized ferrite. Carbon and manganese partition between α-phase (martensite, ferrite) and austenite, resulting in austenite stabilization [46]. Upon further air-cooling, a ferrite-austenite structure is formed in the steel, in which austenite is capable of the TRIP effect during deformation.

When a high level of "Strength/Ductility" is required, it is recommended to use austempering to get the structure of carbide-free nanobainite, as well as Q&P treatment, which will be discussed below. An important advantage of carbide-free nanobainite steels is the possibility of achieving ultra-high strength while maintaining high ductility by obtaining a dispersed (nano-sized) heterophase structure [47]. It is known that the production of classic nanostructured high-strength steels is associated with significant costs due to alloying with the deficient elements, as well as using the warm deformation or thermomechanical treatment for structure refinement [48]. As an attempt to solve this problem, in the early 2000 s, a technology for nanoscale bainite microstructure production (so-called nanobainite) was developed under the guidance of Bhadeshia [47]. This technology requires a specific chemical composition of steel and using a low-temperature ausforming. Nanobainite heat treatment consists of full or partial austenitization [49] and subsequent long (up to 7 days) holding at a temperature slightly above the Ms point (but not above 250 °C) [50–57]. The nanobainite microstructure consists of laths of carbide-free bainite ferrite of thickness less than 100 nm. Between the ferrite laths, the interlayers of retained austenite are positioned. Such structure forms due to low holding temperature which shortens the paths for carbon partitioning and increases the thermodynamic stimulus of transformation [58, 59].

Nanobainite steels contain 0.6–1.0 wt.% C, 0.7–2.0 wt.% Mn, 0.5–2.0 wt.% Cr, ≥ 1.5 wt.% Si. In the heat-treated state, these steels have a unique (for low-alloyed steels) combination of mechanical properties: UTS ≥ ≥ 2000 MPa, the hardness is 600–700 HV, and the TEL is 5–30% [40, 49, 60–63].

The thickness of the ferrite plate in the nanobainite is much lower than that of conventional bainite, providing an effect similar to grain boundary strengthening. Combined with the higher density of crystal lattice defects, this results in high strength of steel. At the temperatures of nanobainite austempering (200–250 °C), carbon atoms retain their diffusion mobility, so the diffusion-free growth of the bainite ferrite plate is accompanied by the partitioning of carbon from the α-phase to austenite [65, 66]. Since the cementite segregation during bainitic transformation is inhibited by the adding of 1.5–2.0 wt.% Si, this leads to austenite enrichment by carbon and its stabilization in the form of thin films. The increased plasticity of the nanobainite steels is closely associated with a presence of a significant volume fraction of austenite and its ability to SIMT (TRIP effect) [67].

An additional important factor of high nanobainite's ductility is the absence of carbides in its structure. This is ensured by adding Si. Silicon greatly inhibits the precipitation of Fe_3C from austenite, which is explained by its very low solubility in cementite [68, 69]. The silicon-induced inhibition of cementite precipitation is described by Bhadeshia [47, 61], Caballero and Garcia-Mateo [47, 57, 61] et al. Earlier it was highlighted by Tkachenko [70] and Kurdyumov [71]. Aluminum has a similar effect on the cementite formation kinetics [72]. It is established that the addition of 1.2% Al to TRIP-assisted steel leads to the refinement of bainitic ferrite plate [72], acceleration of bainite formation [46], and increasing the resistance to crack propagation [73].

When the carbon content exceeds 0.6 wt.%, the martensitic transformation start temperature (Ms) is below 250 °C thus allowing bainite transformation at reduced temperatures (which is the main condition for obtaining nanobainite). As the holding temperature decreases, the bainitic ferrite plate thickness decreases, leading to an increase in the steel strength [74, 75]. However, when the holding temperature is less than 250 °C, the transformation slows down much that the holding required for complete austenite transformation is prolonged to 7–10 days [56, 61, 76, 77]. Such a long heat treatment cycle limits the widespread industrial use of nanobainte steels [78]. This problem is partially solved by the addition of

aluminum and cobalt in the steel, which intensifies bainite transformation, however, cobalt significantly increases the steel cost [79].

Bainite transformation can be accelerated by compression stresses exceeding the austenite's yield strength [80, 81], which is also true for nano-bainitic carbide-free steels [82]. Hot deformation of the steel carried out before austempering at 230 °C, accelerates the nano-bainite formation by reducing the incubation period of transformation [83]. The prior hot strain deformation increases the bainitic transformation rate by increasing the surface area where bainitic nuclei may occur [84]. However, there is evidence that prior deformation at 300 °C inhibits bainitic transformation due to the mechanical stabilization of austenite [85–87].

1.3 Q&P steel: chemical composition and heat treatment technology

Currently, the heat treatment, known as "Quenching and Partitioning" (abbreviated as Q&P) is being actively developed for the third-generation AHSS. This technology allows achieving an advanced complex of mechanical properties in relatively cheap low-alloyed steels. The technology is based on the "Constrained Carbon Paraequilibrium" (CPE) concept proposed in 2003 by Speer [42, 43]. Later, this concept was developed in the works of Clarke, Matlock, Santofimia, Wu, and many other researchers [88–91]. According to CPE, when carbides precipitation is inhibited, then Fe-C alloys must have some metastable (paraequilibrium) state with minimal free energy at which the chemical potentials of carbon in austenite and ferrite (martensite) are equalized. This is ensured by a consistent change in the volume fraction and chemical composition of the phases. Under slow diffusion of alloying elements (X), their ratio with iron (Fe/X) is almost unchanged, so the equality of chemical potentials is achieved due to the partition of carbon, which easily diffuses from αFe (martensite) to austenite [43]. The conditions for reaching the CPE state are (a) absence of carbides precipitation from austenite and (b) immobility of the interfacial martensite/austenite boundary. The diffusion of carbon from martensite into austenite in Si-containing steel under Q&P treatment has been experimentally proven using Atomic Probe Tomography [92, 93].

The Q&P treatment process consists of several steps: (a) austenitization followed by quenching cooling, (b) partitioning, and (c) final cooling (Fig. 1.2). The quenching temperature (QT) should be in the temperature range between M_S and M_F in order to transform some of the austenite to

martensite. The next step involves heating to a partitioning temperature (PT) and holding at that temperature to redistribute carbon from C-rich martensite to austenite. The process is completed by final cooling (in water, oil, or air) to room temperature [94]. It is reported [95] that compared to quenching in water, cooling in the air increases the elongation of low carbon steel with some reduction of its strength.

As a result of carbon enrichment, the austenite partially stabilizes to martensitic transformation upon final cooling, which increases the retained austenite amount in the steel structure. The degree of austenite enrichment by carbon depends, among other things, on the volume fractions ratio of martensite and austenite after quenching [96]. Thus, when developing Q & P processing parameters, it is important to know the kinetics of athermic martensitic transformation in order to select the optimal quenching temperature.

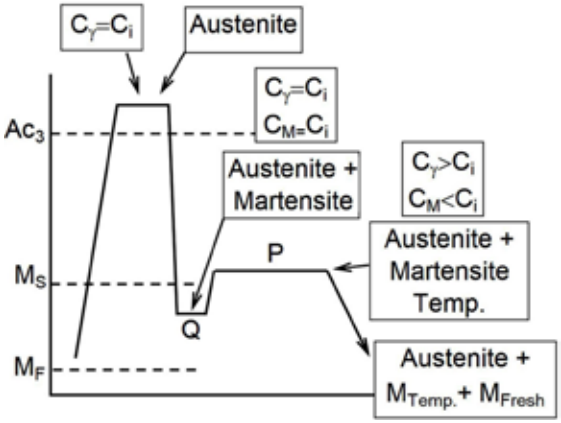

Figure 1.2. Scheme of Q & P heat treatment process

In accordance with the concept, the microstructure of Q & P-treated steel should consist of tempered martensite (formed at the quenching stage), "fresh" martensite formed at the final stage of processing, and retained austenite [97, 98]. This structure combines the areas of different strength and ductility providing improved properties due to the composite strengthening effect.

There are two classic modifications of the Q & P process: one-step partitioning and two-step partitioning [43]. The first modification involves partitioning at the quenching temperature (i.e. between M_S and M_f), and the second one implies partitioning at a higher temperature. In fact, the

one-step partitioning scheme involves the known phenomenon of austenite thermal stabilization, described by Sadovsky [99]. The thermal stabilization of austenite to martensitic transformation is associated with the elastic stress relaxation in the austenitic matrix [100] and the formation of the segregation of C and N atoms at dislocations, which leads to an austenite microheterogeneity [101, 102]. However, as shown in recent works [23, 74, 102, 104], with one-step partitioning, the thermal stabilization of austenite is supported by its chemical stabilization (i.e., carbon saturation diffused from martensite), which provides a notable increase in the RA amount, despite on low holding temperature.

As seen in Fig. 1.1, Q&P-treated steels have a tensile strength similar to martensitic steels at much higher ductility, which gives them an advantage in severe exploitation conditions. After Q&P processing the steels containing 0.2 wt.% C, 1.5 wt.% Si, 1.33 wt.% Mn [98] and 0.22 wt.% C, 0.41 wt.% Si, 1.85 wt.% Mn, 1.46 wt.% Al [105] obtained an increased mechanical properties complex (UTS/TEL) of 1072 MPa/23.7% and 882 MPa/24.4%, respectively, which is a rather high properties level for this class steels [105].

An improvement of mechanical properties after Q&P processing is due to obtaining a multiphase structure containing retained austenite. When loaded, RA transforms into martensite contributing to strength and ductility both [106]. It should be noted that the published data on Q&P processing mainly refer to the low-carbon steels (up to 0.20 wt.% C). The effect of Q&P processing on properties of medium-C and high-C steels is investigated to a much lesser extent, therefore, it requires further detailed study in view of the wide using these steels for automotive and tool applications.

Depending on the Q&P processing mode and the carbon content in steel, the retained austenite amount in the structure may vary in a wide range: 5–20% and even above [107–110]. Q&P processing enables the TRIP effect in cheap low-alloyed steels, making it promising for wide industrial applications. An important parameter of austenite is its stability to SIMT, which influences the deformation hardening coefficient, strength, and ductility of steel [111, 112]. The sasceptibility of RA to SIMT depends on different factors, such as the local carbon and the content of alloying elements in the austenite [3, 113], the size and morphology of the austenitic areas [112–114], the effect of the surrounding phases [115].

After Q&P treatment, the carbon concentration in the austenite can reach high values up to the limit of carbon solubility in γ-phase. The carbon content in austenite determines the SIMT kinetics upon loading, which

significantly affects the strength/ductility ratio. If the carbon content in austenite is less than 0.5 wt.%, then the austenite transforms into martensite under the load too fast deteriorating the steel's mechanical properties. If carbon content ≥1.8 wt.%, then austenite is very stable and it can withstand strain without SIMT [112]. Thus the moderate austenite propensity to SIMT is preferable which is associated with a carbon content of 1.0–1.8 wt.%. With regard to the RA morphology, studies have shown that the filmy austenite has higher stability to SIMT than blocky austenite areas [98].

Another factor that determines the austenite's stability is its area size [116–118]. Large austenitic areas are less stable to SIMT [95]. The austenitic area of 0.01–1.0 μm is considered optimal [119]. The stability and strength of retained austenite also depend on the surrounding phases [120]. The stronger they are, the more stable to SIMT austenite is [120]: the strong surrounding phases interfere through the shear $\gamma \rightarrow \alpha$ transformation, which is accompanied by an increase in the specific volume of steel. Another way of stabilizing austenite to martensitic transformation is thermal stabilization, during the interruption of quenching cooling at a temperature between M_S and M_f and holding at this temperature [121].

It should be noted that the reported experimental data on the amount of retained austenite Q & P-treated steels are lower than the values calculated according to the CPE concept [116]. The discrepancy in experimental and calculated data may be due to the bainite formation at the partitioning stage [88, 122–125] and/or incomplete carbon redistribution. During Q & P treatment, it is difficult to prevent bainite transformation at the partitioning stage, even with the addition of an increased amount of alloying elements [123]. Most likely, this is due to the fact that the bainitic transformation kinetics is accelerated by martensite, which is formed at the stage of interrupted quenching cooling. Martensitic transformation upon cooling leads to straining austenite, thus creating thermodynamic conditions for the accelerated formation of the first nuclei of α-phase [126]. These conditions are associated with a lower energy barrier of transformation in places of lattice defects accumulation. As reported in [126–129], the acceleration of bainitic transformation at temperatures close to M_S was found. Previous studies of the effect of martensite on bainitic transformation kinetics were performed only for low carbon steels. Such study for research medium-carbon and high-carbon steels is of particular scientific interest as well.

In order to address Q & P processing, the steel should belong to a certain alloying system (Si-Mn, Si-Al-Mn, Si-Mn-Cr), which is largely similar

to the nanobainite steel alloying system. The classic Q&P steel composition does not imply adding strong carbide-forming elements (Nb, V), since they bind carbon and reduce the carbon enrichment of austenite. At the same time, elements that prevent the precipitation of cementite from austenite, namely silicon and aluminum, are mandatory for introduction into Q&P steel [130, 131]. Based on this, most Q&P steels contain 0.15–1.0 wt.% C, 0.3–3.5 wt.% Mn, 0.05–1.9 wt.% Al and/or 1.3–3.0 wt.% Si, and up to 2.0 wt.% Cr [105].

Manganese and carbon lower the M_S point, thus increasing the RA volume fraction in the steel. In addition, carbon provides the increase in steel strength through the various strengthening mechanisms. However, increasing the carbon content makes the steel more brittle [110]. The addition of cheap manganese and more expensive chromium in Q&P steel aims at enhancing the hardenability of steel, which is necessary to cool the austenite to quenching temperature without its transformation in the pearlite and bainite areas [132]. In addition, chromium increases the resistance of martensite to decomposition under partitioning tempering, which is important from the point of view of maintaining the strength of steel.

The adding of silicon in Q&P steel effectively inhibits the precipitation of cementite [110], providing maximum austenite enrichment by carbon. The reasons for this are the very low solubility of silicon in cementite [133, 134], and the fact that Si sharply increases the activity of carbon in austenite. As shown by Tkachenko [70], in the case of the cementite nuclei formation silicon should be rejected into the matrix, enriching the austenite next to the interphase boundary. This should lead to a sharp increase in carbon activity in the Si-rich austenite zone, with a corresponding increase in the system's free energy, which thermodynamically disables the cementite precipitation.

However, silicon almost does not inhibit the transitional ε-carbides formation during martensite tempering. Moreover, Si stabilizes ε-carbides, which precipitate from martensite at relatively low temperatures and can continue to exist at long holdings and at higher temperatures [95]. The transitional carbides formation is a competing process that reduces the austenite saturation with carbon. In addition, according to [95], at a content of more than 2 wt.% silicon can stimulate the formation of the carbide.

Aluminum is used as a silicon substitute because it prevents the release of cementite during the holding of steel at bainitic transformation temperature [135]. Aluminum also effectively controls the austenitic grain growth when steel is heating under Q&P treatment [135].

Despite its obvious advantages, basic Q&P technology has some drawbacks. Q&P is difficult to be applied for the parts of large sections. At large thicknesses, it is impossible to ensure the same structure formation at different depths, which leads to a gradient of microstructure and mechanical properties on the cross-section. Basic Q&P technology is constantly being modified, and various modifications are being developed to address the shortcomings or further enhance the steel properties. The following Q&P modifications are currently known as follows:

(a) Q-Q&P is double-quenching processing, which results in double phase recrystallization with obtaining a more dispersed structure. Q-Q&P uses the grain boundary strengthening to more extent as compared to classical Q&P processing. Also, Q-Q&P results in increasing RA fraction due to the fact that fine-grained austenite is more stable to martensitic transformation during quenching [107];

(b) IA-Q&P (IA is Intercritical Austenization) is a modification of Q&P with intercritical annealing. It allows obtaining in the structure a certain amount of polygonal ferrite, along with martensite and austenite, which increases the steel ductility. As a result of IA-Q&P treatment, after partitioning at 400 °C for 10 s steel of composition (0.2 wt.% C; 1.5 wt.% Si; 1.9 wt.% Mn) possessed UTS of 990–1100 MPa and TEL of 29%, which is a good combination of mechanical properties [136];

(c) Q&P-T processing (T is Tempering) is a Q&P modification, in which steel is additionally alloyed with strong carbide forming elements (Mo, Nb, V) [137–139]. This treatment is recommended for applications where a higher strength level of steel is required. The properties enhancement is achieved by dispersion hardening during the precipitation of carbides and carbonitrides during the partitioning stage. Zhong et al. [109] showed that Q&P-T treatment with partitioning at 400 °C provides in steel containing 0.20 wt.% C, 1.18 wt.% Si, 1.44 wt.% Mn, 0.05 wt.% Nb a UTS value of 1200 MPa with an elongation of 18% and a Charpy impact toughness of 48 J/cm^2. Q&P-T treatment can also be applied to steel with a simple alloying system without the addition of expensive carbide-forming elements. As shown in [139], Q&P-T treatment with partitioning at 400 °C provides higher mechanical properties of steel at 0.2 wt.% C–Mn-Si compared to conventional quenching and tempering;

(d) Q-DP (DP is Dynamic Partitioning) is a modification proposed by Li in 2016 [140]. The advantages of this technology include the possibility of achieving higher strength by gradually reducing the temperature at the

partitioning stage (Fig. 1.3, a). In steel containing 0.3 wt.% C, 1.4 wt.% Si, 1.8 wt.% Mn, 1.3 wt.% Cr, 0.3 wt.% Mo, Q-DP led to UTS of 1519 MPa, YTS of 1336 MPa, TEL of 21.3%, and PSE (Product of Strength and Elongation) of 32.4 GPa × % [140];

(e) B-Q&P (B is Bainite). The essence of this technology is obtaining carbide-free bainite before the quenching stage (Fig. 1.3, b) [141]. The carbide-free bainite formed during isothermal holding at the first stage of processing divides austenitic grains, refining the resultant microstructure. B-Q&P treatment was applied for steel containing 0.40 wt.% C, 2.10 wt.% Mn, 1.70 wt.% Si, 0.40 wt.% Cr; the extraordinary properties were obtained: UTS=1495 MPa; TEL=31.8%; PSE=47.5 GPa × % [141]. Holding at temperatures above M_S before quenching can positively result even in the absence of bainitic transformation. As shown by Malinov and Chelyakh [142], a step-quenching with holding in the area of high stability of austenite at 100–400 °C provides both a decrease in the quenching stress level and an increase in RA volume fraction in Cr-Mn austenitic steels. This allows further SIMT which promotes the increase of the mechanical properties complex;

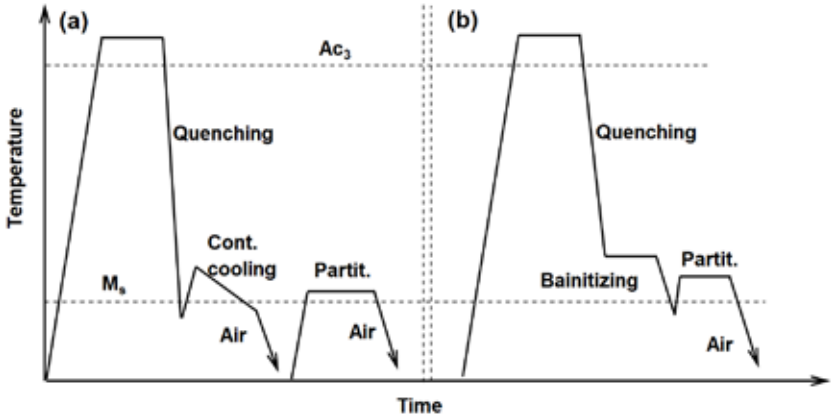

Figure 1.3. The shemes of (a) Q-DP [140] and (b) B-Q&P [141].

(f) Q-T&P (TP is Tempering-associated Partitioning) is a modification in which the chemical composition of steel is tuned so that the quenching temperature coincides with the ambient temperature. This simplifies the application of technology in industrial conditions [135];

(g) Q-LP (L is Long) is a basic Q&P process with prolonged holding at the partitioning stage. This modification was proposed by Huang in 2015

[143] for Q & P processing of bulk products. Q-LP enables the formation of a multiphase microstructure consisting of martensite, bainite, and retained austenite in big cross-section parts.

Despite the technical difficulties, the first data on the use of Q & P technology in the industry has already emerged. Thus, Baoshan Iron & Steel Company (China) has mastered the Q & P-based manufacturing of high-strength automotive steel AHSS980 with YTS ≥ 980 MPa [144–146].

Chapter 2. Mechanisms and kinetics of phase-structural transformations in medium-carbon Si-Mn-Cr-V steels

2.1 Materials and methods

The structural steels of 60Si2CrV, 75CrMn2Si, 55Si3Mn2CrVMoNb, and 75CrMn grades were used in the work as research material, the chemical composition of which is presented in Table 2.1. All steels contained increased amounts of silicon, which is a prerequisite for the steels intended for Q&P processing.

Table 2.1. Chemical composition of the investigated steels

Content of elements (wt.%)									
C	**Si**	**Mn**	**Cr**	**Mo**	**V**	**Nb**	**Al**	**S**	**P**
Grade 60Si2CrV									
0.53	1.46	0.44	0.95	–	0.10	–	–	0.016	0.013
Grade 55Si3Mn2CrVMoNb									
0.56	2.50	1.70	0.50	0.21	0.12	0.05	–	0.011	0.015
Grade 75CrMn2Si									
0.73	0.91	2.10	0.69	0.01	0.01	–	0.08	0.017	0.020
Grade 75CrMn									
0.72	0.37	0.89	0.60	0.14	–	0.05	–	0.008	

The standard steel of 60Si2CrV grade (GOST 14989–79, equivalent to DIN EN10089) was used as a commercial bar with a diameter of 16 mm; the bar was forged into a square cross-section of 12×12 (mm), from which the specimens after annealing (from 850 °C) were machined.

The steels of 75CrMn2Si and 55Si3Mn2CrVMoNb grades were smelted in an induction 60 kg furnace and poured into an 80 mm diametre graphite crucible. The castings were subjected to forging and rolling into a strip 15 mm thick. After annealing from 850 °C the specimens were made for further investigation. The specimens of 75CrMn steel were fabricated from rolled grinding balls produced by PJSC "AzovStal Iron and Steel Works".

Phase-structural transformations under isothermal conditions and under continuous heating (cooling) were investigated by a dilatometric method using a differential optical dilatometer. Samples of 2 mm diameter and 20 mm length were used. Variations in the sample length were recorded by deflection of the light beam. Samples were heated in a dilatometer furnace at a rate of ~5 K/min. The start temperature of the martensitic transformation was determined by bending the dilatometric cooling curves, which corresponds to an increase in sample volume under the γFe → αFe transformation; the temperature was fixed using a welded to the sample chromel-alumel thermocouple.

The TTT (Transformation-Time-Temperature) diagrams and the kinetics of martensitic transformation during cooling were plotted using a magnetometric method with a tensometric system of the magnetic phase gain fixation [147]. Samples of 2 × 10 × 12 (mm) in size were austenized in a laboratory furnace for 5 min, then they were transferred to a magnetometer's bath (molten alloy Sn-38wt.% Pb). The temperature of bath varied from 250 °C to 700 °C. The signal from the bridge circuit was recorded on a personal computer using an "Advantech" analog-to-digital converter. The transformation's onset was referred to as the appearance of the 2–3 vol.% aFe-phase. When determining the martensitic transformation kinetics, the sample was cooled in the air outside the bath; its temperature was fixed by a welded thermocouple.

The heat treatment of the samples was carried out in laboratory muffle furnaces and bath furnaces filled with molten Wood's alloy, Sn-38wt.% Pb alloy, a mixture of salts K_2NO_3 and $NaNO_2$. During austenitization, wood coal was used to prevent oxidation and decarburization of the sample surface. Bath furnaces were used to cool the austenitized specimens at the "Quenching" stage and holding at the "Partitioning" stage.

Tensile tests were performed according to GOST 1497–84 on samples with a gauge diameter of 5 mm. Charpy tests were performed according to GOST 9454–78 on samples of size 7 × 10 × 55 mm with a U-shaped notch. Hardness was measured according to the Rockwell method (scale C). Samples for microstructural analysis were prepared by the standard metallographic procedure of polishing with final etching by 4 vol.% "Nital" solution. The microstructure was examined using "Axiovert 40 MAT" (Carl Zeiss) and "Eclipse M200" (Nikon) optical microscopes, as well as electron scanning microscopes "Ultra 55" (Carl Zeiss) and "Nova 400 Nano" (SEM FEI). The fracture surface was investigated using SEM Ultra-55 (Carl Zeiss).

The phase chemical composition determination was performed using an "INCA" energy dispersion analyzer (Oxford Instruments). The qualitative and quantitative phase composition of the steels was determined by X-ray diffractometers DRON-3 (in FeK_α-radiation) and "Ultima IV-Pro" (Rigaku) (in CuK_α-radiation). In the latter case, the diffraction pattern was recorded at a voltage of 30 kV at a speed of 2 deg/min using monochromator.

The volume fraction of retained austenite (A_{RA}) was calculated using the equation [98]:

$$A_{RA} = \frac{100\%}{1 + G(I_\alpha / I_\gamma)}, \tag{2.1}$$

where G – is the coefficient corresponding to specific combinations of γ – and α-peaks: 2.46 for $I_\alpha(200)/I_\gamma(200)$; 1.32 for $I_\alpha(200)/I_\gamma(220)$; 1.78 for $I_\alpha(200)/I_\gamma(311)$; 1.21 for $I_\alpha(211)/I_\gamma(200)$; 0.65 for $I_\alpha(211)/I_\gamma(220)$; 0.87 for $I_\alpha(211)/I_\gamma(311)$ [98]; I_α, I_γ are the integral intensities of the austenite diffraction peaks (200), (220), (311) and α-phase (200), (211). The austenite volume fraction was found as the average defined for different pairs of lines.

The carbon content of retained austenite was found from the equation [148]:

$$a_\gamma = 0.3556 + 0.00453x_C + 0.000095x_{Mn}, \tag{2.2}$$

where a_γ is austenite lattice parameter, m; x_C is carbon concentration in austenite, wt.%; x_{Mn} is manganese concentration in austenite, wt.%.

The austenite lattice parameter was determined by the equation [149]:

$$\alpha_\gamma = \sqrt{h^2 + k^2 + l^2}\,\frac{\lambda}{2\sin\theta}, \tag{2.3}$$

where h, k, l are plane indexes; λ is X-ray wavelength; θ is Bregg's angle, found using the Gaussian approximation and averaging for the $(200)_\gamma$ and $(220)_\gamma$ peaks.

The fine microstructure was examined using a transmission electron microscope (TEM) "JEM-100-C–XII" (JEOL) with an acceleration voltage of 100 kV. The thin foils made from samples were used. The foil preparation method consisted of mechanical thinning to a thickness of 0.10–0.15 mm, after which discs with a diameter of 3 mm were cut from the foil by the electrospark method. The disks were electrolytic jet polished at the "TENUPOL-2" installation in the electrolyte of composition: 40 ml of HCl, 400 ml of methyl alcohol, and 240 ml of butyl alcohol. The electrolyte temperature (not higher than minus 30 °C) was maintained with a thermostat during polishing.

The impact resistance of steel grinding balls was evaluated by tests on the copra-type equipment where the ball was impacted by a hammer of 125 kg weight which fell from a height of 5.5 m.

Abrasive wear tests were performed according to the "Three-Body Abrasion" scheme at the load on the sample of 10 N. The abrasive was SiO_2 and Al_2O_3. The test duration was 1 hour. The sample wear was evaluated by weight loss, which was determined by weighing on the electronic balance with measurement discretion of 0.0001 g.

2.2 The austenite transformation kinetics under isothermal conditions and morphology of transformation products

As noted above, Q&P treatment allows for achieving high strength in relatively cheap low-alloyed steels, which is of interest from a practical point of view. The application of Q&P treatment to medium- and high-carbon steels remains poorly studied. In this regard, it was of interest to study the prospects of Q&P treatment in enhancing the combination of mechanical properties of structural medium carbon (0.5–0.6% C) steels, which are usually prone to brittle fracture at high strength [150]. In order to accumulate the carbon in γ-phase during the partitioning stage, the steel must contain more than 1.0 wt.% silicon, which effectively inhibits the carbides precipitation from austenite. High-Si spring steels (60Si2, 60Si2CrV, etc.) fully meet this requirement. In this chapter, the results of studies of the use of Q&P treatment to enhance the mechanical properties of commercial steel 60Si2CrV and experimental steel 55Si3Mn2CrVMoNb are presented. The latter steel was designed to maximize the benefits of Q&P treatment: (a) increased silicon content (2.5 wt.%) was intended to inhibit cementite formation at the partitioning stage, (b) adding 1.70 wt.% Mn in combination with the minor amounts of Cr and Mo was aimed at increasing the steel hardenability, (c) microalloying by V and Nb was focused to the grain refinement.

The rational selection of Q&P processing parameters implies the knowledge of phase-structural transformation features and the critical points position of particular steel. In this regard, the kinetics of austenite transformation in steels 60Si2CrV and 55Si3Mn2CrVMoNb were investigated at the initial stage of this research. The critical points Ac_1 and Ac_3 of the steels were found (by dilatometric analysis) as follows: Ac_1= =800 °C, Ac_3 = 840 °C (for 60Si2CrV steel) and Ac_1 = 790 °C, Ac_3 = 840 °C (for 55Si3Mn2CrVMoNb steel). Taking into these values, the optimal

austenitization temperatures were selected as 880 °C for 60Si2CrV steel and 900 °C for 55Si3Mn2CrVMoNb steel. The higher temperature in the latter case was taken due to the presence of Mo in steel, which may impede the carbides dissolution when heated in the austenitic area. The selected temperatures were used for austenitization of steels in the study of phase-structural transformations, as well as for Q & P processing.

The kinetics of austenite transformation in steels under isothermal conditions was investigated at temperatures in the range 250–700 °C with a step of 50 °C with the development of the TTT-diagram. According to Fig. 2.1, a TTT-diagram for 60Si2CrV steel featured the divorced pearlitic and bainitic areas, divided by a zone of austenite stability at 550 °C (which is characteristic of steels alloyed with carbide-forming elements). The kinetic maxima of the transformation in the pearlite region were recorded at 650 °C; in this case, the incubation period was 5 s, and the full transformation time was 35 s. At 550 °C, the incubation period increased sharply to 294 s, and the end of the transformation was fixed after 694 s holding. The kinetic maximum of bainitic transformation referred to 450 °C with an incubation period of 6 s and a total transformation time of 117 s.

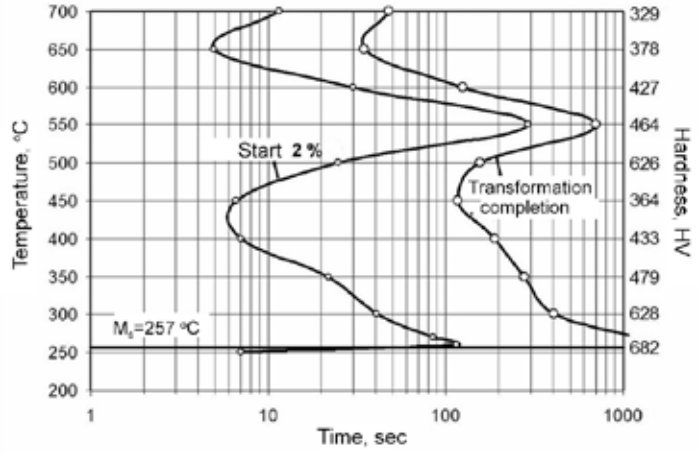

Figure 2.1. TTT-diagram for 60Si2CrV steel

The microstructure of 60Si2CrV steel after isothermal holding is presented in Fig. 2.2. At 600–700 °C, the transformation resulted in lamellar pearlite without proeutectoid ferrite formation (Fig. 2.2, a, b). At 550 °C, the areas of a needle-like morphology (shown by the arrow in Fig. 2.2, b) were detected in the structure along with the pearlite, featuring an over-

lapping of pearlitic and bainitic transformations. Holding at the temperatures in the range "500 °C–M_S" resulted in a structure consisting of bainite, whose appearance changed from differentiated "feathers"-like morphology at 500 °C (Fig. 2.2, c) to a fine-needle morphology at 250 °C (Fig. 2.2, c).

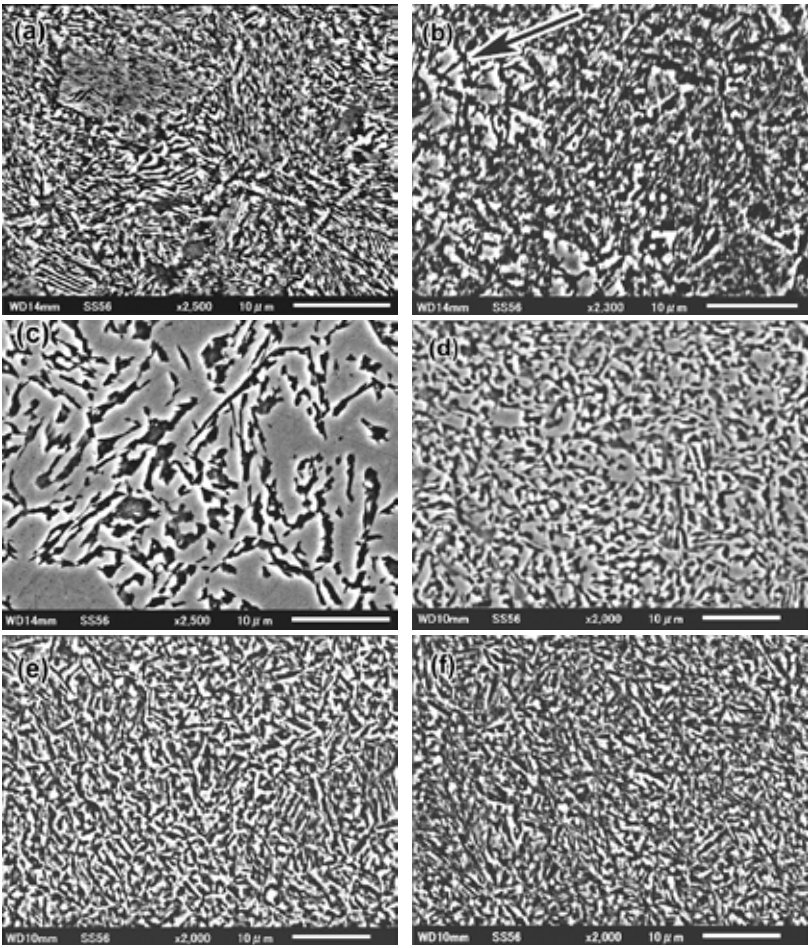

Figure 2.2. Microstructure of 60Si2CrV steel after austempering at (a) 650 °C, (b) 550 °C, (c) 500 °C, (d) 450 °C, (e) 350 °C, (f) 250 °C

Figure 2.3 presents the kinetic curves of austenite transformation for 55Si3Mn2CrVMoNb steel. In this case, a significant slowdown of transformation compared to 60Si2CrV steel was detected for each holding temperature. The TTT-diagram was fully divided into pearlite and bainite

domains with a temperature interval (500–400 °C) where austenite transformation was not recorded during 3000 s holding (Fig. 2.4). The "nose" of the pearlite domain corresponded to 600 °C while the "nose" of bainite domain referred to 350 °C. At 600 °C the incubation period of transformation was 180 s, and the duration of transformation completion was 2400 s. At 350 °C the incubation period of transformation was 60 s, and the transformation finished after 300 s. At 650 °C and 700 °C austenite transformation was not detected during the holding of 3600 s.

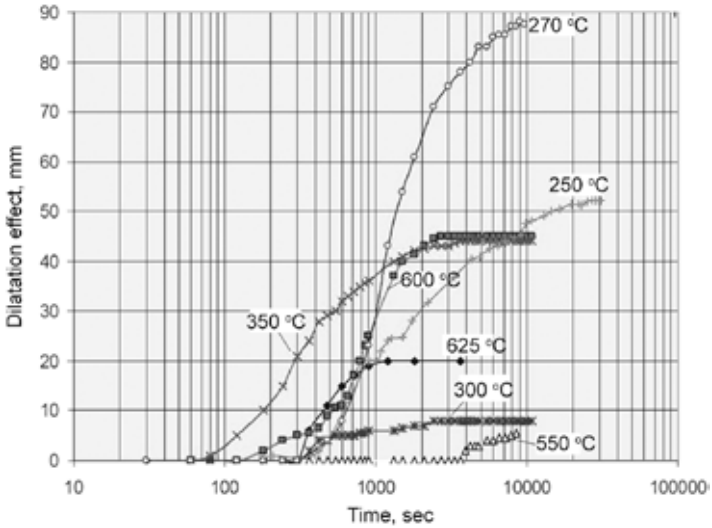

Figure 2.3. Dilatometric kinetic curves of austenite transformation in 55Si3Mn2CrVMoNb steel

According to the kinetic curves (Fig. 2.3), at 300 °C and 550 °C, the transformation proceeded much slower as compared with other holding temperatures. The low transformation rate at 550 °C was explained by the decrease in the diffusivity of alloying element atoms [71]. At 300 °C, the transformation arrest was caused by the carbon over-enrichment of austenite due to higher silicon content (2.5 wt.%) [71, 74, 151–155]: an increase in carbon content during transformation led to stabilization of austenite to bainitic transformation. As a result, at 300 °C the transformation stopped, not even reaching 50%. At 270–225 °C, the transformation proceeded to more extent. At these temperatures, austenite saturation with carbon was much less due to the decreased diffusion mobility of carbon atoms.

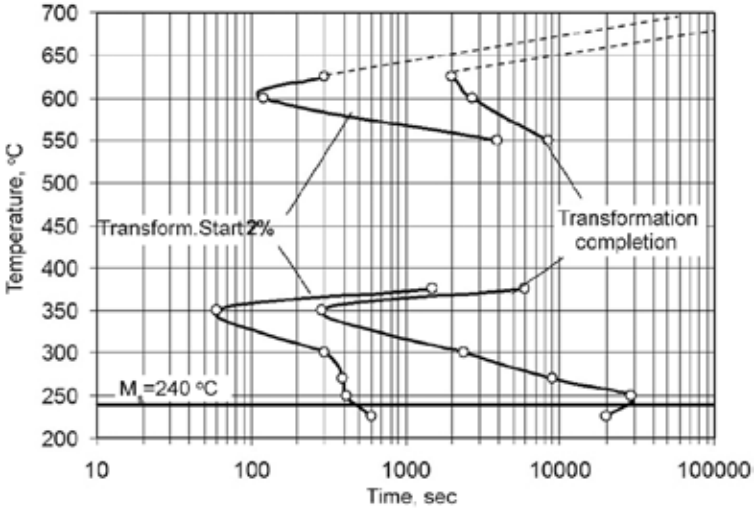

Figure 2.4. TTT-diagram for 55Si3Mn2CrVMoNb steel

The analysis of the transformation kinetics showed that 60Si2CrV and 55Si3Mn2CrVMoNb steels featured fair stability in the pearlite and bainite regions. This allows the cooling of austenite directly to M_S temperature without any transformation that fully meets the requirement of Q&P-principle.

2.3 Determination of M_s temperature and kinetics of athermal martensitic transformation in 60Si2CrV and 55Si3Mn2CrVMoNb steels

Martensitic transformation is extremely important for the improvement of the mechanical properties of steel [156]. The temperature interval of transformation determines the martensite morphology, the amount of retained austenite, and the quenching stress level, thereby affecting the properties and distortion of quenched steel. The data on the kinetics of athermic martensitic transformation allows for the correct selection of the regime of heat treatment, especially if this treatment involves the cooling abortion at the temperature lying within the M_S – M_f interval. This approach is the essence of Q&P processing where the first stage involves the interruption of quenching at a certain temperature (QT), which lies within the interval of M_S – M_f. The correct selection of QT temperature is important in terms of achieving the optimum "martensite/austenite" volume

ratio, which, on the one hand, determines the austenite carbon enrichment, on the other hand, controls the level of steel strength. Experimental data on the kinetics of atermic martensitic transformation in steels are quite rare [157–159]; thus special studies for steels of particular chemical compositions are needed.

The M_S point of the investigated steels was determined by a magnetometric method. The austenized sample was air-cooled being placed between the magnet's poles. As the temperature decreased and the martensitic transformation progressed, the sample was drawn into the magnetometer's magnetic field, generating a signal which is proportional to the volume fraction of α-phase (martensite). The sample's temperature was fixed using a point-welded chromel-alumel thermocouple. The sample was cooled to 50 °C at an average cooling rate of 13.3 K/s inside the magnetometer. After that, the sample was removed from the magnetometer and sequentially cooled to 4 °C, to minus 20 °C and to minus 196 °C (in liquid nitrogen). After cooling, the sample was positioned inside the magnetometer for the ferromagnetic phase increment measurement.

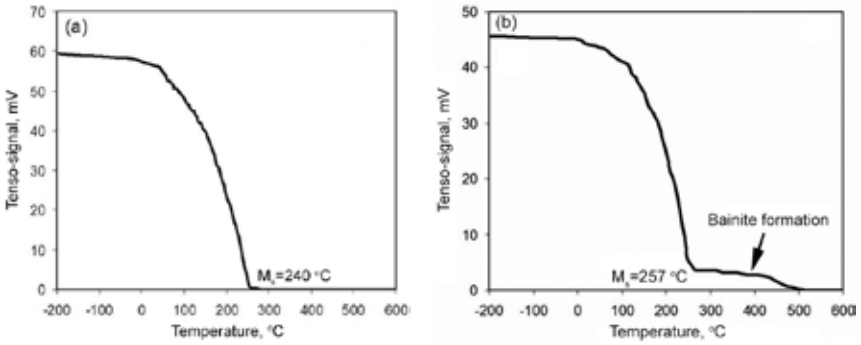

Figure 2.5. Magnetometric cooling curves for:
(a) 55Si3Mn2CrVMoNb steel, (b) 60Si2CrV steel [157]

Figure 2.5 shows the magnetometric curves reflecting the increment of volume fraction of the ferromagnetic phase (martensite) under cooling. In steel 55Si3Mn2CrVMoNb martensite appeared when the sample was cooled to 240 °C, which was adopted as the M_S point for this steel. The peculiarity of 60Si2CrV steel (Fig. 2.5 b) is that during the sample cooling in the air the austenite transformation began in the bainite region by forming at 500–420 °C small amount of bainite. After that, the transformation was suspended until reaching a temperature of 257 °C. Starting at this tem-

perature, the ferromagnetic phase amount began to rise sharply, indicating the martensitic transformation. The temperature of 257 °C was adopted as the M_S point for 60Si2CrV steel. It was presumed that cooling in liquid nitrogen ensured the reaching of the M_f temperature for both steels. Based on this, the obtained magnetometric curves were converted into kinetic curves of martensitic transformation presented in Figure 2.6.

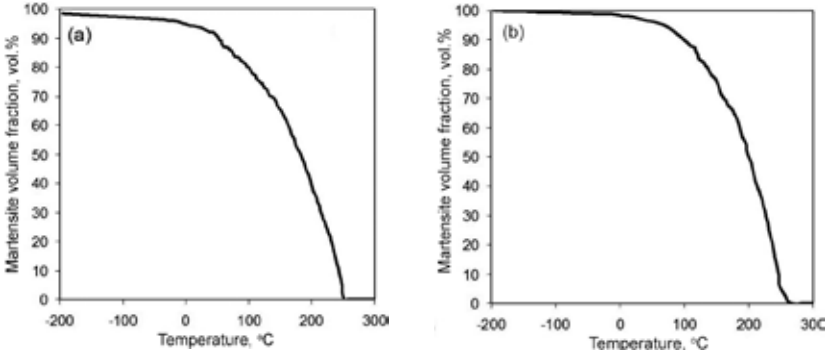

Figure 2.6. Kinetic curves of athermic martensitic transformation for (a) 55Si3Mn2CrVMoNb steel, (b) 60Si2CrV steel [157].

As follows from kinetic curves, the studied steels performed the martensitic transformation close to explosive kinetic, i.e., the most volume of martensite was formed in the temperature range of 120–150 °C. Thus, in 55Si3Mn2CrVMoNb steel, cooling to 200 °C led to the appearance of 38 vol.% of martensite, and at 100 °C its amount increased to 80 vol.%. At lower temperatures, the velocity of martensitic transformation decreased sharply. At room temperature, about 4 vol.% austenite was retained in the 55Si3Mn2CrVMoNb steel structure. For 60Si2CrV steel, the highest increase in the martensite's amount corresponded to the temperature interval of M_s – 200 °C, when 50 vol.% of martensite was formed. At lower temperatures, the growth of martensite volume fraction decreased significantly. At 20 °C steel 60Si2CrV contained 2 vol.% of retained austenite.

Given the complexity in the experimental determination of the martensitic kinetics transformation and martensitic transformation start temperature, mathematical models and empirical equations that allow calculating these parameters are widely used [160, 161]. However, they have limited usage, due to differences in carbon content and alloying systems of different steel classes. In this regard, it was of interest to analyze the known empirical equations for calculating M_S in order to determine their

suitability for medium carbon steels with high Si content. The equation proposed in 1959 by Koistinen and Marburger (K-M) is most commonly used to describe the athermic martensitic transformation kinetic [160]:

$$f = 1 - exp(-a_m \times (M_s - T)) \quad (2.4)$$

where M_S is starting temperature of martensitic transformation, °C; f is the volume fraction of martensite formed at a temperature T (°C) below M_S point; a_m is the fitting coefficient.

The results of calculating M_S temperature values using known empirical equations [160, 161] are presented in Table 2.2. As seen, the equations (2.5)–(2.11) allow sufficient accuracy (±(4–8) °C) when calculating the M_S temperature for 55Si3Mn2CrVMoNb steel. For 60Si2CrV steel, the lowest error in M_S temperature calculation is ascribed to the equations (2.12) and (2.13), and the maximum error corresponds to equations (2.20)–(2.22).

Although K-M equation is developed for non-alloyed iron-carbon alloys, it contains a fitting coefficient a_m, which allows it to fairly accurately describe the transformation's kinetics in alloyed steels of a specific class. Later, Hougardy, van Bohemen, Lee, and Van Tyne were offered modified versions of the "K-M" equation (Table 2.3). In the latter two cases, an attempt to relate the fitting parameter to the steel's chemical composition was made. The theoretical model of Hougardy (2.23), which is based on the "K-M" approach, is distinguished by the introduction of a power parameter q. In the Hougardy equation, both the q parameter and the fitting parameter itself (designated in this case as k) are calculated depending on the temperature M_S. The equation (2.24) proposed by van Bohemen differs by the fitting parameter a_m calculated based on the contents of carbon and alloying elements in steel (this equation can be applied to a limited range of steels that are alloyed by Ni and Mo). The equation (2.25) developed by Lee and Van Tyne includes a fitting parameter K_{LV} and a power parameter n_{LV}, whose values are also calculated depending on the steel's chemical composition.

To evaluate the appropriateness of the equations (2.4) and (2.23)–(2.25) regarding 55Si3Mn2CrVMoNb and 60Si2CrV steels, the kinetics of martensitic transformation was calculated to compare it with experimental kinetic curves. This comparison is presented in Figure 2.7. As seen, the equation of Hougardy fairly described the kinetic, while standard deviations were 2.48 and 2.20 for 55Si3Mn2CrVMoNb and 60Si2CrV steels, respectively. The lowest standard deviations (2.01 for 55Si3Mn2CrVMoNb steel and 1.63 for 60Si2CrV steel) were noted for the "K-M" equation using $a_m = 0.012$.

Table 2.2. Equations (2.5)-(2.22) [160, 161] for M_s calculation. In parentheses, the element contents (wt.%) are given. The steels designated as #1 (60Si2CrV) and #2 (55Si3Mn2CrVMoNb)

Authors	Equation	Calculated M_S temperature (°C) for	
		Steel# 1	Steel# 2
1	*2*	*3*	*4*
Popov A., Popova L.	$M_s = 520–320[C] – 50[Mn] – 30[Cr] – –20[Ni+Mo] – 5[Cu+Si]$ (2.5)	293	224
Capdevila	$M_s = 764.2–302.6[C] – 30.6[Mn] – –16.6[Ni] – 8.9[Cr] + 2.4[Mo] – 11.3[Cu] +8.58[Co] + +7.4[W] – 14.5[Si]$ (2.6)	288	229
Krauss	$M_s = 561–474[C] – 33[Mn] – 17[Cr] – -17[Ni] – 21[Mo]$ (2.7)	279	227
Zhichao	$M_s = 540 – 420[C] – 35[Mn] – 12[Cr] – - 20[Ni] – 21[Mo] – 10.5[Si] – 10.5[W] + + 20[Al] + 140[V]$ (2.8)	289	225
Sverdlin and Ness	$M_s = 561.1 – 473.9[C] – 33[Mn] – - 16.7[Cr+Ni] – 21.1[Mo]$ (2.9)	293	224
Payson and Savage	$M_s = 498.9 – 316.7[C] – 33.3[Mn] – –7.8[Cr] – 16.7[Ni] – 11.1[Si+Mo+W]$ (2.10)	274	221
Van Bohemen	$M_s = 565 – 31[Mn] – 13[Si] – – 10[Cr] – 18[Ni] – 12[Mo] – – 600(1-exp(– 0.96[C]))$ (2.11)	284	223
Andrews	$M_s = 539–423[C] – 30.4[Mn] – – 17.7[Ni] – 12.1[Cr] – 11[Si] – 7[Mo]$ (2.12)	258	199
Rowland, Lyle	$M_s = 498.9–333.3[C] – 33.3[Mn] – – 27.8[Cr] – 16.7[Ni] – 11.1[Si+Mo+W]$ (2.13)	265	212
Liu	$M_s = 525 – 350([C]–0.05) – 45[Mn]–30[Cr] – - 20[Ni] – 16[Mo] – 5[Si] – 8[W] + 6[Co] + + 15[Al] – 35[V+Nb+Zr+Ti]$ (2.14)	298	233
Mahieu	$M_s = 539–423[C] – 30.4[Mn] – – 7.5[Si] + 30[Al]$ (2.15)	290	232

1	*2*	*3*	*4*
Nehrenberg	$M_s = 498.9 - 300[C] - 33.3[Mn] - 22.2[Cr] - - 16.7[Ni] - 11.1[Si+Mo]$ (2.16)	288	233
Grange, Stewart	$M_s = 537 - 361.1[C] - 38[Mn+Cr] - 19[Ni] - - 27.[Mo]$ (2.17)	292	244
Hougardy	$M_s = 0.95\ M_п + 0.0095\ M_п^2 + 40$ (2.18)	301	243
Kunitake	$M_s = 560. - 407.[C] - 37.8[Mn] - 14.8[Cr] - - 19.5[Ni] - 4.5[Mo] - 7.3[Si] - 20.5[Cu]$ (2.19)	303	242
Tamura	$M_s = 520 - 361[C] - 39[Mn] - 20[Cr] - - 17[V] - 17[Ni] - 10[Cu] - - 5[Mo+W] + 15[Co] + 30[Al]$ (2.20)	321	268
Jaffe and Hollomon	$M_s = 550 - 350[C] - 40[Mn] - 35[V] - - 20[Cr] - 17[Ni] - 10[Cu] - 10[Mo] - 8[W] + + 15[Co] + 30[Al]$ (2.21)	324	270
Carapella	$M_s = 496 \times (1-0.44[C]) \times (1-0.051[Mn]) \times (1-0.18[Si]) \times (1-0.025[Ni]) \times (1-0.39[Cr]) \times \times (1-0.016[Mo])\ (1-0.10[W]) \times (1-0.067[Co])$ (2.22)	372	341

Table 2.3. Equations [160] to calculate the kinetic of athermic martensitic transformation and the standard deviation relatively the experimental data for 55Si3Mn2CrVMoNb and 60Si2CrV steels (in all cases, M_S is given in °C)

Authors	**Expression**	**Standard deviation for**	
		Steel# 1	**Steel# 2**
1	*2*	*3*	*4*
Koistinen, Marburger	$f = 1 - exp(-a_m \times (M_s - T))$ (2.4)	1.63	2.01
Hougardy	$f = 1 - exp(-k \times (M_s - T)^q)$. where $k = 0.36 \times \times 10^{-3} + 10^{-5} \times M_s - 0.34 \times 10^{-6} M_s^2 + 0.32 \times \times 10^{-8} M_s^3 - 0.52 \times 10^{-11} \times M_s^4$; $q = 2.08 - 0.76 \times \times 10^{-2} M_s + 0.16 \times 10^{-2} \times M_s^2 - 0.9 \times 10^{-8} \times M_s^3$ (2.23)	2.20	2.48

1	*2*	*3*	*4*
Van Bohemen	де $a_m = 0.0224 - 0.01007[C] - 7 \times 10^{-4}[Mn] - 5 \times 10^{-5}[Ni] - 12 \times 10^{-5}[Cr] - 10^{4}[Mo]$ (2.24)	4.29	3.99
Lee, VanTyne	$f = 1 - exp(-K_{LV}(M_s - T)^{nLV}$. where $K_{LV} = 0.0231 - 0.0105[C] - 0.0017[Ni] + 0.0074[Cr] - 0.0193[Mo]$; $n_{LV} = 1.4304 - 1.1836[C] + 0.7527[C]^2 + 0.0258[Ni] - 0.0739[Cr] + 0.3108[Mo]$ (2.25)	6.71	6.99

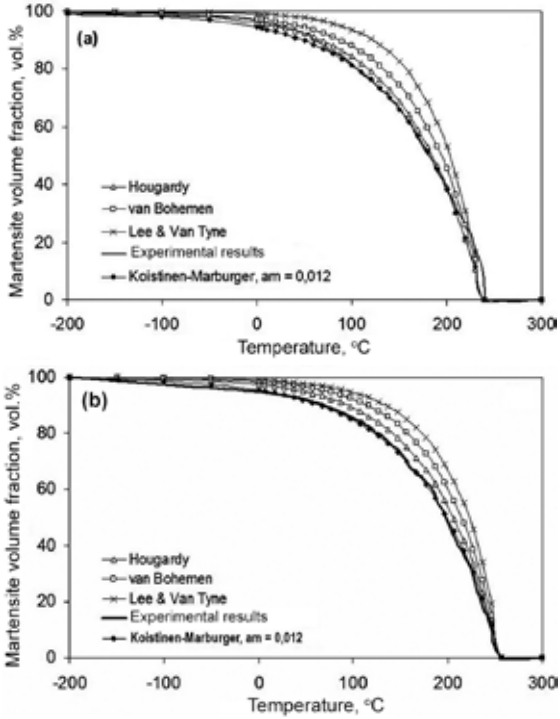

Figure 2.7. Comparison of experimental and calculated kinetics curves of martensitic transformation in (a) 55Si3Mn2CrVMoNb steel and (b) 60Si2CrV steel [157]

2.4 Effect of athermic martensite on the bainitic transformation kinetics

Bainite transformation is a competitive process in the partitioning stage resulting in a decrease in the austenite volume fraction. The prediction of the

bainitic transformation during Q&P processing can be based on the analysis of TTT-diagram. But it should be considered, that before the partitioning stage start, a certain amount of martensite is present in the structure, which may affect the kinetics of bainitic transformation [162–163]. Therefore, TTT-diagram is not appropriate for predicting Q&P processing. In this connection, the effect of athermal martensite on the bainitic transformation kinetic in 55Si3Mn2CrV-MoNb steel and 60Si2CrV steel was investigated [164]. The studies were carried out similarly to the TTT-diagram building but with pre-cooling to the interval of martensite transformation. The pre-cooling temperatures were 200 °C and 160 °C. Further, the isothermal holding was conducted at different temperatures within the interval of 270–350 °C for 60Si2CrV steel and of 225–300 °C for 55Si3Mn2CrVMoNb steel. Fig. 2.8 presents the kinetic curves of "austenite → bainite" transformation in 60Si2CrV steel with pre-cooling (Q+IH scheme) and without pre-cooling (IH scheme) (Q means "quenching", IH means "isothermal holding").

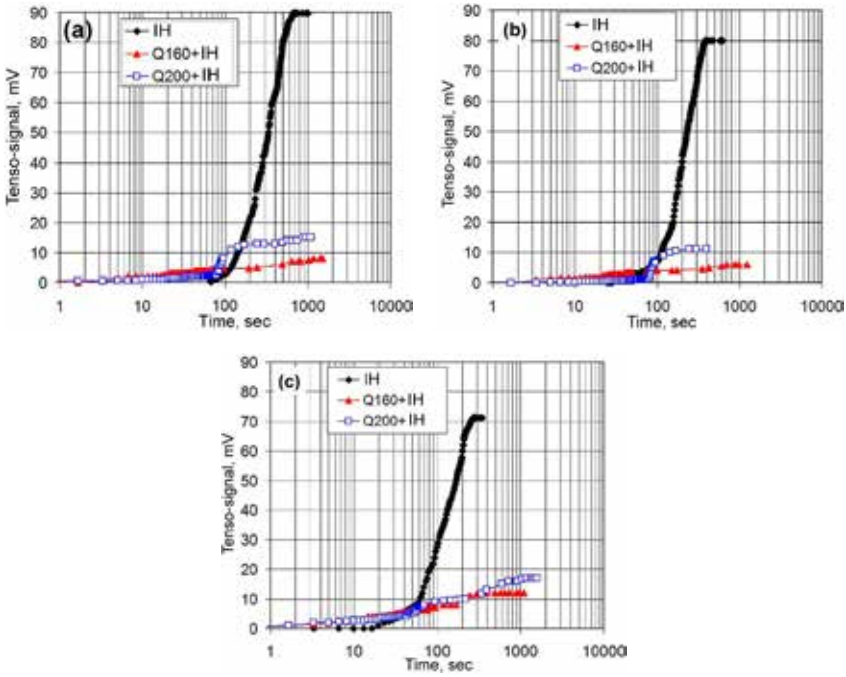

Figure 2.8. Kinetics of austenite transformation in 60Si2CrV steel with pre-quenching to 160 °C (200 °C) and without it at (a) 270 °C, (b) 300 °C, and (c) 350 °C [164]

The comparison of the curves (Fig. 2.8) showed that pre-cooling (a) accelerates the start of bainitic transformation and (b) decreased its velocity at further stages (at any holding temperature). Pre-cooling sharply reduces the maximum amount of bainitic α-phase, and this effect is manifested to a greater extent with a decreasing pre-cooling temperature. This is explained by the partial martensitic transformation before isothermal holding; this reduces the amount of austenite that can be transformed into bainite. As follows from Fig. 2.9, 55Si3Mn2CrVMoNb steel featured similar transformation behaviour to 60Si2CrV steel. The difference was a very small deflection of the beam at 300 °C (or even the absence of deflection at holding at 225 °C and 250 °C for 60 min). This indicates a significant inhibition of bainitic transformation at 300 °C, which is also characteristic of the isothermal holding of 55Si3Mn2CrVMoNb steel without pre-cooling (Fig. 2.4).

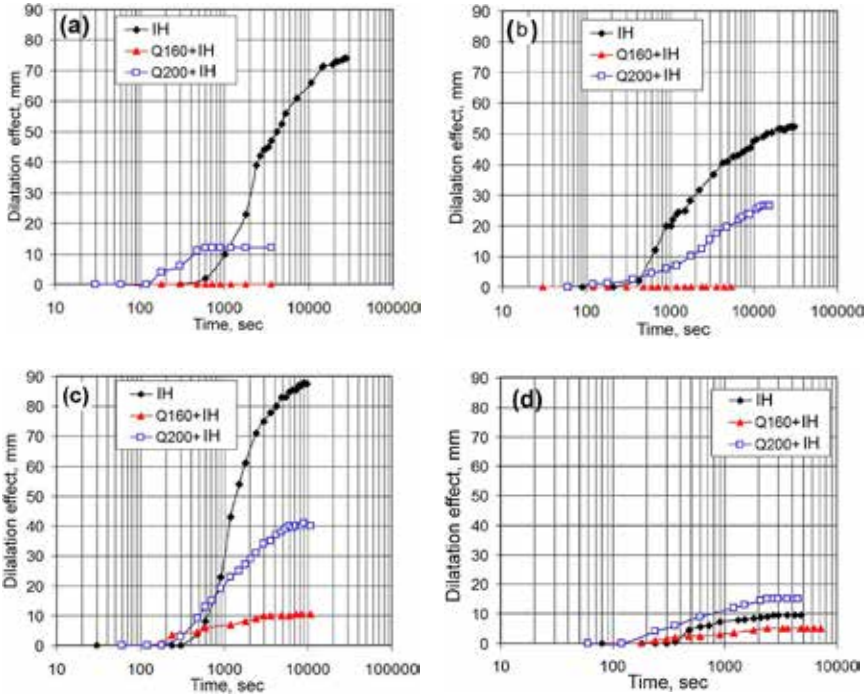

Figure 2.9. Kinetics of austenite transformation in 55Si3Mn2CrVMoNb steel with pre-cooling to 160 (200) °C and without it at: (a) 225°C, (b) 250 °C, (c) 270 °C, (d) 300 °C [164]

Thus, for both steels, an acceleration of bainite transformation induced by pre-cooling was documented. However, pre-cooling to 160 °C resulted in a sharp inhibition of the transformation in 55Si3Mn2CrVMoNb steel at low holding temperatures (225 °C and 250 °C).

Figure 2.10 presents the comparison of the values for the incubation period of bainite transformation with and without pre-cooling. It is seen that for steel 60Si2CrV pre-cooling reduced the incubation period for each holding temperature. The highest accelerating effect corresponded to holding at 270 °C (7-fold reduction of the incubation period); by increasing the holding temperature to 300 °C, this effect is reduced by 2 times. For steel 55Si3Mn2CrVMoNb, the character of the dependence was generally similar, although the accelerating effect was lower, being 3 times at 225–250 °C and 1.3 times at 270–300 °C.

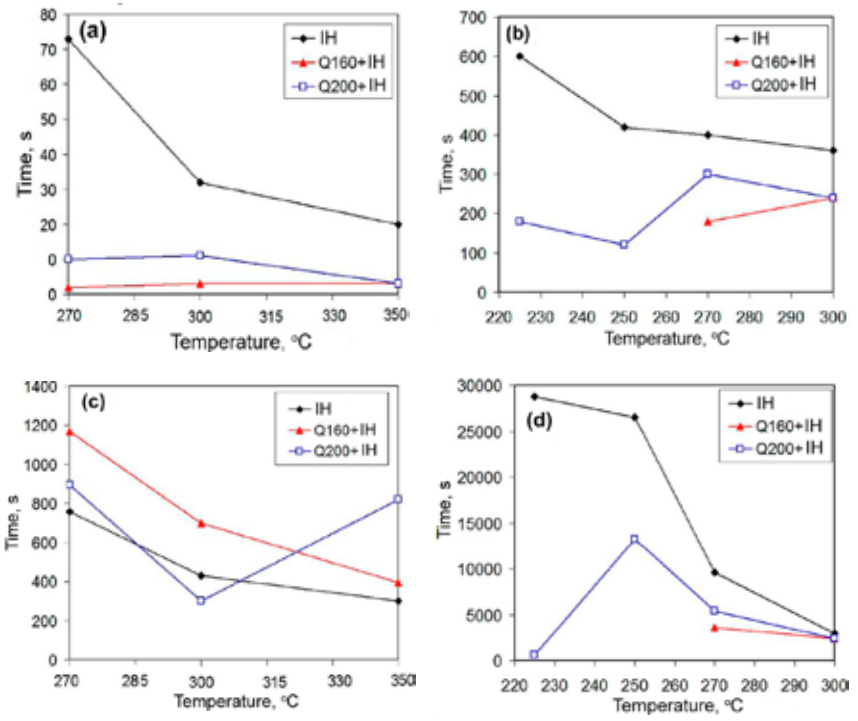

Figure 2.10. Effect of pre-cooling to 160 °C (200 °C) on (a, b) incubation period and (c, d) total duration of bainitic transformation (a, c – 60Si2CrV steel, b, d – 55Si3Mn2CrVMoNb steel) [164]

As for the effect of pre-cooling on the total duration of bainitic transformation, an increase in the duration under the effect of athermic martensite was recorded for steel 60Si2CrV (Fig. 2.10, c). The opposite pattern was observed for steel 55Si3Mn2CrVMoNb (Fig. 2.10, d): here the pre-cooling accelerated the completion of the transformation, and most sharply – at 225 °C.

The obtained results indicate that there is a significant effect of athermal martensite on the bainitic transformation kinetics in the investigated steels, for which a significant acceleration of the transformation's beginning under the influence of pre-cooling is highlighted. The formation of martensitic crystals during pre-cooling causes strain in the surrounding austenite, creating the cites for α-phase nuclei's emergence on the crystal defects [129]. An increase in martensite volume fraction results in a higher number of the sites of potential α-phase formation thus accelerating the bainite transformation.

After a quick start, bainite transformation gradually decelerated due to: (a) carbon diffusion from the bainitic α-phase to austenite; (b) carbon partitioning from athermal martensite to austenite [116]. These processes led to the saturation of austenite by carbon and its stabilization to transformation. The C-enrichment was facilitated by the increased amount of silicon that inhibited the precipitation of cementite carbides from austenite. The stabilization factors also included the mechanical stabilization by the compressive elastic stresses induced in austenitic regions by martensite crystals. In this regard, pre-cooling to 160 °C more effectively stabilized austenite due to the larger volume fraction of athermic martensite. Moreover, in steel 55Si3Mn2CrVMoNb complete inhibition of the transformation at 225–250 °C was characteristic due to imposition of the following factors such as (a) austenite enrichment by carbon, (b) increased austenite resistance to shear transformation due to higher solution strengthening (because of higher Si, Cr, Mn, Mo contents), (c) martensite-induced stresses, (d) decreasing the carbon diffusion mobility by soluted alloying elements and lower holding temperature.

Despite the fact that with holding increase, the effect of factor "c" gradually decreased (due to the partitioning of carbon from martensite to austenite, which reduces the α-phase lattice's tetragonality and the stress in austenite), the total stabilization effect, obviously, manifested in inhibition the transformation, especially in its final stages. This conclusion, at first glance, is inconsistent with the data for 55Si3Mn2CrVMoNb steel (Fig. 2.16, a),

which shows the acceleration of transformation's completion due to pre-cooling. However, we suppose that this is a quasi "acceleration"; in fact, it is an early transformation arresting due to the extensive austenite stabilization. This was a result of increased contents of alloying elements, especially of silicon, the content of which in 55Si3Mn2CrVMoNb steel was 1.7 times higher than that in 60Si2CrV steel. During the holding at 225 °C after pre-cooling to 200 °C the transformation was suspended after 600 s of holding, which corresponds to a 33-fold "acceleration" of transformation's completion. Actually, at low holding temperatures, in 55Si3Mn2CrVMoNb steel martensite retained its lattice tetragonality for a longer time, providing effective austenite stabilization through residual compression stresses.

It can be assumed that due to austenite stabilization, the transformation continuation requires ever-increasing holdings for more pronounced carbon redistribution, needed to form another portion of bainitic ferrite. In such a scenario, the transformation has a "stepped" character that manifests in alternating stabilization periods ("step") and periods of α-phase amount growth. Such character is exactly shown in the Figure. 2.11 in the form of a "staircase" profile of kinetic transformation curves for 60Si2CrV steel. Thus, the effect of athermal martensite on the bainitic transformation kinetics in investigated steels has a complex character, which must be taken into account when selecting the Q&P treatment mode.

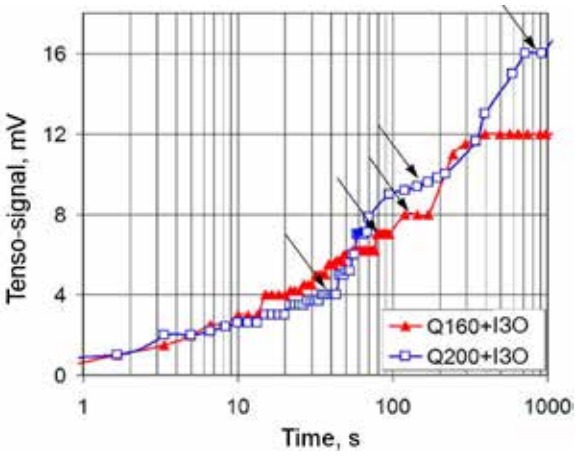

Figure 2.11. The "stepped" kinetics of bainite transformation in 60Si2CrV steel at 350 °C in the case of pre-cooling in the martensitic interval [164]

2.5 The selection of quenching temperature for Q&P treatment based on the "Constrained ParaEquilibrium" concept

The methodology of selecting the optimal quenching temperature for Q&P treatment was proposed in [42–43, 116] with the aim of obtaining the maximum amount of retained austenite in the resultant structure. This methodology is based on the hypothesis of complete carbon partitioning from martensite to austenite under the condition of full suppression of all competing reactions such as bainitic transformation, cementite or transition carbide precipitation. This approach presumes (a) the immobility of the interfacial α/γ boundary, (b) the interstitial diffusivity of carbon atoms, and (c) the absence of diffusion of iron and alloying atoms in a solid solution. According to the model, carbon redistribution ("partitioning") finishes when martensite (ferrite) reaches the state of metastable equilibrium with austenite. This means that at all points in the system the same chemical potential value of carbon is reached. This final state corresponds to a conditional (constrained) paraequilibrium. Given the above assumptions, the final chemical composition of austenite will be determined by the total carbon concentration in the steel and the α/γ phase ratio during partitioning.

Under immobility of the interfacial boundary, the final state of the system can be described by the set of equations that refer to (a) the balance of iron (it is assumed that the number of iron atoms in α-phase and γ-phase during partitioning remains unchanged); (b) carbon balance; (c) the condition of carbon chemical potentials equality in austenite and ferrite (in the latter case the effect of alloying elements is not taken into account):

$$f_{CPE}^{\gamma}(1-X_{C_{CPE}}^{\gamma}) = f_i^{\gamma}(1-X_{C_i}^{\gamma}) \text{ (balance for iron)}, \tag{2.26}$$

$$f_{CPE}^{\alpha}X_{C_{CPE}}^{\alpha} + f_{CPE}^{\gamma}X_{C_{CPE}}^{\gamma} = X_C^{alloy} \text{ (balance for carbon)}, \tag{2.27}$$

$$X_{C_{CPE}}^{\gamma} = X_{C_{CPE}}^{\alpha} \cdot \exp\left[\frac{76789 - 43{,}8T - (169105 - 120{,}4T)X_{C_{CPE}}^{\gamma}}{RT}\right], \tag{2.28}$$

$$f_{CPE}^{\alpha} + f_{CPE}^{\gamma} = 1, \tag{2.29}$$

where T is absolute temperature; X_C^{alloy} is total carbon content in steel; f_i^{γ} is austenite fraction before "Partitioning"; $X_{C_i}^{\gamma}$ is initial carbon content in austenite; f_{CPE}^{α} and f_{CPE}^{γ} are the fractions of α-phase and austenite,

respectively; $X^{\alpha}_{C_{CPE}}$ and $X^{\gamma}_{C_{CPE}}$ are the carbon concentrations in α-phase and austenite, respectively, when equilibrium is reached.

The contents of iron and carbon in austenite are given as for binary alloy:

$$X^{\gamma}_{Fe} = 1 - X^{\gamma}_{C}. \tag{2.30}$$

The selection of quenching temperature for Q&P treatment of 60Si2CrV steel and 55Si3Mn2CrVMoNb steel was carried out in four stages. In the first stage, assuming heating to the austenite domain, 100% of austenite was taken as an initial structure with a carbon concentration equal to the total carbon concentration in the steel. In the second stage, calculations of the martensite and austenite volume fractions were performed at a specific quenching temperature using the Koistinen-Marburger equation (2.4) taken with a fitting parameter a_m of 0.012. In the third stage, the austenite chemical composition after the completion of partitioning was calculated using the equations (2.26)–(2.30). In the fourth stage, the amount of C-rich austenite, which will transform into fresh martensite in the final stage of Q&P treatment was determined. For this purpose, the Koistinen-Marburger equation was used again, and M_S temperature was calculated according to Andrews' equation (2.12) for 60Si2CrV steel and by Kunitake' equation (2.19) for 55Si3Mn2CrVMoNb steel.

The results of the calculations are presented in Fig. 2.12. They show that the volume fraction of retained austenite after Q&P treatment should vary by a curve with a maximum corresponding to quenching temperature of 196 °C for 60Si2CrV steel and 177 °C for 55Si3Mn2CrVMoNb steel. In this case, the RA volume fractions were calculated as 48.4 vol.% for 60Si2CrV steel and 47.8 vol.% for in 55Si3Mn2CrVMoNb steel. After completion of carbon redistribution, the carbon content in austenite should be 1.08 wt.% and 1.12 wt.% for 60Si2CrV steel and 55Si3Mn2CrVMoNb steel, respectively. At this carbon concentration, the M_S point of the steels decreases to room temperature, and, accordingly, "fresh" martensite should not appear upon final cooling.

As the further quenching temperature decreases, the carbon concentration in the retained austenite increases continuously (to 3.48 wt.% at 100 °C in 60Si2CrV steel and to 2.84 wt.% in 55Si3Mn2CrVMoNb steel), however, RA volume fraction decreases because of continuous increase in quenching martensite volume fraction. Thus, regarding the Q&P treatment mode for investigated steels, it is necessary to select the quenching temperature close to the listed above temperatures. Too high (above 220 °C) and excessively low (below 150 °C) quenching temperatures will result in decreased volume fraction of retained austenite.

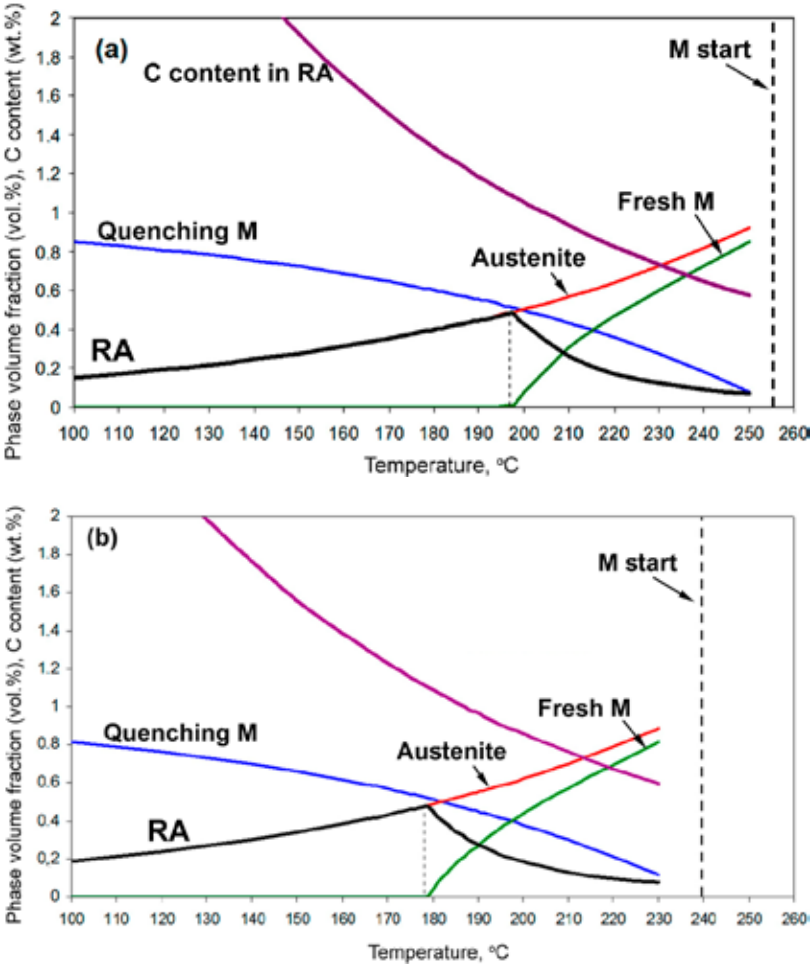

Figure 2.12. Effect of quenching temperature on the phase composition and carbon content in austenite after Q&P treatment. (a - 60Si2CrV steel, b – 55Si3Mn2CrVMoNb steel) [165]

2.6 Dilatometric study of Q&P-treated steels

The application of Q&P heat treatment aims to a heterogeneous microstructure with a high volume fraction of retained austenite. The final structure is dependent on several parameters such as quenching temperature, partitioning temperature, and partitioning duration. Experimental selection

of optimum parameters is costly taking into account a large number of samples and tests needed. Therefore, in this work, the dilatometric method was used for a preliminary selection of the Q&P mode parameters [166]. Dilatometric samples of both steels were subjected to Q&P treatment according to the modes presented in Table 2.4. The target values of quenching temperature were chosen as 160 °C and 200 °C, close to the calculated optimal temperatures for both steels. For comparison, the variants with a quenching temperature outside the optimum region (120 °C and 240 °C) were investigated as well. The partitioning temperature (220–300 °C) was selected close to the M_S temperature. After Q&P treatment, the specimens were heated in a dilatometer furnace to record the differential dilatometric curves (when the studied sample is heated along with the reference sample). The reference was the sample of the same steel previously subjected to quenching and tempering at 650 °C (with a holding time of 4 h). After such treatment, it was believed that the reference sample was stabilized to phase transformations at temperatures below the Ac_1 temperature.

Table 2.4. Parameters of Q&P treatment of dilatometric samples (final air cooling)

Quenching temperature, °C	**"Partitioning" stage**	
	Holding temperature, °C	**Holding duration, sec**
60Si2CrV steel		
120	220	30, 60, 300
	260	30, 60, 300
	300	30, 60, 300
160	220	10, 20, 30, 45, 60, 300, 600
	260	10, 20, 30, 45, 60, 300, 600, 1800, 36000
	300	10, 20, 30, 45, 60, 300, 600, 1200
200	220	10, 20, 30, 45, 60, 300, 600, 1200
	260	10, 20, 30, 45, 60, 300, 600, 1200
	300	10, 20, 30, 45, 60, 300, 600, 1200
240	260	300, 600, 1200
	300	300, 600, 1800
55Si3Mn2CrVMoNb steel		
160	260	60, 120, 240, 540, 720, 2400, 6000
200	300	60, 120, 480, 1000, 2400, 5400, 7200, 12000, 13200, 18000

Figure 2.13 depicts the dilatometric curve of the Q&P-treated sample in comparison with the sample, quenched to room temperature (both samples are 60Si2CrV steel). On the dilatometric curve of the quenched specimen, several characteristic areas can be identified. In the "AB" interval (100–260 °C), the curve is upward, meaning the prevailed extension of the standard sample; in the "BC" interval (260–400 °C) the curve goes slightly down indicating a more significant extension of the quenched sample. In the "CD" interval (400–500 °C) the curve sharply goes up, changing than with a slower growing section "DE". Comparing the curve's profile with the classical dilatometric heating curve of quenched steel [167], one can conclude that these areas are associated with different transformations occurring during tempering.

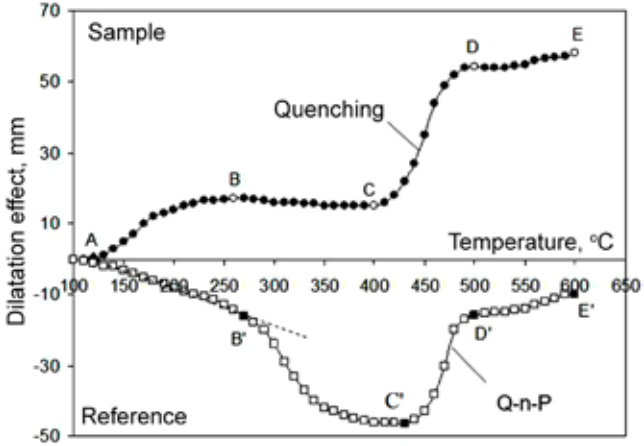

Figure 2.13. Differential dilatometric heating curves of 60Si2CrV steel in quenched state and after Q&P (QT is 160 °C, partitioning temperature is 300 °C, partitioning duration is 300 s) [166]

Thus, the increase in the "AB" interval was associated with the first transformation during tempering, which is the initial stage of martensite's decomposition (precipitation of ε-carbide) accompanied by a decrease in the quenched sample's volume. Within the "BC" interval, the quenched sample expanded more intensively than the standard sample. It resulted from the second transformation during tempering [167], which is a decomposition of retained austenite (accompanied by increasing steel volume). Starting at ~400 °C, the main contribution to the change in the quenched sample's length was attributed to the third transformation: it was

a complete decomposition of martensite with the cementite precipitation, which led to the most intensive reduction of the sample's specific volume (decreasing the sample length). At temperatures above ~500 °C the curve slightly increased. It was associated with the recrystallization of ferrite, which was also accompanied by a decrease in the specific volume of the quenched sample.

Q & P treatment significantly changed the pattern of dilatometric heating curves which shifted downward relative to the quenched specimen. The volumetric effect's magnitude on the "B′C′" interval (similar to the "BC" interval for quenching) increased sharply. If adopt this effect as a result of γFe → αFe transformation (retained austenite decomposition), one can conclude a sharp increase in the volume fraction of retained austenite in the Q & P-treated sample as compared to the quenched sample. This assumption was later confirmed by XRD analysis which showed that the volume fractions of retained austenite were 15 vol.% and 5 vol.% for Q & P-treated and quenched samples, accordingly. Thus, the magnitude of the "BC" interval is proportional to the amount of retained austenite.

The presence of an increased RA amount in the Q & P-treated sample was confirmed not only by the "B′C′" effect's magnitude but also by the curve's downward in the interval A′B′ which means a more active expansion of the Q & P-sample at temperatures in the range of 100–270 °C. This resulted from (a) a higher amount of RA and (b) a higher value coefficient of thermal expansion for austenite ($\alpha_T = 2.30 \times 10^{-5}$ K^{-1}) as compared to ferrite ($\alpha_T = 1.15 \times 10^{-5}$ K^{-1}) [106]. Thus, the mixture of martensite and austenite in the Q & P-sample expanded during heating more intensively than the ferrite-cementite structure in the reference sample.

A "CD" ("C′D′") interval refers to the third transformation under tempering. As seen, in Q & P-sample "C′D′" interval begins at a higher temperature (430 °C) than in the quenched sample (400 °C). This is explained by higher RA resistance to decomposition due to the enrichment of austenite by carbon during the partitioning stage.

As follows from Fig. 2.14–2.15, the character of dilatometric curves for most Q & P modes is similar to that shown in Fig. 2.13. Since Q & P treatment is aimed at increasing the RA volume fraction, the analysis of the magnitude of the "B′C′" effect depending on the mode parameters was of interest. Under QT=160–240 °C the magnitude of the "B′C′" effect increases first along with the partitioning duration increase (Fig. 2.16, b-d).

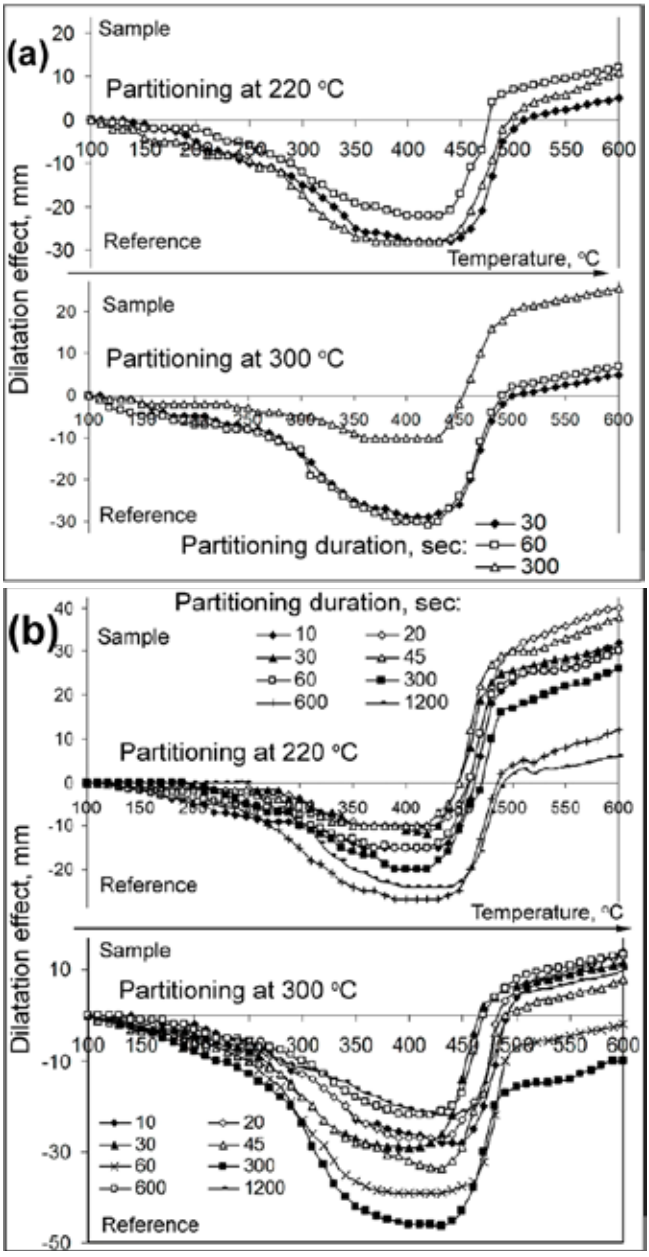

Figure 2.14. Differential dilatometric heating curves of Q&P-treated 60Si2CrV steel: (a) QT=120 °C, (b) 160 °C

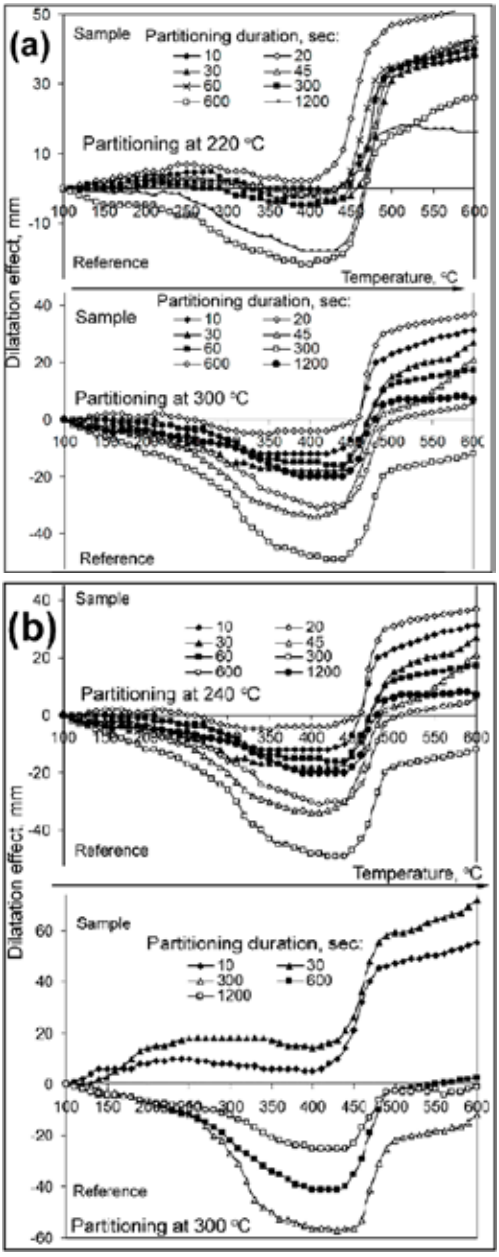

Figure 2.15. Differential dilatometric heating curves of Q & P-treated 60Si2CrV steel: (a) QT= 200 °C, (b) 240 °C

After reaching a maximum, the effect's magnitude decreases with holding prolongation. At the same time, the partitioning holding necessary for maximum effect is in inverse proportion to the partitioning temperature. Under QT=120 °C the picture has the opposite character: the "B′C′" effect value is maximal at initial holdings; as the holding time increases, the effect value decreases or remains unchanged (Fig. 2.16, a).

If assume that the magnitude of the "B′C′" effect is directly proportional to the RA volume fraction, then it becomes apparent that the Q & P parameters significantly influence the amount of retained austenite in 60Si2CrV steel. As follows from Fig. 2.17 at the partitioning temperature of 260 °C and 300 °C, the RA amount increases significantly as a "QT" increases. At the same time, at a lower partitioning temperature (220 °C), the austenite's amount is not affected by the quenching temperature.

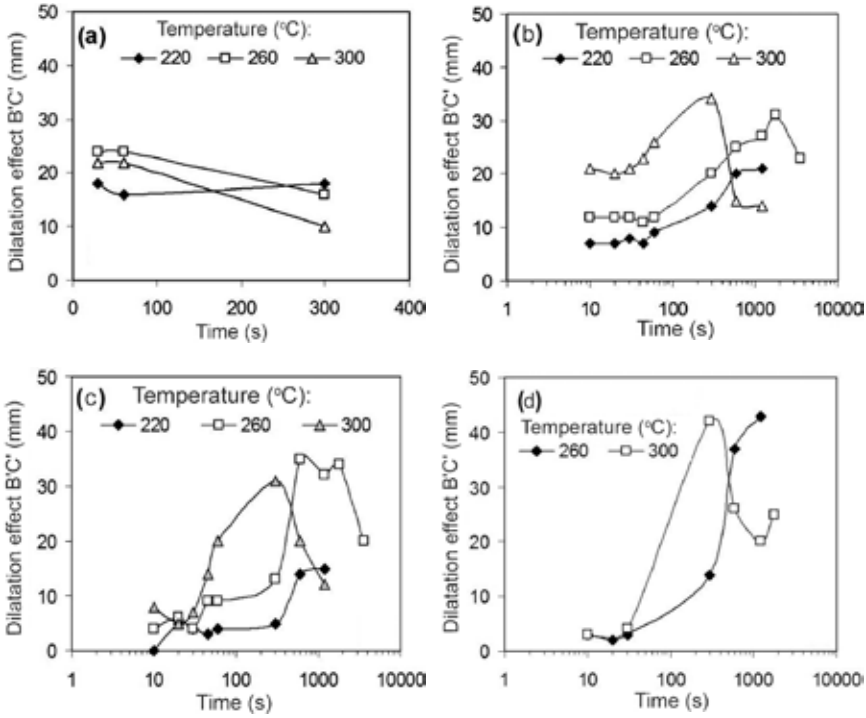

Figure 2.16. The variation of dilatation effect "B′C" magnitude for 60Si2CrV steel, depending on the partitioning duration for different quenching temperatures: (a) 120 °C, (b) 160 °C, (c) 200 °C, (d) 240 °C [166]

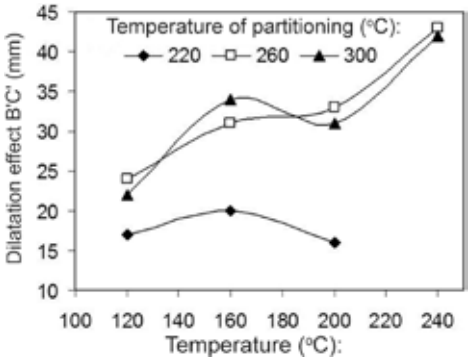

Figure 2.17. Maximum value of the "B′C′" effect depending on quenching temperature [166]

The obtained results can be explained by the action of two factors. First, with a "QT" increasing, the martensite amount decreases and, accordingly, the "basic" proportion of austenite increases, which can be stabilized by carbon partitioning. Second, the partitioning temperature, which determines the diffusivity of carbon atoms and the austenite saturation rate, is important. Obviously, at PT=260–300 °C, the redistribution of carbon proceeded more actively than at 220 °C. In the latter case, carbon diffusion inhibition was the key factor reducing RA amount in the structure. Thus, in order to obtain an increased amount of austenite in 60Si2CrV steel, the "QT" temperature and partitioning temperature should not be less than 160 °C and 260 °C respectively.

When selecting Q & P parameters, it should be taken into account that as the "QT" temperature decreases, the optimum partitioning duration decreases as well. This is due to the increase in the martensite amount that results in an increase in the area of the "Austenite/Martensite" interphase surface through which carbon redistribution occurs. It should also be considered that excessive prolongation of the partitioning stage leads to a decrease in the austenite volume fraction, apparently due to its decomposition with carbide precipitation.

The same study was performed for 55Si3Mn2CrVMoNb steel. The corresponding dilatometric curves are shown in Fig. 2.18. Their profiles are similar (in general) to the profile of the curves for 60Si2CrV steel. A specific feature of 55Si3Mn2CrVMoNb steel was less pronounced upward curve in the "C′D′" interval. This was probably due to increased austenite stability to decomposition during heating, which was caused by higher al-

loying elements content in austenite. More stable austenite was not fully decomposed in the "B′C′" interval, so its further transformation was shifted to the higher temperature region (to the "C′D′" interval), where it was superimposed with the cementite precipitation from martensite. Since these processes have the opposite effect on the specific volume of the sample, the dilatometric effect on the "C′D′" area was lower as compared with 60Si2CrV steel.

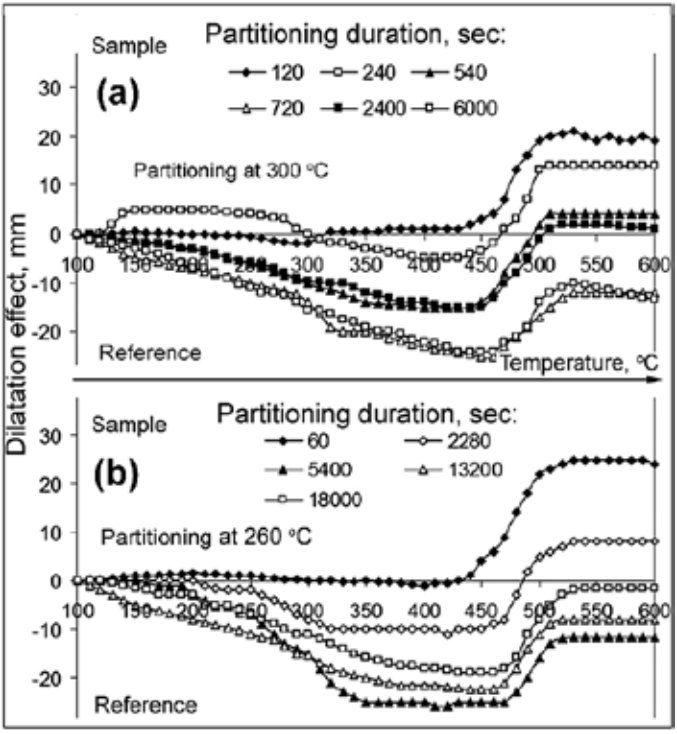

Figure 2.18. Differential dilatometric heating curves of Q&P-treated 55Si3Mn2CrVMoNb steel: (a) QT=160 °C, (b) QT=200 °C

Chapter 3. Effect of Q&P treatment on the microstructure and mechanical properties of 60Si2CrV and 55Si3Mn2CrVMoNb steels

3.1 Microstructure and mechanical properties of 60Si2CrV steel subjected to Q&P treatment

The standard steel of 60Si2CrV grade is intended for high-loaded springs used in different vehicles. According to GOST 14959–79, after quenching and tempering at 470 °C, this steel has the following mechanical properties: YTS ≥ 1470 MPa, UTS ≥ 1670 MPa, TEL ≥ 6%.

The parameters of Q&P treatment for 60Si2CrV steel were selected based on the values of critical points Ac_1, Ac_3, and M_S (presented in Fig. 3.1). The austenitization of the samples was performed at 880 °C for 10 min. After that, the samples were pre-cooled in the air to 700 °C and quenched in a bath of Wood alloy to a quenching temperature (240 °C, 200 °C, 160 °C) with a short (60 s) holding at this temperature. Further, the samples were held in a bath of "Sn-38wt.% Pb" melt at partitioning temperature (270 °C, 300 °C) for 300–3600 s. After partitioning the samples were cooled in calm air. To be short, the regimes of Q&P-treatment were designated as, for example, "$Q_{160°C}/P_{300°C}$ (300 s)", where Q and P are the temperatures of quenching and partitioning, respectively, and partitioning duration is given in the perentheses.

For comparison, the samples were subjected to conventional Q-T treatment: oil-quenching from 880 °C and tempering at 300–600 °C for 1.5 hours. Mechanical properties of steel after Q-T treatment are given in Table. 3.1. After tempering at 300–400 °C steel had a fairly high strength (1844–1861 MPa) with very low ductility and impact toughness. A noticeable increase in ductility occurred only after tempering at 500 °C, when the tensile strength decreased by almost 500 MPa (up to 1349 MPa). The product of strength and elongation (PSE) is used for the estimation of a combination of strength and ductility [106]. PSE values for quenched and tempered 60Si2CrV steel varied from 1.8 GPa · % to 14.5 GPa·%, where high strength corresponded to low PSE values.

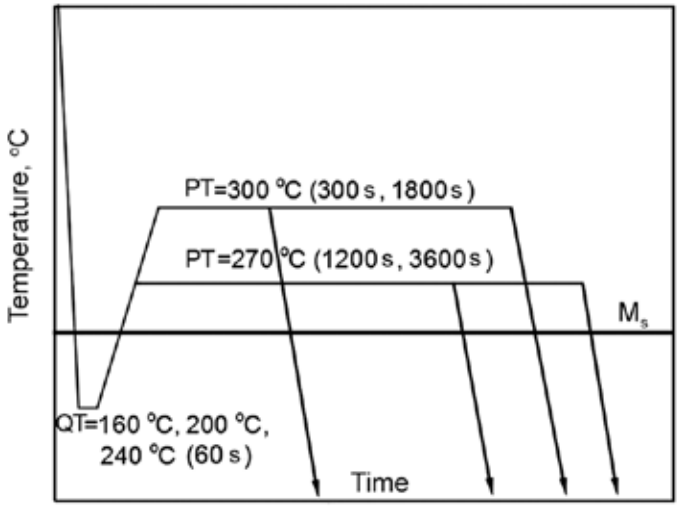

Figure 3.1. Scheme of Q & P treatment modes for 60Si2CrV steel [168]

As follows from Table 3.1 the application of Q & P treatment [168–170] allowed increasing the UTS values to 1980–2060 MPa, i.e. by 6–12% relative to the maximum of Q-T-treated samples. At this strength, the steel performed an increased ductility: total elongation increased to 6% and an area reduction (AR) – to 19%. The impact toughness ($KCU_{+20^\circ C}$) was improved more significantly: from 14 J/cm^2 (quenching and tempering at 300 °C) to 38–67 J/cm^2 (Q & P treatment).

Table 3.1. Mechanical properties, RA amount and carbon content in austenite (C_γ) in 60Si2CrV steel after heat treatment [168]

Quenching (holding) temperature, °C	***YS*, MPa**	***UTS*, MPa**	***TEL*, %**	***(AR)*, %**	***KCU*$_{20}$, J/cm^2**	**Hardness, HRC**	***RA*, %**	***C*$_\gamma$, %**	***PSE*, GPa·%**
1	***2***	***3***	***4***	***5***	***6***	***7***	***8***	***9***	***10***
Quenching and tempering (Q-T)									
300	1861	1861	1,5	0	14	57	6	-	2.8
400	1844	1844	1	0	16	53	0	-	1.8
500	1240	1349	7	26	44	47	0	-	9.4
600	1025	1113	13	48	47	45	0	-	14.5
Q & P treatment (QT=160 °C)									
PT=270 °C(1200s)	1920	1988	2	4	38	53	19	0.95	4.0
PT=270 °C(3600s)	1818	1874	2	4	42	54	17	1.05	3.8

1	*2*	*3*	*4*	*5*	*6*	*7*	*8*	*9*	*10*
PT=300 °C(300s)	1811	2022	5	19	72	53	17	1.00	10.1
PT=300 °C(1800s)	1899	2002	4	16	44	53	11	1.28	8.0
Q&P treatment (QT=200 °C)									
PT=270 °C (1200s)	1855	2086	4	6	52	52	16	1.01	8.3
PT=270 °C (3600s)	1884	2021	3	6	55	53	15	1.16	6.1
PT=300 °C (300 s)	1777	2003	6	19	64	53	17	1.05	12.0
PT=300 °C (1800s)	1963	2048	4	15	67	52	12	1.32	8.2
Q&P treatment (QT=240 °C)									
PT=270 °C (1200s)	1821	2060	3	6	60	52	16	0.79	6.2
PT=270 °C (3600s)	1822	2021	3	6	48	52	12	1.19	6.3
PT=300 °C (300s)	1786	1980	6	8	55	53	15	0.90	11.9
PT=300 °C (1800s)	1799	1990	3	11	56	53	6	1.29	6.0

The best combination of mechanical properties was attributed to Q&P treatment with the parameters $Q_{160°C}/P_{300°C}$ (300s) and $Q_{200°C}/P_{300°C}$ (300––1800 s). These Q&P modes resulted in UTS of 2003–2048 MPa, hardness of 53 HRC, total elongation of 4–6%, area reduction of 13–19%, and impact toughness of 59–67 J/cm^2. Accordingly, the PSE values were in the ranges of 8.2–12.0 GPa·%. The same ductility (TEL of 6%) and PSE (1.9 GPa · %) were characteristic for the $Q_{240°C}/P_{300°C}$ (300 s) mode, but in this case, the tensile strength (1980 MPa) and the toughness (55 J/cm^2) were somewhat lower.

The effect of the Q&P treatment mode on the mechanical properties of 60Si2CrV steel is seen in the data presented in Figure 3.2. The maximum strength (UTS of 2110 MPa) referred to $Q_{160°C}/P_{300°C}$ (300s) mode (Fig. 3.2, a). In the case of PT = 270 °C, the higher strength corresponded to the modes with QT = 200 – 240 °C. There was a general tendency to decrease the tensile strength with increasing the duration of partitioning. At the same time, for some modes, this trend was either absent ($Q_{240°C}/P_{300°C}$) or reversed ($Q_{200°C}/P_{300°C}$). In general, it can be stated that at a partitioning holding up to 2000 s, there was no clearly pronounced dependence of the tensile strength on the Q&P treatment modes, and the distribution of UTS values has a fluctuating character with a deviation within 130 MPa.

The maximum TEL values (5–6%) referred to the partitioning at PT = 300 °C for 300 s (Fig. 3.2, b). As partitioning duration increased, the TEL values decreased to 3–4%. At PT=270 °C, the holding duration did not affect TEL, while the minimum ductility corresponded to QT = 160 °C. The samples treated at PT = 300 °C had a higher (by ~15%) impact toughness as compared with PT = 270 °C (Fig. 3.3, a). The partitioning duration had almost no effect on the impact toughness (except $Q_{160°C}/P_{300°C}$ mode). After Q & P treatment by $Q_{160°C}/P_{300°C}$ (300 s) mode, the impact toughness exceeded 70 J/cm^2.

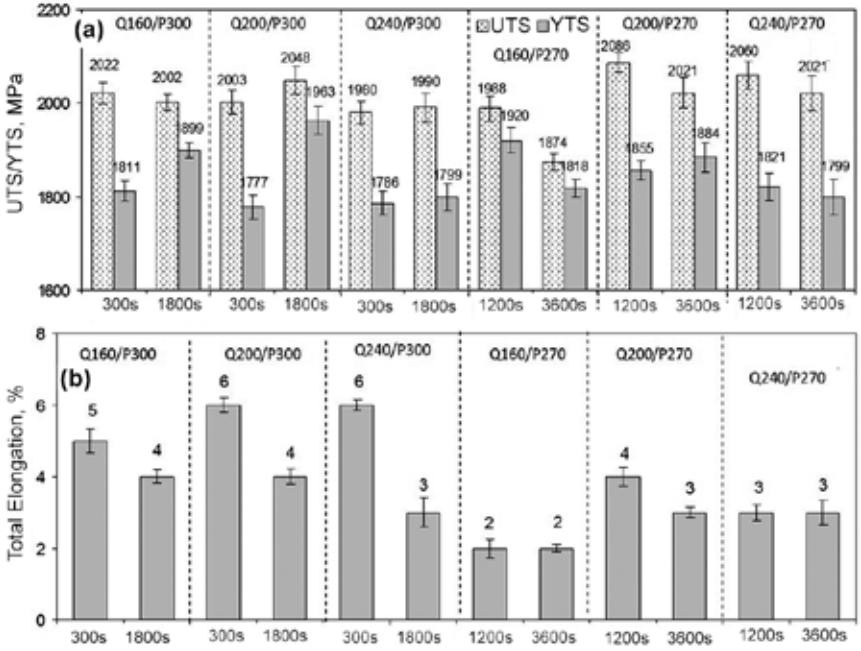

Figure 3.2. Effect of partitioning duration on
(a) UTS/YTS and (b) TEL of 60Si2CrV steel

The results obtained showed that due to Q & P treatment 60Si2CrV steel gained an improved "high-strength/ductility" complex which is characteristic of martensitic Ni-containing steels [171]. The properties improvement was associated with the increased volume fraction of retained austenite in the structure [3, 43, 172]. To confirm this, XRD studies of Q & P-treated samples were performed (Figs 3.4 and 3.5, Table 3.1).

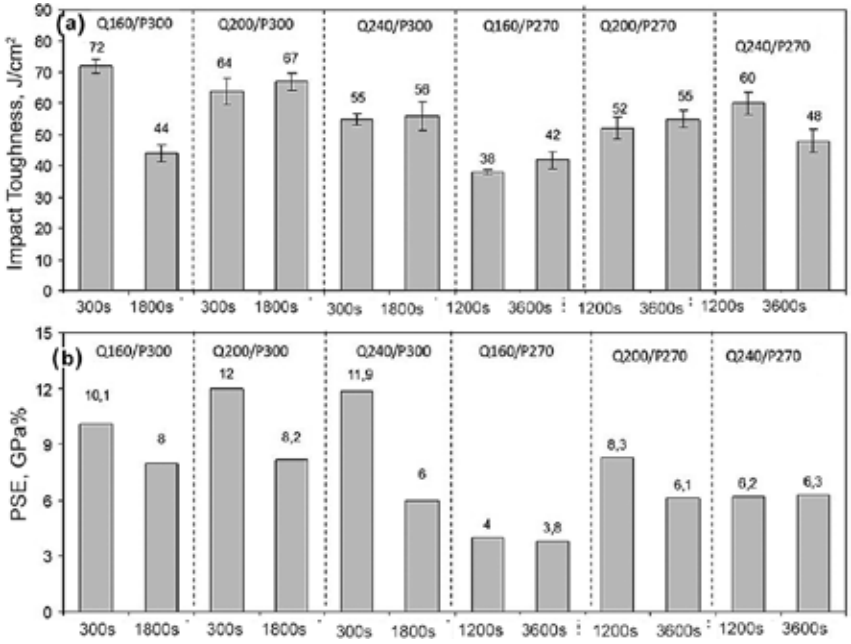

Figure 3.3. Effect of partitioning duration on (a) impact toughness and (b) PSE of 60Si2CrV steel

The XRD pattern of the sample, subjected to quenching and tempering at 300 °C, presented only one weak peak (200)γ of austenite, indicating a low austenite amount in the structure (6 vol.%). In contrast, diffraction patterns of samples Q & P-treated at QT = 160 °C and 200 °C clearly showed a full set of austenite peaks lying in the range $2\theta = 40 - 110$ degrees: (111)γ, (200)γ, (220)γ, and (311)γ. This displayed an increased volume fraction of retained austenite which was 16–19 vol.% (Table 3.1) which is 3 times as compared with the Q-T regime. Increasing the QT temperature from 160 °C to 240 °C led to a small decrease in RA amount (to 13–16 vol.%). As follows from Fig. 3.5, the maximum amount of retained austenite is referred to QT = 160 – 200 °C with short partitioning holding; with increasing holding duration, the RA volume fraction decreased. An increase in RA volume fraction resulted from the enrichment of austenite with carbon at the partitioning stage. As the duration of partitioning increased, the carbon content in austenite increased as well. The highest carbon content (1.30–1.35 wt.%) corresponded to Q & P treatment with higher partitioning temperature (PT = 300 °C). In the case of QT = 240 °C (which is close to

M_S point) the carbon content in RA reduced noticeably for any partitioning temperature.

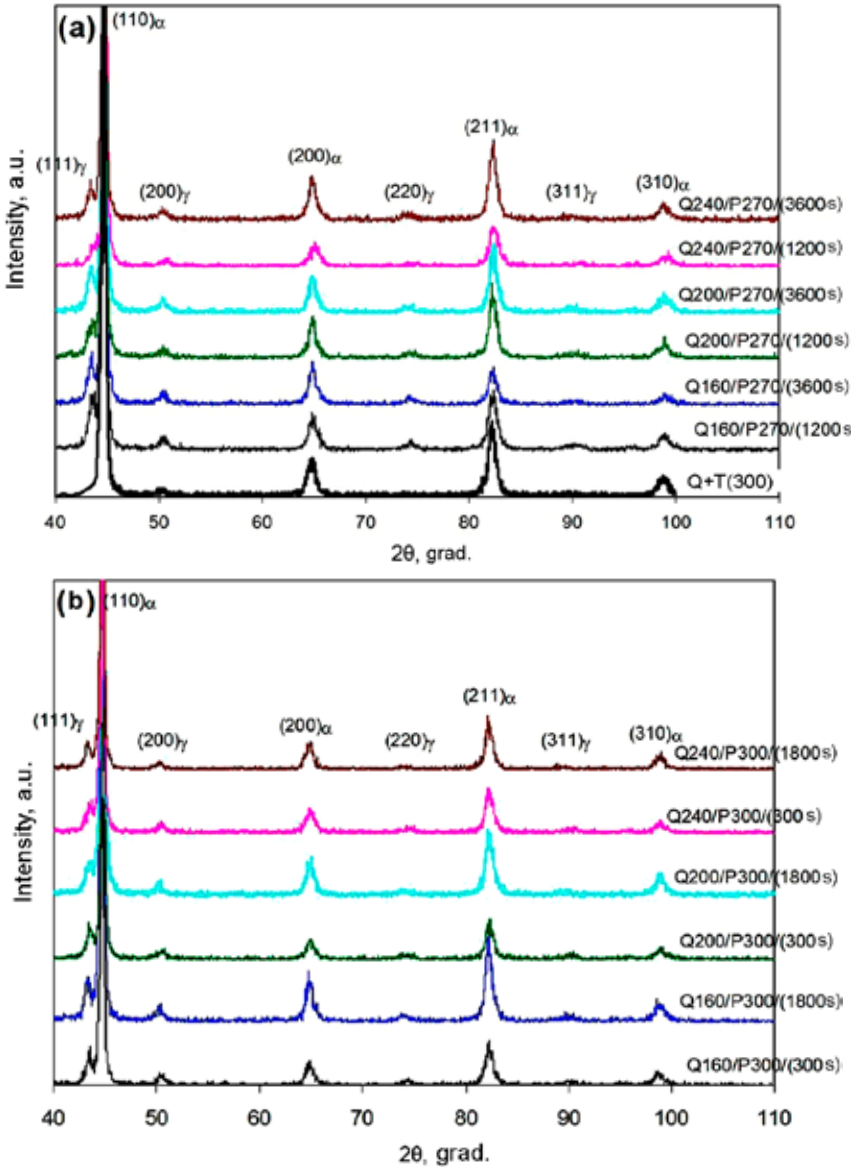

Figure 3.4. XRD patterns of 60Si2CrV steel subjected to Q & P treatment: (a) PT = 270 °C, (b) PT = 300 °C [168]

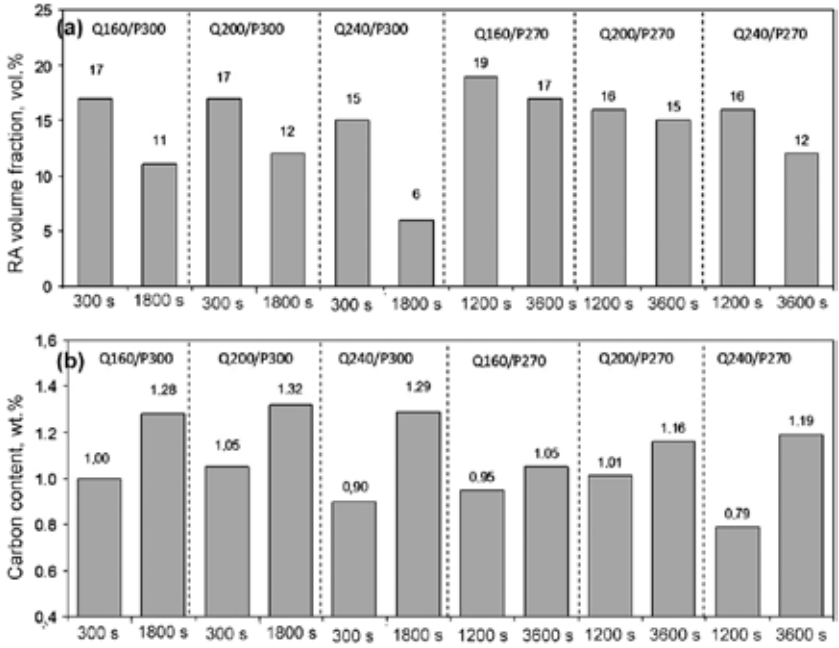

Figure 3.5. Effect of partitioning holding on (a) RA volume fraction and (b) carbon content in austenite in Q & P-treated 60Si2CrV steel

After quenching and tempering at 300 °C 60Si2CrV steel had a microstructure of tempered martensite (Fig. 3.5, a) with granular particles of vanadium carbide up to 1 μm in diameter (Fig. 3.5, b). The microstructure of Q & P treated samples consisted of martensite, occasional areas of bainite and retained austenite (shown by the arrows in Fig. 3.5, c). The structure also included granular VC precipitates (Fig. 3.5, g).

The fine structure of the samples was studied using TEM. In areas of bainite, parallel laths of bainite ferrite with a thickness of 100 to 470 nm were revealed; they alternate with austenite film-like interlayers with a thickness of 20 to 70 nm (Fig. 3.7a). The structure also contains martensite, which has a higher dislocation density than bainite [173, 174] (Fig. 3.8b). The presence of austenite was confirmed by dark-field images of the structure made in reflections of the γ-phase (Fig. 3.7 c) and the selected area electron diffraction (SAED) analysis (Fig. 3.7 d).

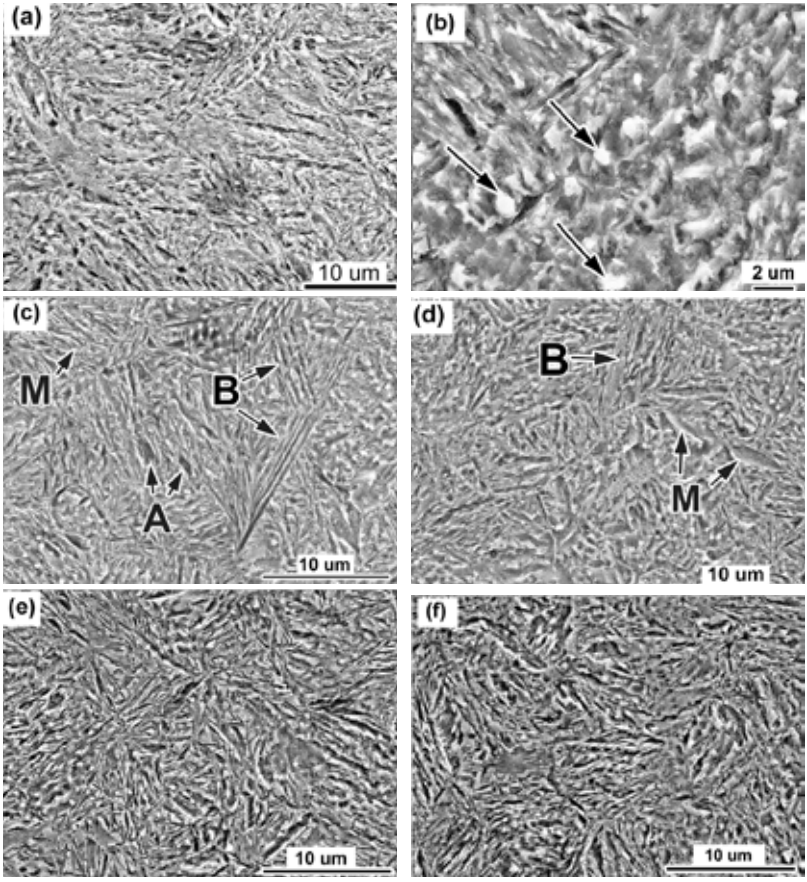

Figure 3.6. Microstructure of 60Si2CrV steel after: (a, b) Q+T300, (c) $Q_{160^{\circ}C}/P_{300^{\circ}C}$ (300 s), (d) $Q_{160^{\circ}C}/P_{270^{\circ}C}$ (1200 s), (e) $Q_{240^{\circ}C}/P_{300^{\circ}C}$ (300 s), (f) $Q_{240^{\circ}C}/P_{270^{\circ}C}$ (1200 s) [168]

A distinctive feature of the fine structure of Q & P samples was the absence of cementite carbides. At the same time, transitional carbides were found within the martensite laths (shown by arrows in Fig. 3.7, e), precipitated from martensite at the partitioning stage. The precipitation of intermediate (ε) carbides in steels with a high silicon content during Q & P treatment was repeatedly described in previous works [58, 60]. The results obtained confirm the data of Speer et al. [74] that silicon suppresses only cementite, exerting a weak inhibitory effect on the formation of ε-carbide.

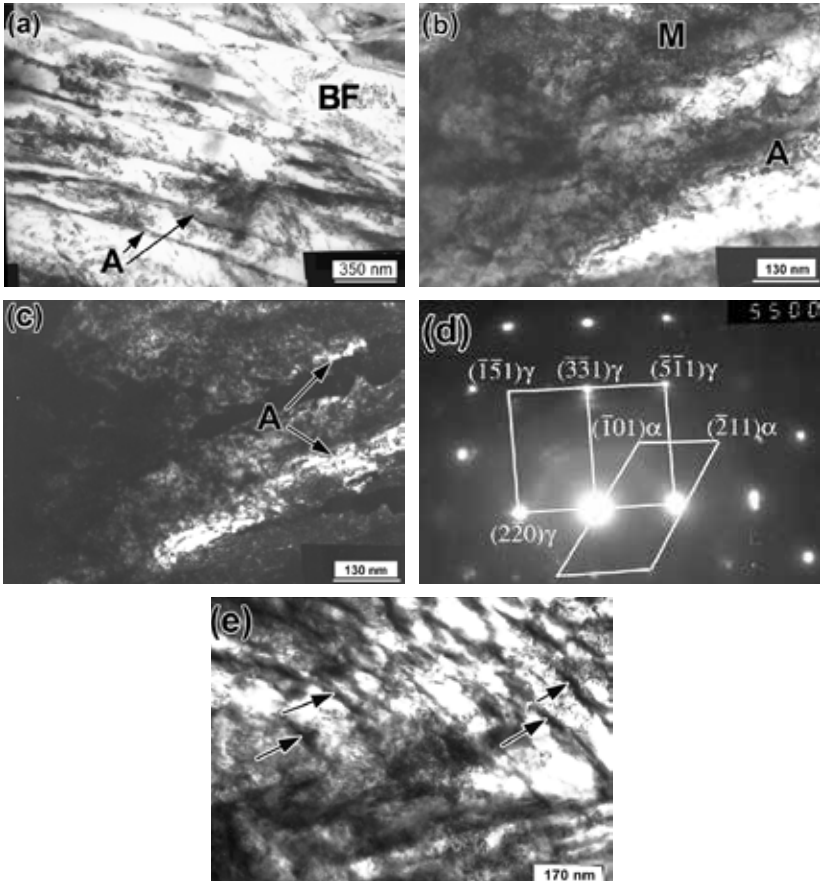

Figure 3.7. TEM images of the microstructure of 60Si2CrV steel after Q-n-P treatment according to the $Q_{160^{\circ}C}/P_{300^{\circ}C}$ (300 s) mode: (a) bainitic ferrite (BF) and austenite interlayers (A), (b) martensite (M) and austenite (bright-field), (c) dark-field image of (b) in austenite reflection, (d) SAED from (b), (e) transitional carbides within ferrite lath [168]

The increase in the austenite amount (resulted from Q & P treatment) led to a change in the mechanism of sample fracture under the dynamic load (Fig. 3.8). The fractured surface of steel subjected to quenching and tempering at 300 °C was characterized by the large facets oriented along the cleavage planes (shown by the arrows in Fig. 3.8, a), which alternated with of the quasi-cleavage rupture and the dimple areas. In Q & P-treated speci-

mens, the cleavage area was reduced (Fig. 3.8, b), while the fracture surface was mostly formed by the quasi-cleavage areas with rough relief (Fig. 3.8, c), as well as the ductile zones of the dimples tearing-off (Fig. 3.8, d). The dimples arose from the micropores' coalescence initiated by dispersed inclusions of vanadium carbides (shown by arrows in Fig. 3.8, d). Thus, the fracture pattern indicated a more energy-consuming mechanism for the Q & P specimens' rapture, consistent with a significant increase in the impact toughness as compared to Q+T heat treatment.

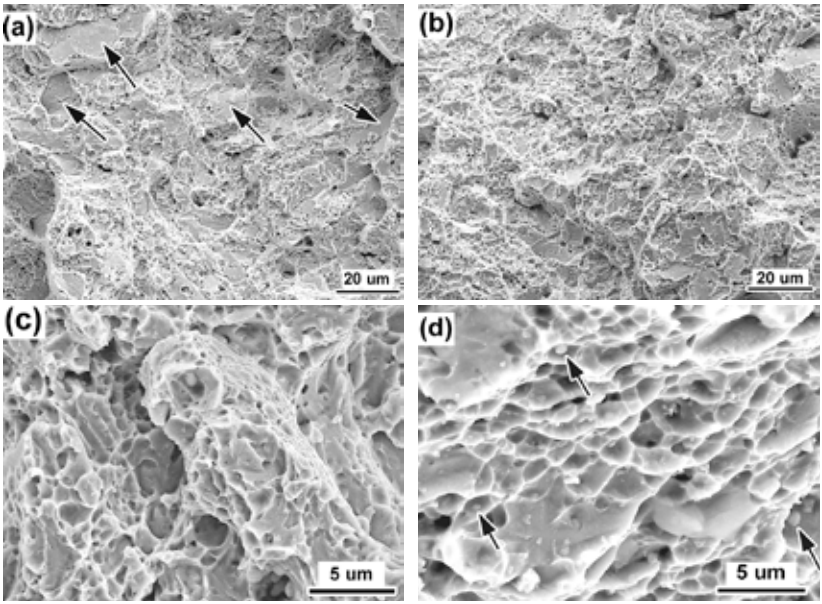

Figure 3.8. The fractured surface of Charpy samples after: (a) Q+ + T(300 °C); (b-c) Q & P treatment ($Q_{160°C}/P_{300°C}$ (300 s)), (d) Q & P treatment ($Q_{160°C}/P_{300°C}$ (300 s)) [168]

The mechanism of microstructure formation at the "Partitioning" stage is a key to understanding the processes occurring under Q & P treatment. In this sense, two scenarios are possible. According to one of them, carbon partitions from martensite to austenite, and in the second scenario, a bainitic transformation is imposed on this process, which reduces the austenite amount. Most authors favor the second scenario [116]. The carbon enrichment of retained austenite (and the increase in RA volume fraction) during Q & P treatment might be the result of bainite transformation which is accompanied by the rejecting carbon from the bainitic α-phase to

remaining austenite [175]. This is especially true for steels with high silicon content, which prevents the cementite precipitation from austenite, contributing to the carbide-free bainite formation with high retained austenite content [71]. Since carbide-free bainite has a high mechanical properties level [61, 176, 177], its presence in the Q & P-treated steel is preferable.

We suppose that in 60Si2CrV steel, the second scenario of structure formation under Q & P treatment occurred. As shown in Chapter 2, the martensite formation at the quenching stage dramatically accelerates bainitic transformation. As follows from Fig. 2.10, b, quenching (pre-cooling) to 160 °C reduces the incubation period at 300 °C from 26 s to 3 s. In the case of quenching to 160 °C, bainite transformation was completed at 300 °C and 270 °C within 300 s and 700 s, respectively, and in the case of quenching to 200 °C – within 820 s and 300 s, respectively. A comparison of these data with the Q & P treatment schedule (Fig. 3.1) showed that for all Q & P regimes, the duration of the partitioning stage exceeded the duration of bainitic transformation until its completion, thus the transformation contributed to the final structure of 60Si2CrV steel.

The volume fraction of formed bainite was obviously minor. This was due to: (a) the transformation of a major part of austenite into martensite at the quenching stage and (b) the inhibition of bainitic transformation because of austenite enrichment with carbon with partitioned to γ-phase from martensite. The analysis of kinetic of bainite transformation at 300 °C (Fig. 2.10, b) showed that, in the athermic martensite presence, the increment of α-phase is very small as compared to the transformation without pre-cooling below the M_S point. Thus, one can assume that bainite was minor present in the structure of Q & P-treated 60Si2CrV steel (it was difficult to distinguish it due to the similarity in morphologies of lower bainite and martensite).

Considering the complexity of the Q & P process, the carbon accumulation in austenite in different parts of the structure probably occurred by different mechanisms (Fig. 3.9). Leaving the martensite lattice, carbon enriches the austenite layer adjacent to the martensitic crystal. This layer is very thin (within 5 nm [116]) due to the reduced (relative to α-phase) carbon diffusivity in austenite: carbon did not have enough time to move into austenite deeply thus accumulating at the interphase boundary. Carbon-rich austenite layer was extensively deformed by martensite, that is, it acquired an increased dislocation density on which the bainite α-phase embryos might appear. However, the saturation of this austenite with carbon prevents the rapid progress of bainitic transformation. The zone of

plastic deformation extended beyond the saturated austenitic layer. At some distance from the martensitic crystal, where the carbon content was decreased, bainite transformation began. It was accompanied by carbon redistribution with alternation of enriched and depleted austenite areas. The depleted areas transformed into α-phase laths, and the enriched ones remained as austenite film layers or austenite "islands". The precipitation of carbides from bainitic austenite was prevented due to the high content of silicon in steel. As partitioning temperature decreased, the width of the enriched zone around martensite decreased as well. This resulted in a decrease in the thickness of austenitic layers in bainite because of limitations in carbon atoms' diffusion mobility.

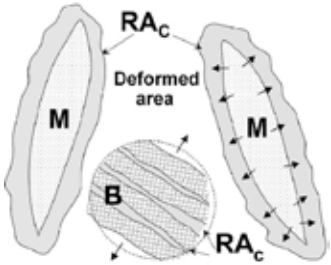

Figure 3.9. Scheme of formation of C-enriched austenite (RA_c) during the partitioning stage [168]

The Q&P modes with QT=160 °C and QT=200 °C provided a similar RA amounts. In contrast, raising the QT temperature to 240 °C led to a decrease in RA volume fraction. This was due to the difference in amount of martensite formed during the quenching stage. The calculation by the Koistinen-Marburger equation showed that the martensite amount at QT = 240 °C, 200 °C and 160 °C was 18 vol.%, 50 vol.% and 69 vol.%, respectively. Thus, a relatively small martensite volume fraction occurred during cooling to 240 °C, which was apparently not sufficient to create a long interfacial martensite/austenite boundary through which carbon could redistribute at the partitioning stage. Therefore, when selecting the Q&P treatment mode, it is necessary to focus on obtaining 50–70 vol.% of martensite before partitioning stage. In this case, a triplex structure (tempered martensite, carbide-free bainite, and retained austenite) can be formed by Q&P treatment ensuring improved mechanical properties. An increase of martensite fraction by more than 70 vol.% leads to a sharp decrease in the bainite fraction in favor of martensite, with a corresponding decrease in ductility and impact toughness of steel.

As follows from Fig. 3.5, an increase in partitioning duration reduces RA volume fraction affecting in some cases the steel's strength and ductility. Since long partitioning holdings goes beyond the bainitic transformation completion (Fig. 2.1), the decrease in the retained austenite fraction was caused by the processes occurring precisely in carbon-stabilized austenite areas. Carbon saturation increased the austenite's free chemical energy, so presumably, this austenite was prone to decompose under prolonged holding. The most active decomposition took place at an elevated partitioning temperature (300 °C) due to an increased diffusivity of carbon atoms. The partitioning duration should be selected in such a way as to achieve complete or permanent suspension of the bainitic transformation at a given temperature. In the case of short holdings, part of the austenite can transform into "fresh" martensite at the final stage of treatment leading to an increase in steel brittleness. On the other hand, very long holdings can cause the decomposition of C-rich austenite with the cementite formation, which will also lead to a decrease in mechanical properties.

The presented results show that Q & P treatment effectively enhances the mechanical properties of medium carbon low-alloy steel, allowing a high strength state (UTS ≥ 2000 MPa, hardness ≥ 50 HRC) while maintaining the ductility and impact toughness at a higher level. For 60Si2CrV steel, Q & P treatment should be done with quenching cooling to 160–200 °C with subsequent holding at 300 °C for 300–1800 s (at QT= =160 °C, the partitioning duration should not exceed 300 s). This provides the heterogeneous multiphase structure consisting of tempering martensite, carbide-free lower bainite (or nanobainite), and retained austenite with an increased proportion of the latter (17–19 vol.%).

3.2 Effect of low tempering on the microstructure and mechanical properties of Q & P-treated 60Si2CrV steel

Quenching-Partitioning-Tempering (Q & P+T) is one of the modifications of Q & P treatment [137]. Its peculiarity is the additional tempering at 400 °C or prolonged holding at this temperature at the partitioning stage. Q & P-T treatment is recommended for steels microalloyed with strong carbide-forming elements (V, Ti, Nb), considering that it increases the steel's strength due to the dispersion hardening mechanism [109]. At the same time, the effect of tempering lower temperatures (≤ 300 °C) on the properties of Q & P-treated steels remained mostly unexplored [178]. Such

tempering can be useful in terms of stress relaxation that appear during the final cooling stage of Q&P treatment due to the austenite partial transformation to "fresh" martensite. This is especially true for medium- and high-carbon steels, since martensite in these steels has a tetragonal lattice, which causes significant volumetric changes leading to high residual quenching stresses. At the same time, low tempering can cause the decomposition of retained austenite, which may adversely affect the mechanical properties of Q&P-treated steel. In order to clarify these issues, the effect of 200–300 °C tempering on the phase-structural state and mechanical properties of Q&P-treated 60Si2CrV steel was investigated. The samples of 60Si2CrV steel were subjected to Q&P treatment by the regime: QT= = 160 °C, partitioning at 300 °C for 300 s. After Q&P treatment, the samples were tempered at 200 °C, 250 °C and 300 °C for 90 min; after the tempering the samples were cooled in the calm air.

The SEM (Fig. 3.10) and TEM (Fig. 3.11) observations revealed no visible changes in the microstructure after tempering compared to Q&P treatment. The samples tempered at 200 °C and 250 °C structure contained retained austenite of "film" and "island" morphology, with dispersed transitional carbides seen within the α-phase's laths (Fig. 3.11, a-c). Cementite carbides were absent in the structure. In the samples tempered at 300 °C, cementite carbides were revealed within RA areas, which was confirmed by characteristic reflexes of Fe_3C carbide on SAED pattern (Fig. 3.11, d).

XRD patterns of the samples presented the diffraction maxima of the α-phase and γ-phase; the maxima for carbide were not found. According to the intensity of lines $(110)_a$, $(200)_a$ and $(211)_a$, α-phase was major in the structure. At the same time, the XRD pattern of the Q&P-treated sample clearly showed austenite $(111)_\gamma$, $(200)_\gamma$, $(220)_\gamma$, $(222)_\gamma$ indicating an increased RA volume fraction (17 vol.%) (Fig. 3.12). The same RA amount was present in the sample tempered at 200 °C (17 vol.%). Increasing the tempering temperature caused the decrease of austenite amount to 14 vol.% at 250 °C and to 10 vol.% at 300 °C. The decrease in RA volume fraction was accompanied by the gradual increase in carbon content in retained austenite: from 1.11 wt.% in after Q&P treatment to 1.32 wt.% after tempering at 250 °C and 1.42 wt.% after the tempering at 300 °C. As seen from the results, the carbon partitioning continued during tempering, which led to an additional austenite C-enrichment as compared to to Q&P treatment.

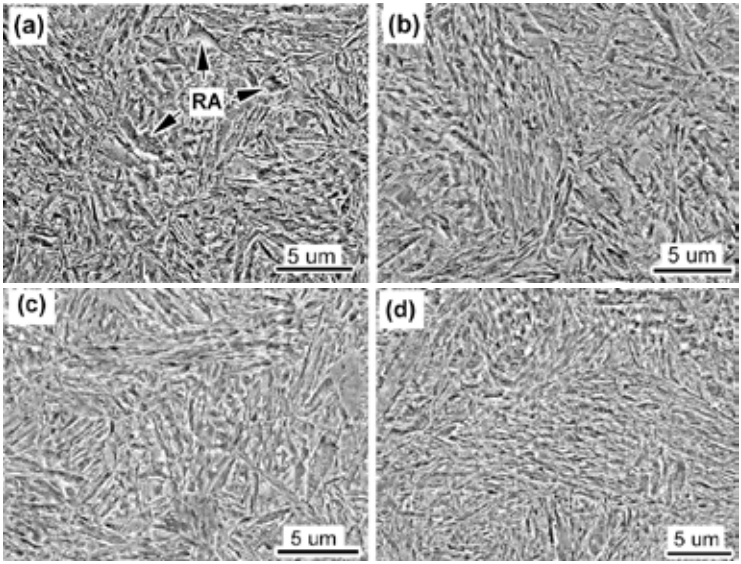

Figure 3.10. Microstructure of Q & P-treated 60Si2CrV steel (a) without tempering, (b) with tempering at 200 °C, (c) 250 °C, (d) 300 °C

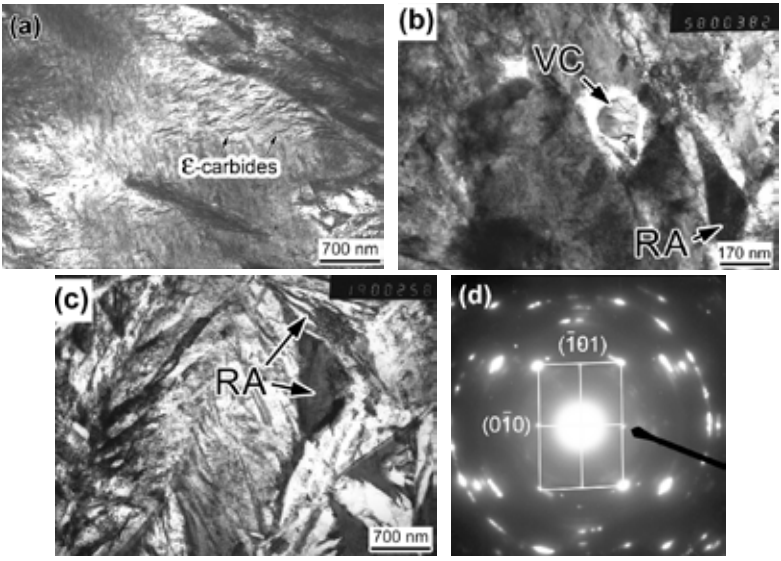

Figure 3.11. TEM images of Q & P-samples after tempering at (a) 200 °C, (b, c) 250 °C. TEM images of Q & P+T(300 °C) sample: (d) SAED pattern from the cementite zone [101]

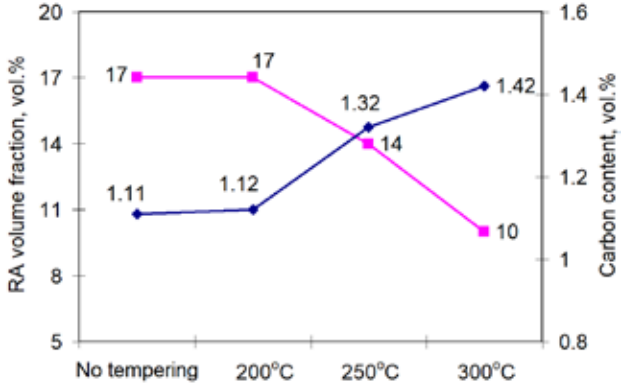

Figure 3.12. Volume fraction of retained austenite and carbon content in RA in 60Si2CrV steel depending on heat treatment mode

As follows from Fig. 3.13, tempering at 200–250 °C after Q & P caused a slight increase in UTS (from 2022 to 2065 MPa) and a 1.5–2-fold increase in ductility (TEL up to 6–8%, area reduction (AR) up to 22%) and a maximum impact toughness (62–63 J/cm^2). Tempering at a higher temperature (300 °C) further increased ductility (TEL is 9%, AR is 24%), but caused a 30% decrease in impact toughness (48 J/cm^2). With tempering temperature increase the PSE value gradually increased (to 18 GPa·%), reaching a 125% increment relative to Q+300 °C treatment. It should be also noted that in all the experimental modes (Q & P/Q & P+T), which resulted in a sharp increase in ductility and impact toughness, the hardness remained at a fairly high level (~52 HRC), indicating that an improved complex of mechanical properties was obtained in steel.

Figure 3.14 illustrates the fracture pattern of Q & P-treated Charpy samples. It is seen that after tempering at 200–250 °C the fracture was predominantly ductile with the dimples pattern (Fig. 3.14, c). With the tempering temperature was 300 °C an increase in cleavage/quasi-cleavage areas was observed while dimples areas decreased. This observation complies with the decrease in impact toughness after 300 °C tempering. Concluding, tempering at 200–250 °C was beneficial for 60Si2CrV steel since it allowed to maintain the ductile fracture characteristic for Q & P treatment.

The results presented above indicated the positive effect of low-temperature tempering on the mechanical properties of medium carbon steel subjected to Q & P treatment. The main factor was the tempering of "fresh" martensite formed during the final stage of Q & P treatment. The

tempering occurred both through the ε-carbides precipitation and carbon partitioning from "fresh" martensite to retained austenite. This reduced the lattice distortion of α-phase facilitating the microstrain process in front of the micro-crack tip thus inhibiting the crack growth.

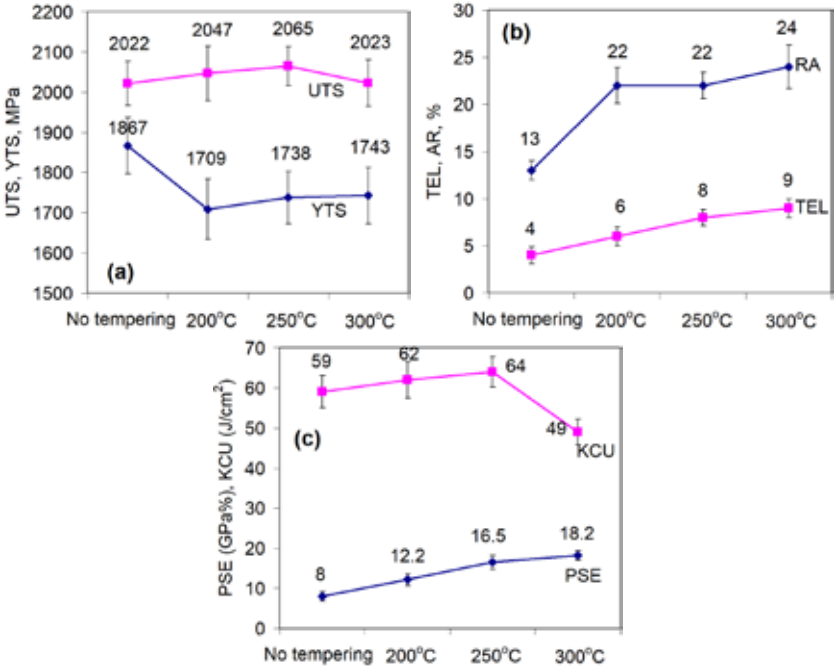

Figure 3.13. The mechanical properties of 60Si2CrV steel depending on the heat treatment mode: (a) strength (YTS, UTS), (b) ductility (TEL, AR), (c) impact toughness, PSE

The XRD analysis (Fig. 3.12) allowed suggesting that during tempering the following processes occurred in Q & P-treated 60Si2CrV steel: (a) relief of residual stress caused by the "fresh" martensite formation, (b) carbon partitioning from "fresh" martensite to retained austenite, (c) precipitation of ε-carbides within "fresh" martensite, (d) the transformation of retained austenite (occurred at 250–300 °C). Processes "b" and "c" led to austenite C-enrichment. As the tempering temperature increased the carbon content in austenite increased continuously reaching 1.42 wt.% after tempering at 300 °C. The explanation is that during tempering, the decomposition occurred in the low-carbon austenite areas whereas the carbon-rich areas remained in the structure. Carbon enrichment ensured increased austen-

ite stability for SIMT. This is indirectly confirmed by the increase in area reduction, i.e. by thin "neck" formation; this was ascribed to the absence of a "running neck" characteristic to the TRIP effect [179].

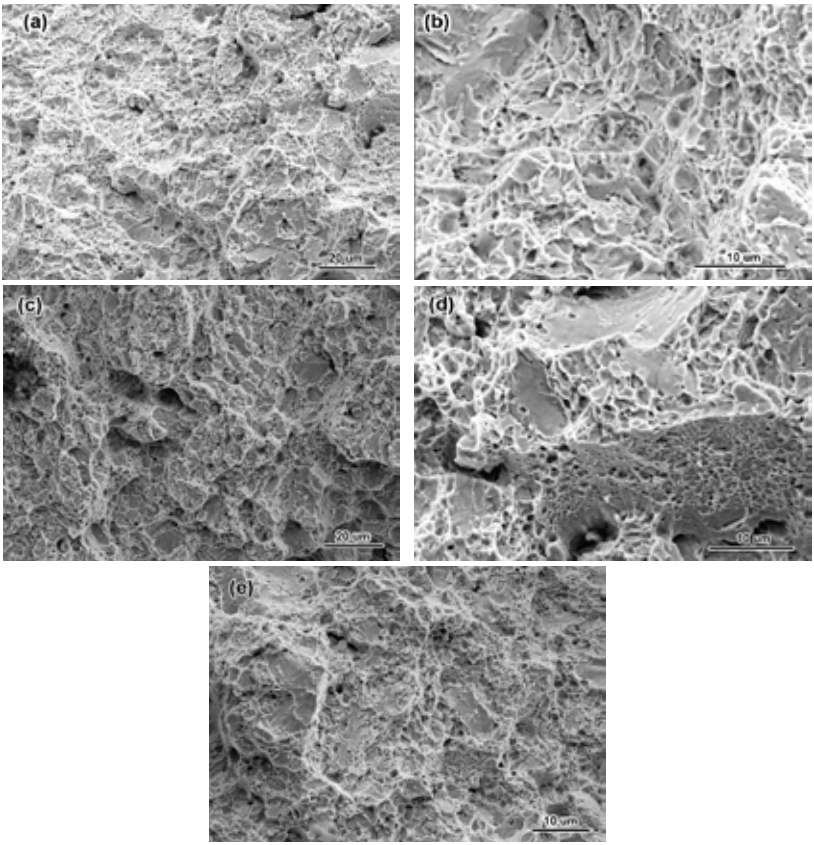

Fig. 3.14. The rupture surface of the Charpy specimens:
(a, b) Q&T, (c, d) Q&T+270 °C, (e) Q&T+300 °C

Austenite's transformation at 250 °C proceeded through carbide-free bainite formation, which is confirmed by TEM observation and higher impact toughness. In this case, the decrease in RA volume fraction was compensated by the formation of carbide-free bainite, which possessed improved impact toughness. Tempering at 300 °C caused a significant (by 30%) decrease in impact toughness caused by precipitation of cementite carbides revealed by TEM studies. Silicon in the amount of ~1.5% was not able to prevent the cementite appearance due to sharply increased

carbon diffusivity at 300 °C, which changed the balance between the chemical free energy and elastic free energy. As a result, carbon partially left the austenite lattice to form cementite which reduced the stresses in the austenite lattice associated with the carbon solution effect.

The results above allowed concluding that low-temperature tempering is a useful technological complement in Q & P treatment of medium carbon steels. Obtaining an improved "Strength/Ductility/Impact toughness" complex in the Q & P-treated 60Si2CrV steel can be ensured by tempering at 200–250 °C. Regarding the PSE parameter, it is more desirable to conduct tempering at 300 °C because of the increase in ductility while maintaining high strength. The optimum tempering temperature for specific Q & P-treated steel grades should be determined additionally.

3.3 Effect of heat treatment modes on microstructure and mechanical properties of 55Si3Mn2CrVMoNb steel

3.3.1 (Q+T)-treatment and austempering

The effect of Q & P treatment on the mechanical properties of 55Si3Mn2CrVMoNb steel was evaluated in comparison with standard heat treatments which are (a) quenching and tempering, and (b) austempering for lower bainite structure [180, 181]). The austenitization temperature was 900 °C that corresponded to the single-phase (γ) domain. The austenitized samples were oil-quenched to room temperature. The tempering was carried out at 200–600 °C with a holding duration of 1.5 hours. During austempering, the austenitized samples were held in the bath of Wood alloy at the constant temperature (300 °C, 270 °C, 250 °C) for 5 min with further transfer to a laboratory furnace heated to the same temperature for prolonged holding from 45 min to 600 min. The holding duration was selected by taking into account the transformation kinetics at a given temperature (Chapter 2). After holding, the samples were cooled in calm air. As follows from Table 3.2, the tensile strength of steel after (Q+T) treatment varied from 2144 MPa (200 °C) to 1605 MPa (600 °C) while TEL and impact toughness remained low: after tempering at 600 °C they did not exceed 6.5% and 45 J/cm^2, respectively. PSE was also low, its values reached the maximum (10.2 GPa·%) after tempering at 600 °C.

Austempering has provided a significant increase in the mechanical properties complex compared to quenching with tempering. A combina-

tion of high strength (UTS = 1397–1733 MPa) with competitive elongation (10–21%) and impact toughness (105–139 J/cm^2) was achieved. Accordingly, the PSE increased sharply, reaching 15.1–28.8 GPa · %.

The highest complex of the properties for this steel was provided by austempering at 300 °C for 45–120 min. In this case, the steel had a tensile strength of 1397–1522 MPa, hardness of 45–47 HRC, TEL of 18–21%, impact toughness of 105–116 J/cm^2, while PSE reached maximum values of 27.5–28.8 GPa · %. The tensile curves of austempered specimens corresponded to the ductile materials with a long interval of a plastic flow above the yield point (Fig. 3.15). As the austempering temperature decreased, the length of this interval decreased.

Table 3.2. Mechanical properties, RA amount and carbon content in austenite (C_γ) in 55Si3Mn2CrVMoNb steel after Q+T and austempering (H means Rockwell hardness)

Tempering (austempering) temperature, °C	YTS, MPa	UTS, MPa	TEL %	AR, %	KCU, J/cm^2	H, HRC	RA,%	C_γ,%	PSE, GPa·%
Quenching and tempering									
200 °C	2140	2144	1	2	–	–	–	–	2.1
300 °C	2105	2116	3	2	29	54	–	–	6.3
400 °C	1895	1895	3	33	38	53	–	–	6.1
500 °C	1617	1617	3.5	14	32	47	–	–	5.6
600 °C	1573	1605	6.5	31	45	44	–	–	10.2
Austempering at 300 °C									
300 °C (45 min)	1210	1522	18	35	105	47	33	0.94	27.5
300 °C (120 min)	1162	1397	21	34	116	45	–	–	28.8
300 °C (240 min)	1171	1397	12	38	139	43	31	1.08	16.9
Austempering at 270 °C									
270 °C (160 min)	1353	1585	10	30	126	50	19	1.04	15.1
270 °C (240 min)	1337	1542	12	39	133	49	–	–	18.4
270 °C (300 min)	1447	1604	11	39	136	49	19	1.06	17.5
Austempering at 250 °C									
250 °C (400 min)	1496	1697	12	32	107	52	17	0.94	20.9
250 °C (600 min)	1418	1733	10	30	114	48	–	–	1700

Maximum strength (UTS=1733 MPa, YTS=1697 MPa) was reached after holding at 250 °C for 600 min. There was a clear tendency of strength to decrease as the holding temperature.

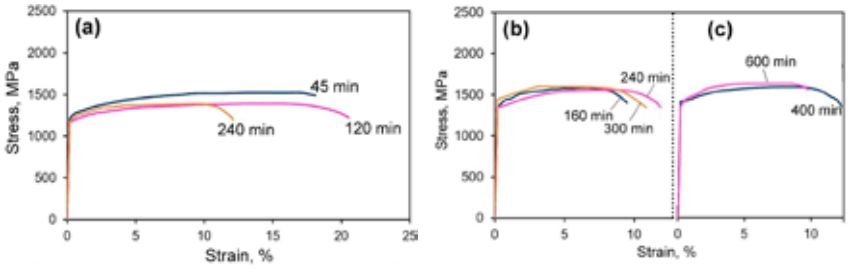

Figure 3.15. Tensile curves of 55Si3Mn2CrVMoNb steel samples after austempering at (a) 300 °C, (b) 270 °C, (c) 250 °C.

Maximum ductility (18–21%) referred to austempering at 300 °C for 120 min. Under austempering at 300 °C and 270 °C the TEL values varied by a curve with a maximum. The increase in TEL at the initial holding stages was due to a decrease in "fresh" martensite (appeared after the austempering completion) as the bainitic transformation progressed. The decrease in TEL at the prolonged holding stages resulted from a decrease in RA volume fraction. As for austempering at 250 °C, the minimum holding time at this temperature (400 min) corresponded to the completion of bainite transformation at this temperature. Therefore, there was only a slight decrease in ductility when the holding time approached 600 min.

The PSE level reached its maximum (27.6–28.8 GPa · %) after holding at 300 °C for 45–160 min. The samples austempered at 270 °C and 250 °C performed a lower PSE level due to reduced ductility.

The maximum hardness value (52 HRC) was referred to holding at 250 °C for 400 min. As the holding time increased to 600 min, the hardness decreased to 48 HRC due to carbide precipitation from the bainitic α-phase with a corresponding decrease in the crystal lattice distortion. The tendency of hardness decreasing at holding time was characteristic of higher holding temperatures; here it was explained by the decrease in the "fresh" martensite fraction in favor of bainite. The minimum hardness level (43 HRC) corresponded to austempering at 300 °C for 240 min.

In contrast to hardness, impact toughness gradually increased with holding duration increase; this was the case for any holding temperature. This behavior was related to the increase in the bainite volume fraction. A rather high impact toughness (≥100 J/cm^2) was characteristic for all performed austempering modes. Holding at 270–300 °C gives a higher toughness level compared to holding at 250 °C.

The microstructure of austempered samples is presented in Figure 3.16. Holding at 300 °C for 240 min led to the structure consisting of bainite packages with a parallel α-phase laths combined with a large number of RA areas evenly distributed throughout the structure (Fig. 3.16, a). By reducing the holding temperature to 250 °C, a decrease in the bainitic plates' thickness was observed to be in agreement with [61] (Fig. 3.16, c).

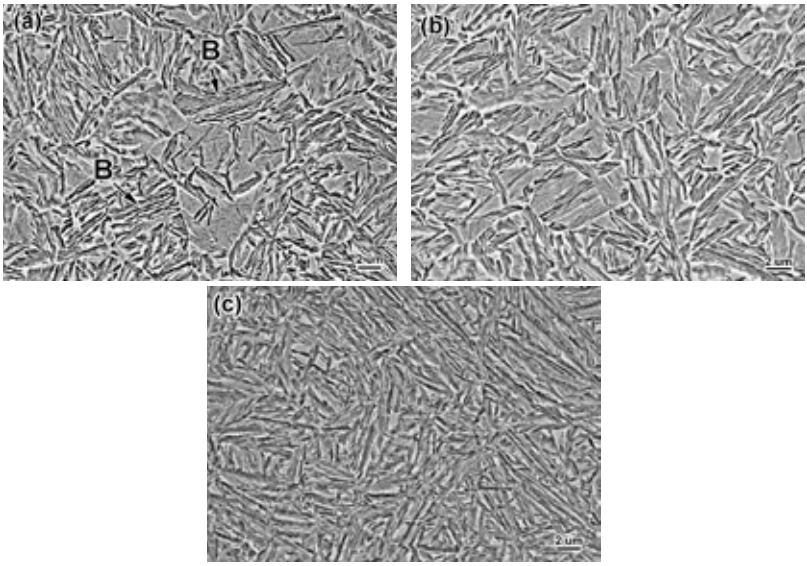

Figure 3.16. Microstructure of 55Si3Mn2CrVMoNb steel after austempering at (a) 300 °C (240 min), (b) 270 °C (300 min), (c) 250 °C (400 min)

The fracture patterns of austempered Charpy specimens are shown in Fig. 3.17. After an initial holding at 300 °C (45 min), the quasi-cleavage areas (shown by arrows) surrounded by the ductile dimples zones (Fig. 3.17, a) were seen on the fracture surface. As the holding time increased (Fig. 3.17, b), the ductile component in the fracture increased, which is generally consistent with an increase in impact toughness.

The XRD data on RA volume fraction and carbon content in austenite are presented in Fig. 3.18. The maximum austenite amount (33 vol.%) was detected after holding at 300 °C for 45 min, with carbon content in austenite of 0.94 wt.%, which is almost 2 times to average carbon content in the steel. With increasing the holding duration to 240 min, the RA amount was slightly decreased to 31 vol.% with increasing carbon content to

1.08 wt.%. Thus, holding at 300 °C was accompanied by C-enrichment of austenite leading to its stabilization followed by full suspension of bainite transformation (Fig. 2.3).

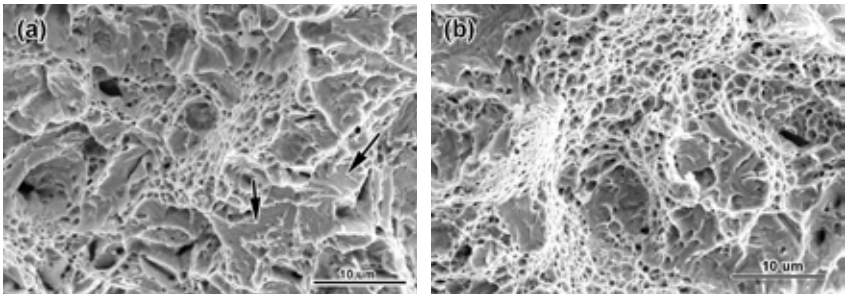

Figure 3.17. The fracture patterns of Charpy samples of 55Si3Mn2CrVMoNb steel austempered at 300 °C for: (a) 45 min, (b) 240 min

After holding at 270 °C and 250 °C, lower RA volume fractions (18–19 vol.%) were recorded with a carbon content of 1.04–1.06% and 0.94%, respectively. The increased carbon content in austenite was explained by the presence of 2.5% Si in the steel composition, which apparently inhibited the cementite precipitation at holding in the range of 250–300 °C. The increase in carbon content in RA with increasing holding duration was attributed to carbon redistribution from α-phase to austenite. As the holding temperature increased, this process became more intensive due to the promotion of carbon diffusivity.

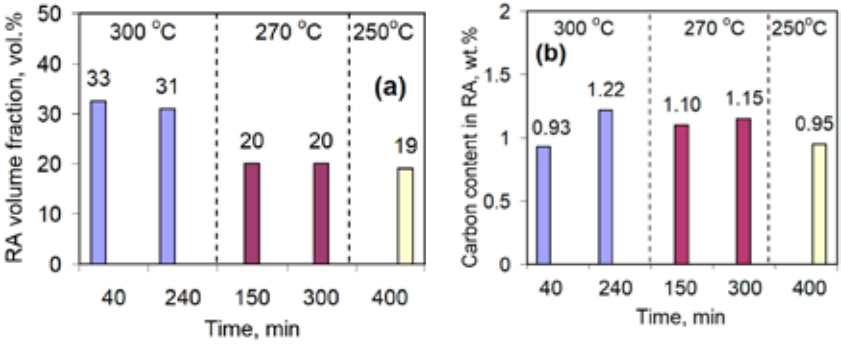

Figure 3.18. The effect of austempering duration on (a) RA volume fraction and (b) carbon content in RA

3.3.2 Effect of Q & P treatment modes on the mechanical properties of 55Si3Mn2CrVMoNb steel

Q & P treatment of 55Si3Mn2CrVMoNb steel was performed according to the following modes: QT = 160 °C (200 °C), partitioning temperature = 200 °C (225 °C, 250 °C, 270 °C, 300 °C) with holding from 10 to 300 min. The austenitization temperature was 900 °C (15 min holding). Before transfer to bath with Wood alloy melt, the samples were pre-cooled in the air to ~700 °C. The samples were held in the bath for 60 s with a further quick transfer to the laboratory furnace for prolonged holding. After finishing the partitioning stage, the samples were cooled in air. Taking into account the positive effects of tempering (Chapter 3.2), the Q & P-treated specimens were tempered at 200 °C for 1.5 hours. Q & P modes and mechanical properties of 55Si3Mn2CrVMoNb steel are given in Table 3.3.

The data presented in Table 3.3 allow to conclude that Q & P treatment provided 55Si3Mn2CrVMoNb steel with a particularly high strength (UTS = 1535–2374 MPa) which was by 10–11% with respect to (Q+T) treatment. At the same time, there was a significant increase in ductility: the total elongation was up to 23% and area reduction was up to 36%. The impact toughness also increased from 29–45 J/cm^2 (Q+T) to 48–117 J/cm^2 (Q & P).

The highest mechanical properties complex was recorded after Q & P treatment according to the regimes of $Q_{160\,^{\circ}C}/P_{270\,^{\circ}C}$ (50–120 min) and $Q_{200\,^{\circ}C}/P_{300\,^{\circ}C}$ (100 min): YTS of 1275–1506 MPa, UTS of 1535–1830 MPa, TEL of 20–23%, impact toughness of 75–101 J/cm^2. For these modes, the PSE reached an advanced level of 35.6–36.5 GPa · %. The regimes $Q_{160\,^{\circ}C}/P_{225\,^{\circ}C}$ (90 min) and $Q_{160^{\circ}C}/P_{250\,^{\circ}C}$ (90 min), which provided UTS of 1935–2077 MPa with TEL of 15–18%, also performed an improved PSE of 30.5–35.0 GPa · %.

The maximum strength (YTS of 1978 MPa, UTS of 2378 MPa, hardness of 57 HRC) corresponded to the regime of $Q_{160^{\circ}C}/P_{200^{\circ}C}$ (90 min). It should be noted that such high strength was accompanied with an elongation of 9% and impact toughness of 61 J/cm^2. A similar properties complex is characteristic to steels with nanostructured carbide-free bainite after prolonged (a week or more) austempering [56]. In our case, it was obtained in a much shorter mode (less than 2 hours).

The effect of the Q & P treatment mode on the mechanical properties of 55Si3Mn2CrVMoNb steel can be followed by the data presented in Figure 3.19 and Figure 3.20. It is seen that with increasing temperature and

Table 3.3. Mechanical properties, RA volume fraction and carbon content (C_γ) in austenite in 55Si3Mn2CrVMoNb steel after Q&P heat treatment (followed by the tempering at 200 °C)

Partitioning temperature, °C	UTS, MPa	YTS, MPa	TEL %	AR, %	KCU, J/cm²	Hardness, HRC	RA,%	C_γ,%	PSE, GPa×%
Q&P treatment (QT=160 °C)									
300 °C (10 min)	1841	1142	13	25	71	53	18	1.16	23.9
300 °C (40 min)	1597	1265	12	30	117	51	–	–	18.4
300 °C (120 min)	1565	1340	18	36	113	50	28	1.21	27.6
270 °C (20 min)	1764	1270	9	24	74	51	18	0.99	15.5
270 °C (50 min)	1830	1418	20	20	75	51	–	–	36.6
270 °C (120 min)	1743	1506	21	24	79	51	22	1.17	36.5
250 °C (40 min)	1736	1480	12	4	62	53	–	–	21.7
250 °C (90 min)	1935	1327	18	30	73	52	13	1.23	35.0
250 °C (200 min)	1747	1325	16	26	111	50	–	–	28.3
250 °C (300 min)	1783	1532	18	33	117	51	8	1.32	31.1
225 °C (40 min)	2090	1470	11	10	59	55	11	0.75	22.8
225 °C (90 min)	2077	1692	15	6	62	54	–	–	30.5
225 °C (200 min)	2011	1434	14	19	86	54	22	0.97	27.9
200 °C (90 min)	2374	1978	9	10	61	57	13	0.93	22.0
200 °C (200 min)	2066	1848	8	21	–	56	13	0.94	16.3

Table 3.3 (continuantion)

Q&P treatment (QT=200 °C)									
300 °C (10 min)	1592	1063	11	26	75	48	20	1.14	18.2
300 °C (50 min)	1575	1250	21	34	96	47	–	–	33.6
300 °C (100 min)	1535	1275	23	34	101	49	25	1.22	35.6
270 °C (40 min)	1798	1197	20	6	66	47	18	1.22	35.2
270 °C (120 min)	1687	1379	14	30	81	48	–	–	23.3
270 °C (200 min)	1666	1429	13	28	89	51	25	1.14	21.8
250 °C (40 min)	1960	1509	9	18	73	54	–	–	18.1
250 °C (90 min)	1889	1253	11	23	63	52	15	1.18	21.1
250 °C (200 min)	1837	1413	17	14	83	52	–	–	30.4
250 °C (300 min)	1747	1353	15	18	106	50	15	1.26	26.4
225 °C (40 min)	1965	1405	7	0	48	50	13	1.00	13.9
225 °C (90 min)	1939	1277	9	8	49	53	–	–	17.2
225 °C (200 min)	1962	1211	17	23	75	53	15	1.00	33.9

holding time at the partitioning stage, the strength decreased. It was induced by more intensive tempering of martensite; furthermore, increasing the holding temperature led to the formation of bainite with lower strength which also contributed to the decrease in steel strength [182].

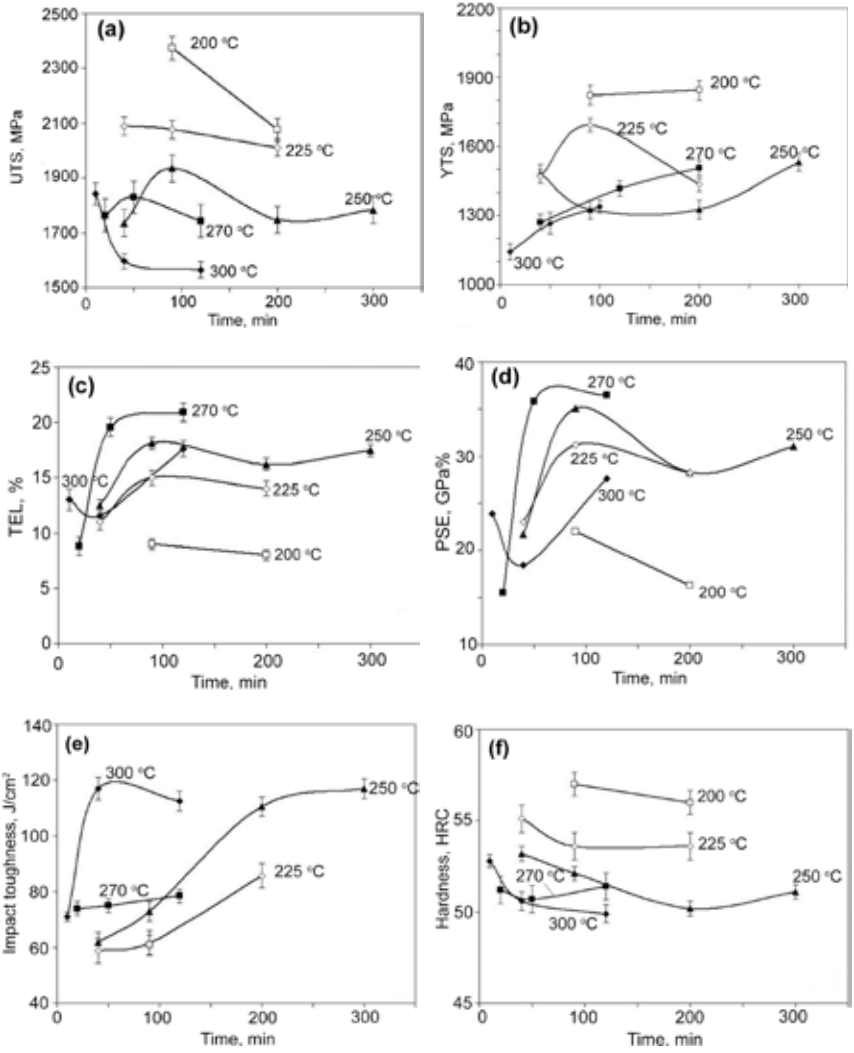

Figure 3.19. Effect of partitioning duration on mechanical properties of Q&P-treated 55Si3Mn2CrVMoNb (QT=160 °C)

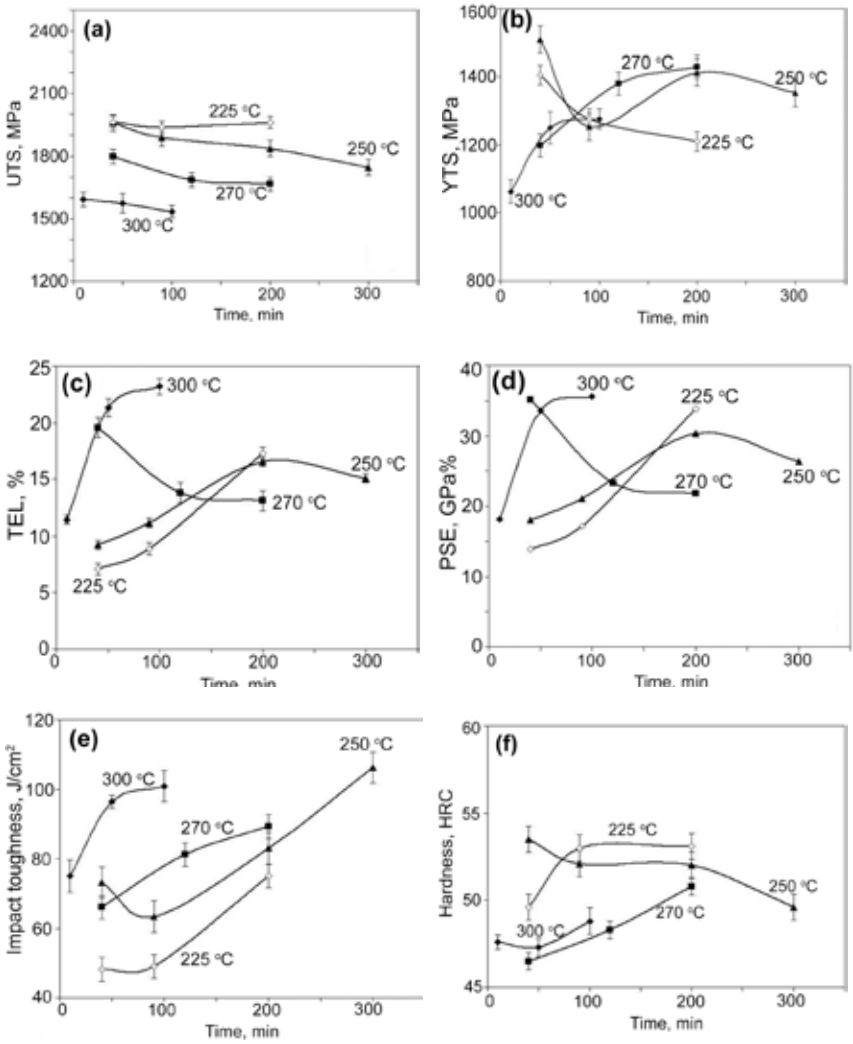

Figure 3.20. Effect of partitioning duration on mechanical properties of Q & P-treated 55Si3Mn2CrVMoNb (QT=200 °C)

Increasing the partitioning duration reduced the steel strength due to the more complete martensite tempering and austenite transformation to bainite (Figs. 3.19, a, b and 3.20, a, b). The latter decreased the contribution of the TRIP effect to the steel strengthening. Increasing QT temperature from 160 °C to 200 °C resulted in a slight decreasing strength due to

the decrease in the martensite amount at the quenching stage. All these structural changes led to a minimum strength level (YTS = 1275 MPa, UTS = 1535 MPa) after the mode of $Q_{200^\circ C}/P_{300^\circ C}$ (100 min). This mode was characterized by a maximum TEL value of 23%, which provided a very high PSE value (35.6 GPa · %).

The effect of Q&P mode on ductility (Figs. 3.19, c and 3.20, c) was opposite to the strength trend. There was a tendency of decreasing elongation as the partitioning temperature decreased and of a slight increasing as the partitioning duration increased. These trends were explained by the tempering of martensite formed during the quenching stage, as well as by austenite saturation with carbon, which reduced its tendency to deformation martensite transformation. Thus, stabilized austenite remained in the structure at higher tensile stress, increasing the steel ductility.

In Figs. 3.19, e and 3.20, e the effect of Q&P treatment mode on the impact toughness is illustrated. From these figures, the tendency of impact toughness increasing with the temperature and duration of the partitioning stage can be clearly seen. In addition, after Q&P treatment with QT = = 160 °C, the steel acquired a higher impact toughness than that of QT = = 200 °C. The maximum impact toughness (117 J/cm^2) is referred to $Q_{160^\circ C}/P_{300^\circ C}$(40 min) and $Q_{160^\circ C}/P_{250^\circ C}$(300 min) modes, and the minimum (48 J/cm^2) – to $Q_{200^\circ C}/P_{225^\circ C}$ (40 min). The growth of impact toughness was due to an increase in volume fraction of ductile components (retained austenite and carbide-free bainite) with a corresponding decreasing the amount of brittle phase (martensite). Also, martensite tempering was an important factor contributing to advanced steel toughness.

Q&P treatment promoted a fairly high hardness (≥ 50 HRC) for all treatment modes. The maximum hardness (57 HRC) corresponded to $Q_{160^\circ C}/P_{200^\circ C}$ (90 min) mode. In general, modes with quenching to 160 °C with the initial stages of holding were characterized by decreased hardness as a result of martensite tempering. In the later partitioning stages, the hardness increased owing to austenite transformation into lower bainite. For modes with QT = 200 °C (Fig. 3.20, f), there was a significant increase in hardness as the partitioning holding increased. In this case, the structure contained less martensite, thus the carbon redistribution from martensite to austenite was not as fast as at QT = 160 °C. With increasing holding time, austenite was enriched with carbon and partially transformed to high-carbon martensite, which enhanced hardness. The character of the change in hardness during $Q_{200^\circ C}/P_{250^\circ C}$ mode was close to that for modes

with QT = 160 °C to be associated with a lesser RA amount in the steel structure.

The Q&P-treated samples of 55Si3Mn2CrVMoNb steel were characterized by high impact toughness reaching 117 J/cm^2. Noteworthy, the improved impact toughness was obtained with fairly high hardness (≥50 HRC). As follows from Fig. 3.21, the fracture surface of the Q&P-treated specimens was predominantly ductile, as evidenced by transcrystalline quasi-cleavage and dimples areas. The formation of the dimples proceeded through merging micro-voids that originated on the lattice defects or on the dispersed inclusions of vanadium carbide (shown by the arrows in Fig. 3.21, a).

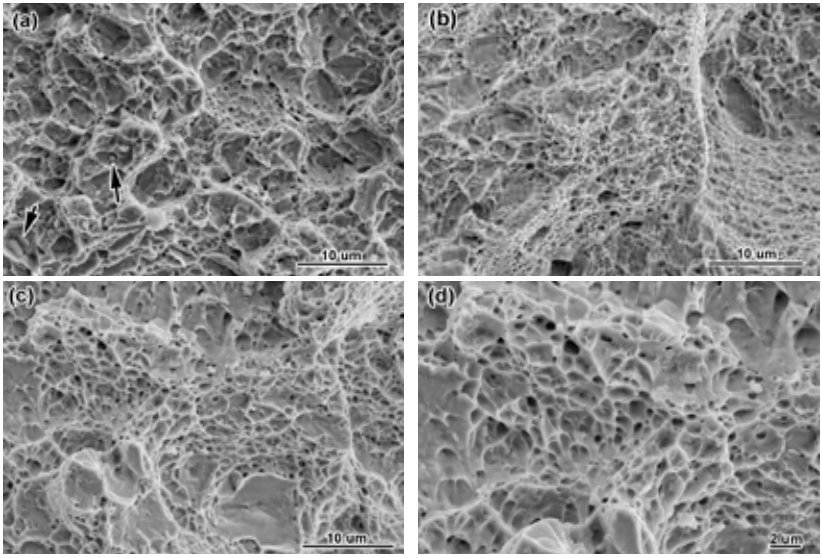

Figure 3.21. Rupture surface of Charpy samples of 55Si3Mn2CrVMoNb after Q&P treatment by modes: (a) $Q_{160°C}/P_{250°C}$ (90 min), (b) $Q_{160°C}/P_{250°C}$ (300 min), (c, d) $Q_{200°C}/P_{300°C}$ (100 min)

3.3.3 Microstructure and phase constituents of Q&P-treated 55Si3Mn2CrVMoNb steel

After Q+T(300 °C) treatment the microstructure of 55Si3Mn2CrVMoNb steel consisted of a mixture of tempered martensite (lath and plate morphologies) and a minor amount of retained austenite, evenly distributed in structure (Fig. 3.22). RA was of two morphological types: "islands" and thin elongated areas of lath shape.

The microstructure of 55Si3Mn2CrVMoNb steel after Q&P treatment is presented in Figures 3.23, 3.24. After treatment by $Q_{160°C}/P_{300°C}$ (10 min) mode structure consisted of tempered martensite and copious areas of retained austenite (Fig. 3.30, a, b). Increasing the holding duration led to a significant reduction in the size and number of austenitic areas; in their place, lower carbide-free bainite laths appeared. The latter divided the former austenitic grain into smaller areas leading to fine-needle martensite formation at the final cooling stage after partitioning (Fig. 3.30, c).

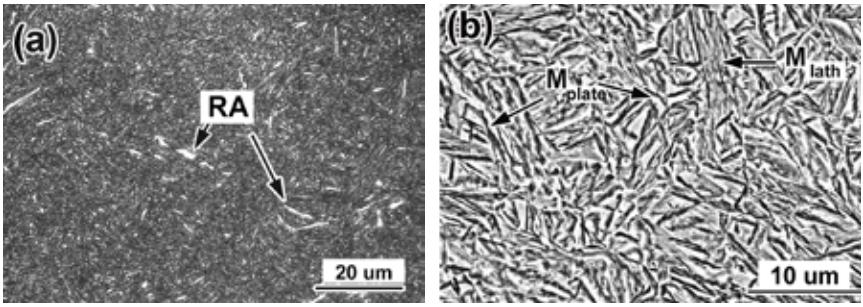

Figure 3.22. Microstructure of 55Si3Mn2CrVMoNb steel after quenching and tempering at 300 °C: (a) optical microscope, (b) SEM

As the partitioning temperature decreased, the number of austenite areas decreased also to be explained by low carbon diffusion mobility leading to lower C-enrichment of retained austenite (Fig. 3.31, a, c, e, Fig. 3.32 a, e, g). These features were typical for modes with QT = 160 °C and QT = 200 °C.

The local chemical composition of an austenitic area was determined by EDX analysis (spectra 2 and 3 in Fig. 3.25). As follows from Table 3.5, the austenitic area had higher Mn content (2.10–2.26 wt.%) as compared to bainite (1.63–1.73 wt.%, spectra 4, 5) and to martensite (0.97–1.80 wt.%, spectra 6, 7). The austenite area contained the least Si content (2.39–2.40 wt.%) while martensite was depleted in Cr (0.54–0.55%). These data showed that austenitic areas were enriched in austenite-forming manganese and depleted on ferrite-forming silicon (Fig. 3.26). Given the low diffusion mobility of these elements at partitioning temperatures, it can be assumed that these elements' segregations resulted from ingot solidification. Accordingly, the retained austenite formation was facilitated in Mn-enriched segregational areas. The areas depleted with Mn and Cr during Q&P treatment transformed into martensite due to the higher M_S temperature.

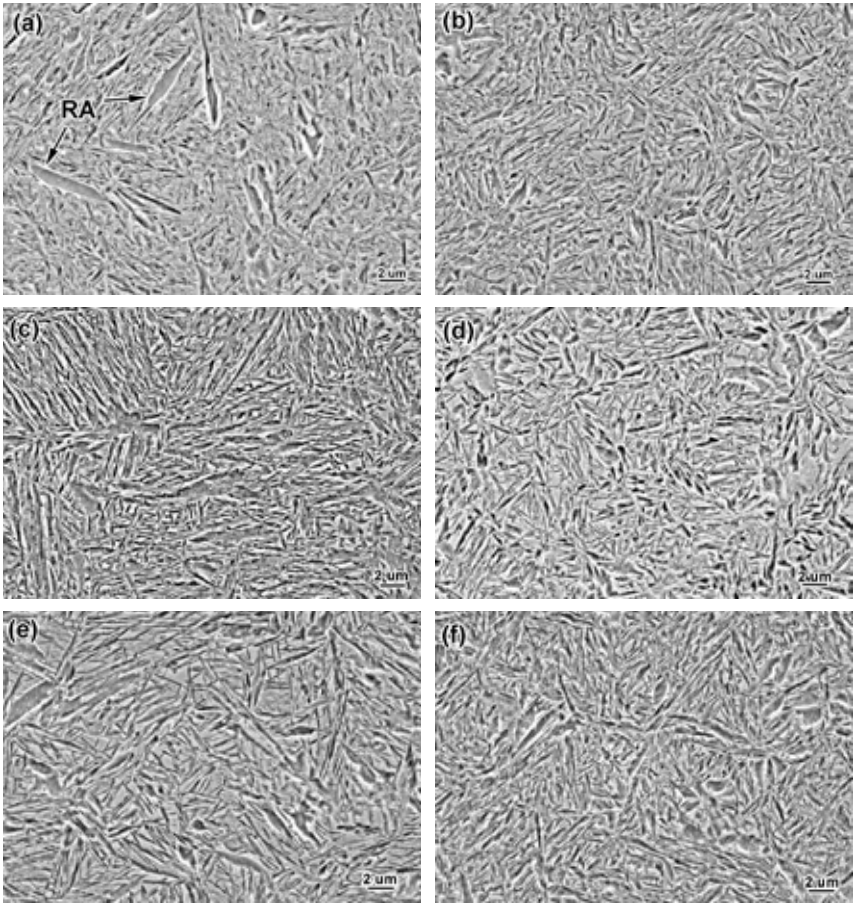

Figure 3.23. Microstructure of 55Si3Mn2CrVMoNb steel after Q & P treatment with QT=160 °C and partitioning at 300 °C for (a) 10 min and (b) 120 min; at 250 °C for (c) 90 min and (d) 300 min; at 225 °C for (e) 40 min and (f) 250 min

Figs. 3.27–3.29 present the fine structure of Q & P-treated 55Si3Mn-2CrVMoNb steel. In the sample treated by $Q_{160^{\circ}C}/P_{300^{\circ}C}$ (10 min) mode, partially twinned martensite with high dislocation density, as well as the films and massive "islands" of RA were observed (Fig. 3.27, a, b). The presence of austenite is confirmed by SAED analysis (Fig. 3.27, c).

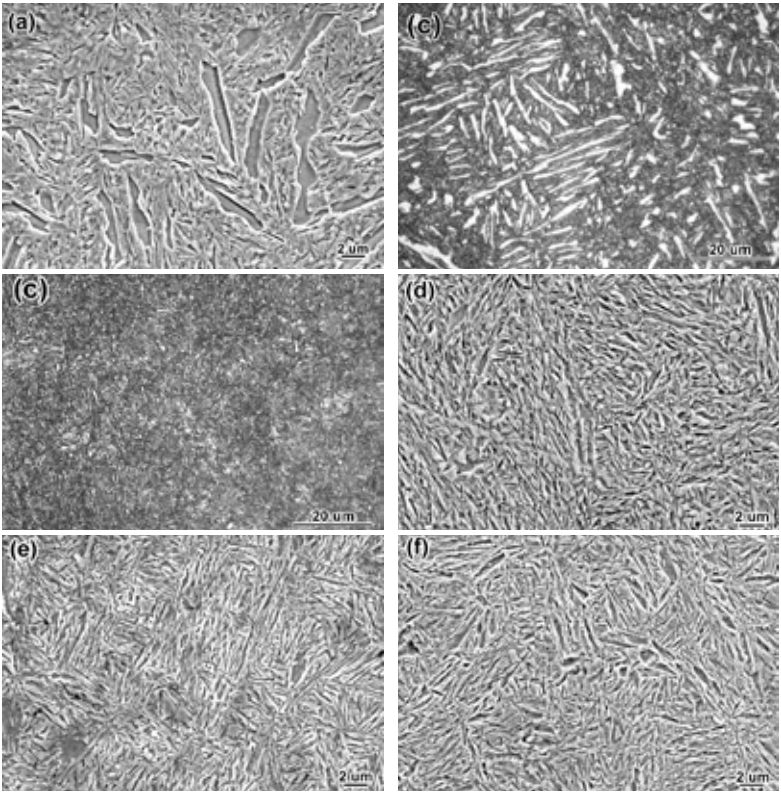

Figure 3.24. Microstructure of 55Si3Mn2CrVMoNb steel after Q-n-P treatment with QT = 200 °C and partitioning at 300 °C for (a) 100 min; at 250 °C for (b) 20 min and (c, d) 120 min; at 225 °C for (e) 40 min and (f) 200 min

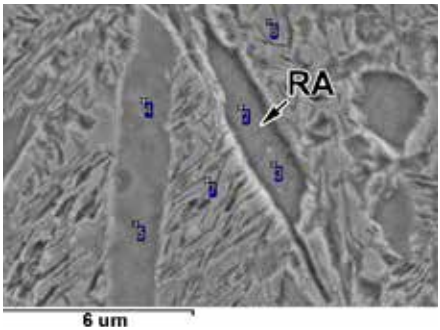

Figure 3.25. Locations of point EDX analysis in the sample of 55Si3Mn2CrVMoNb steel after $Q_{200\,^{\circ}C}/P_{300\,^{\circ}C}$ (100 min) mode

Table 3.4. The results of EDS point analysis of Q & P-treated 55Si3Mn2CrVMNb steel

Spectrum number (Fig. 3.25)	Content, wt.%				
	C	Si	Cr	Mn	Fe
2	8.28	2.39	1.12	2.26	85.95
3	7.95	2.40	0.81	2.10	86.74
4	10.03	2.93	0.89	1.63	84.52
5	8.05	2.64	0.96	1.73	86.62
6	12.82	3.06	0.54	1.80	81.78
7	14.57	4.05	0.55	0.97	79.86

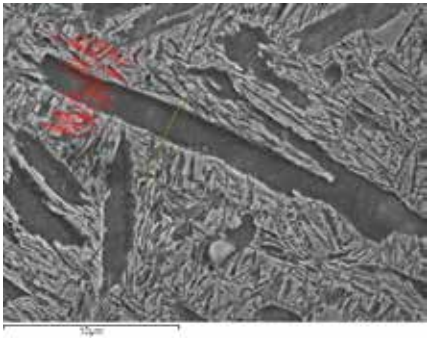

Figure 3.26. The profile of Si across the austenite area

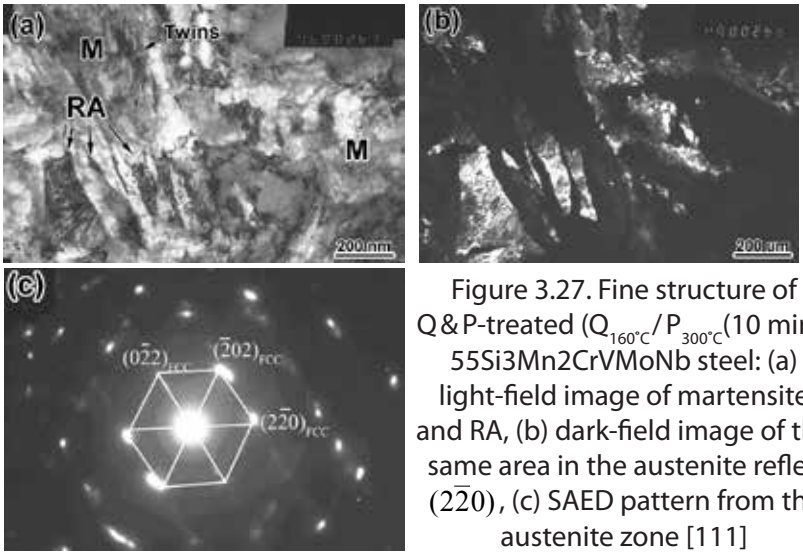

Figure 3.27. Fine structure of Q & P-treated ($Q_{160°C}$ / $P_{300°C}$(10 min)) 55Si3Mn2CrVMoNb steel: (a) light-field image of martensite and RA, (b) dark-field image of the same area in the austenite reflex $(2\bar{2}0)$, (c) SAED pattern from the austenite zone [111]

In martensite there were transitional carbides, which were released within the a-laths during the partitioning stage; carbides formed the fiber-shaped clusters positioned at an angle of ~40–50° to the long axis of the laths. In some laths, twins were detected, indicating a high carbon content (this could be due to the austenite C-enrichment at the partitioning stage, with its subsequent transformation to high carbon martensite). The 55Si3Mn2CrVMoNb steel contained an increased amount of retained austenite as seen in dark-field image in Fig. 3.28, b. where RA is well identified as light-contrast layers.

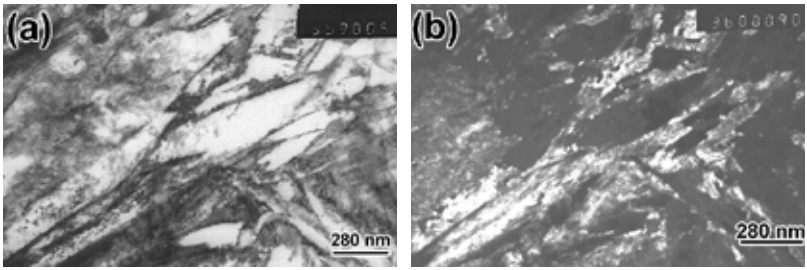

Figure 3.28. Martensite laths and RA ("islands" and films) in Q&P-treated ($Q_{160°C}/P_{250°C}$ (40 min)) 55Si3Mn2CrVMoNb steel

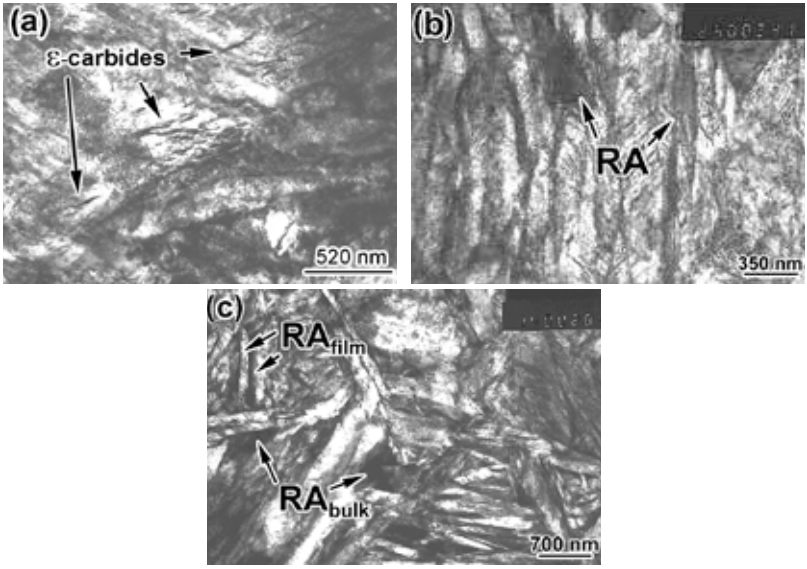

Figure 3.29. Martensite laths and RA ("islands" and films) in 55Si3Mn2CrVMoNb steel after Q&P treatemnt ($Q_{160°C}/P_{200°C}$ (90 min))

By lowering the partitioning temperature to 200 °C, the structure retained its character specific for higher holding temperatures. The images showed α-phase lath packages with the transitional carbides inside the laths (Fig. 3.29, a). Retained austenite was of two morphological types: "filmy" and "blocky" (Fig. 3.29, b, c). The thickness of the α-phase laths varied in the range of 57–350 nm (Fig. 3.30), with almost half of them (45.7%) being nano-sized and having less than 100 nm thick. Taken that martensite in 55Si3Mn2CrVMoNb steel was both of needle and lath morphologies, it was difficult to identify martensitic and bainitic laths uniquely. It can be assumed that the wider (> 100 nm) α-phase laths referred to martensite formed at the quenching stage (as evidenced by the transitional carbides formed inside them during the partitioning stage). Then the finer laths referred to nanobainite that formed during the partitioning stage, or to "fresh" martensite formed upon final cooling. The latter assumption was based on the fact that austenitic grains, at the end of the partitioning stage, became fragmented by bainitic laths that further reduced the "fresh" martensite laths size.

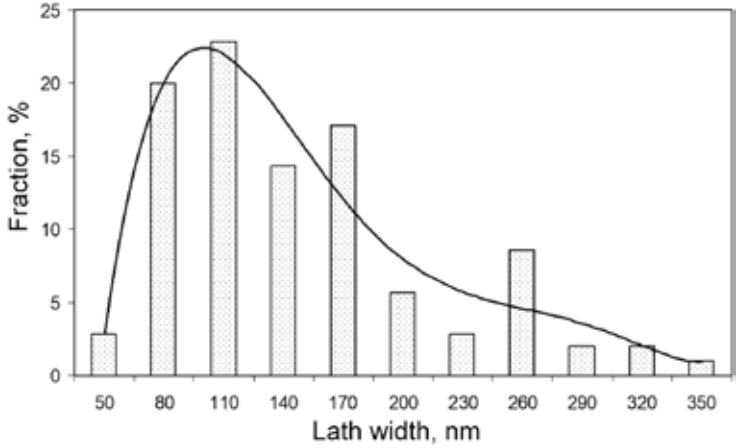

Figure 3.30. Frequency distribution of martensitic laths thickness in sample of 55Si3Mn2CrVMoNb steel after Q&P treatment ($Q_{160\,°C}$ / $P_{200\,°C}$ (90 min))

For different Q&P treatment modes, the RA amount varied from 11 vol.% to 28 vol.%, increasing as the partitioning temperature increased (Fig. 3.31, a). Under partitioning at 270–300 °C with increasing holding time, the RA volume fraction reached 28 vol.% at $Q_{160\,°C}$/ $P_{300\,°C}$ and 25 vol.% at

$Q_{200\,^{\circ}C}/P_{270\,^{\circ}C}$. At lower partitioning temperatures, the effect of holding time became less pronounced (or even absent at 200 °C), although at QT = 160 °C the austenite amount increased more intensively than at QT = 200 °C.

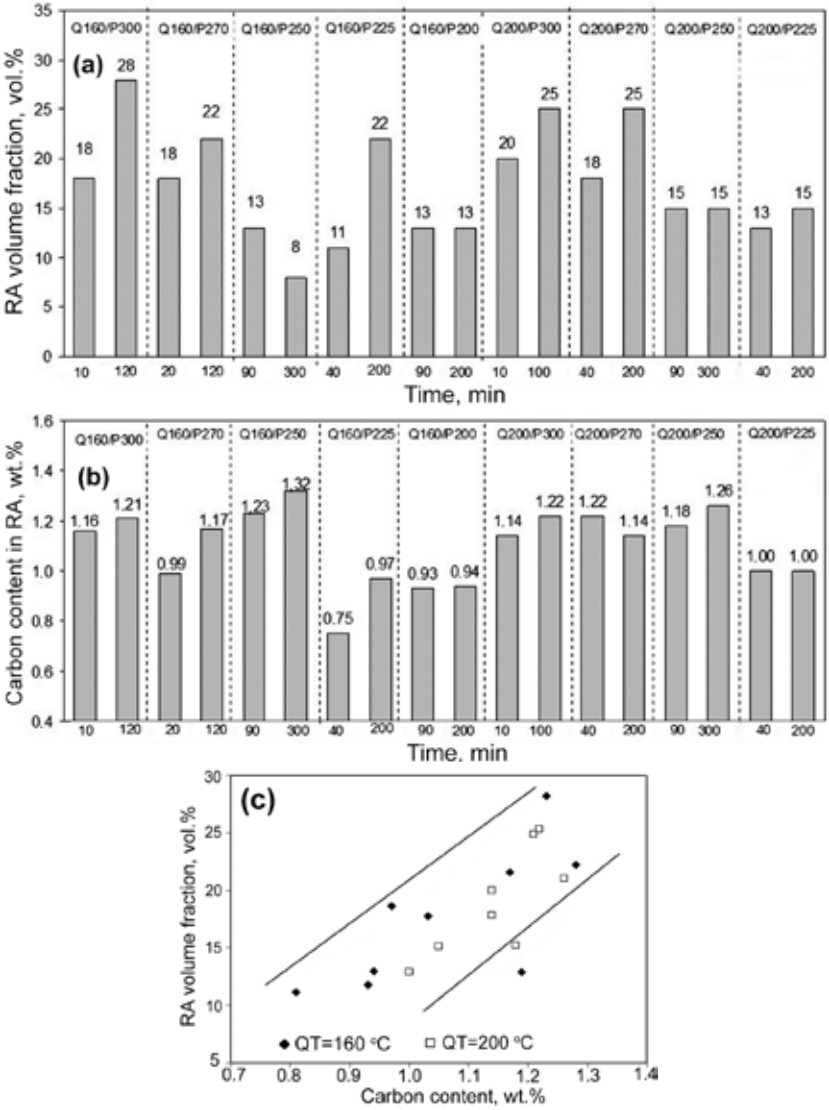

Figure 3.31. Effect of Q&P treatment mode on (a) RA volume fraction, (b) carbon content in austenite and (c) its relationship with RA volume fraction in Q&P-treated 55Si3Mn2CrVMoNb steel

The carbon content in retained austenite increased as the partitioning duration increased (Fig. 3.31, b). At a partitioning temperature of 270––300 °C the carbon content increased to 1.17–1.21 wt.%; at 200–225 °C it reached 0.94–0.97 wt.%. As follows from Fig. 3.31, c there was a directly proportional relationship between the carbon content and the amount of retained austenite which is described by the regression equation:

$$RA\ (vol.\%) = 50.3 \times [\%C]^2 - 70.2 \times [\%C] + 35.8\ (R^2 = 0.70). \quad (3.1)$$

Thus, microstructural and XRD studies have shown that, due to Q & P treatment, 55Si3Mn2CrVMoNb steel gained a heterogeneous microstructure comprising α-phase, retained austenite, and transitional carbides. As follows from the austenite transformation kinetics, bainite transformation occurred at the partitioning stage, therefore, the α-phase was represented by both tempered martensite and carbide-free bainite.

Exactly this structure provided an advanced combination of strength, ductility, and impact toughness of this steel.

3.4 Q & P-integrated steel heat treatment modes and their effect on the mechanical properties of 55Si3Mn2CrVMoNb steel

Since its appearance, the Q & P concept has been constantly evolving and modified to address its shortcomings and further enhance the mechanical properties of steel. In this regard, it was of interest to test several Q & P-integrated heat treatment modes concerning the 55Si3Mn2CrVMoNb steel. The following modes were proposed:

(a) LQ & P (Long Quenching) presented prolonged (60 min) holding at the quenching temperature (160 °C) and partitioning at 200 °C for 90 min) (Fig. 3.32, a);

(b) IA-Q & P (Intercritical Annealing) included austenitization held in the intercritical interval. The austenitization temperature (810 °C) corresponded to the intercritical interval of 55Si3Mn2CrVMoNb steel was determined by dilatometric analysis to ensure about 20 vol.% of ferrite in the structure. After the intercritical annealing the quenching was performed to QT=120 °C, 140 °C and 160 °C, followed by holding at PT=250 °C for 90 min (Fig. 3.32, b);

(c) B-Q & P included holding at 225 (80 min) and 250 °C (40 min) to form bainite before the quenching (Fig. 3.32, c);

(d) TCT-Q & P was a thermocyclic Q & P treatment with a 3 cycle performed as 160 °C ↔ 250 °C or 160 °C ↔ 225 °C (Fig. 3.32, d).

After all types of treatment, tempering was performed at 200 °C for 1.5 hours. LQ & P treatment aimed to increase ductility at high strength (above 2000 MPa) due to an increase in the RA volume fraction through thermal stabilization of γ-phase. For this case, the basic mode $Q_{160^\circ C}/P_{200^\circ C}$ (90 min) was selected since it ensured the highest strength (UTS of 2373 MPa) at TEL of 9% (Table 3.3).

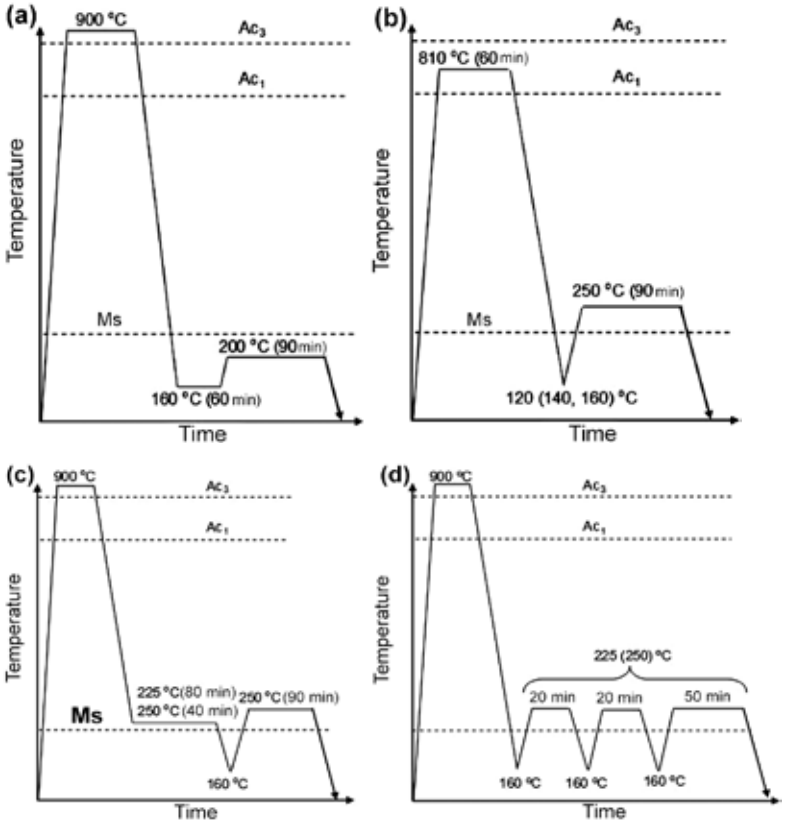

Figure 3.32. The schemes of Q & P-integrated modes:
(a) LQ & P, (b) IA+Q & P, (c) B-Q & P, (d) TCT-Q & P

The IA+Q & P treatment mode pursued an additional increase in ductility by obtaining proeutectoid ferrite. The B-Q & P mode aimed to obtain fine-needle martensite by pre-forming a certain lower bainite fraction, which

was supposed to fragment austenitic grains. The TCT-Q&P mode aimed to stimulate diffusion and phase-structural transformations by changing the stress-strain state as a result of heating/cooling cycles. The $Q_{160^\circ C}/P_{250^\circ C}$ (90 min) mode was selected as the base for the "b"–"d" modes, since it provided one of the best combinations of mechanical properties: UTS of 1935 MPa, TEL of 18%, AR of 30%, PSE of 35 GPa · %. The mechanical properties after Q&P-integrated modes are presented in Table. 3.5.

Table 3.5. Mechanical properties of 55Si3Mn2CrVMoNb steel after Q&P-integrated heat treatments

Temperature and duration of holding	UTS, MPa	YTS, MPa	TEL, %	AR, %	KCU, J/cm²	Hardness, HRC	PSE, GPa · %
LQ&P (200 °C (90 min))							
QT=160 °C (60 min)	2160	1692	9	16	–	56	18.9
IA-Q&P (250 °C (90 min))							
QT=160 °C	1858	1262	9	13	55	45	17.4
QT=140 °C	1694	1145	5	8	58	47	8.9
QT=120 °C	1719	1176	6	9	47	49	10.1
B-Q&P(250 °C (90 min))							
250 (40 min)	2001	1613	10	30	79	50	20.0
225 (80 min)	2116	1561	9	8	62	54	18.2
TCT-Q&P (250 °C (90 min))							
160 °C ↔ 250 °C	1941	1405	16	25	74	50	31.5
160 °C ↔ 225 °C	2108	1509	10	10	–	54	21.1

As follows from Table 3.6, the thermal stabilization at 160 °C for 60 min resulted in a slight increase in the total elongation narrowing, but it significantly (by 200 MPa) lowered the tensile strength relative to the base mode.

Heat treatment with intercritical annealing resulted in 15–20% structurally free ferrite in the structure (Fig. 3.33), which, however, did not provide an expected increase in ductility. On the contrary, the ductility decreased almost twice compared to the basic Q&P mode, while impact toughness decreased by 25%. As the quenching temperature decreased to 140–120 °C, the ductility reduced even to a greater extent. Such change was accompanied by a general decrease in strength: by ~100 MPa at QT=160 °C and by ~200 MPa at QT=120–140 °C (the hardness also reduced by 3–7 HRC). The decline in the properties compared to the basic Q&P modes was probably due to the carbon redistribution between ferrite and austenite under intercritical holding which led to a significant increase in carbon content in the

austenite after the partitioning stage. This resulted in the formation of high-carbon brittle martensite after final cooling, which decreased steel ductility. A decrease in quenching temperature reduced a martensite volume fraction causing an additional reduction in ductility and impact toughness. The presence of ferrite expectedly reduced the yield strength, while the reduction of tensile strength was caused by steel embrittlement. Thus, quenching from intercritical interval had an adverse effect on the properties of Q & P-treated 55Si3Mn2CrVMoNb steel. These results contradict the conclusions of [183], where the positive effect of intercritical annealing on the mechanical properties of 60Si2 and 60Si2CrV steels was reported.

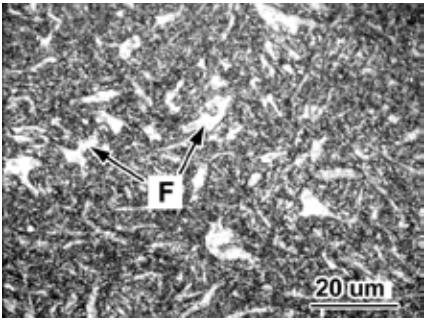

Figure 3.33. Microstructure of 55Si3Mn2CrVMoNb steel after IA + Q & P treatment (QT = 160 °C)

Better results were obtained after B-Q & P mode: UTS was 2001–2116 MPa while ductility was similar to IA+Q & P mode (TEL = 9–10%, AR = = 8–30%) with some increase in impact toughness (up to 79 J/cm^2). The yield strength increased significantly (compared to basic Q & P treatment), reaching 1561–1613 MPa. Obviously, this was due to a decrease in the amount of retained austenite during the bainite transformation in the previous stage. The increase in pre-bainitization temperature caused the increase in UTS value accompanied by a decrease in total elongation and impact toughness. The B-Q & P mode can be used when it is necessary to increase the yield strength and impact toughness of steel, but the PSE remains low (18–20 GPa · %).

The TCT-Q & P mode with partitioning temperature 250 °C provided almost the same properties as the base treatment (PSE of 31.5 GPa · %). At a partitioning temperature of 225 °C strength slightly increased but ductility decreased by 1.5 times; as a result, the PSE reduced to 21.1 GPa · %. Thus, the TCT-Q & P mode can compete with the basic Q & P treatment mode, however, additional studies are needed to determine its optimal

parameters (number of cycles, temperature, holding time, etc.) to obtain an improved complex of steel properties.

3.5 Deformation stability of retained austenite in Q & P treated 55Si3Mn2CrVMoNb steel

As shown above, retained austenite plays a key role in mechanical properties of Q & P treated steels, since its ductility allows to achieve high strength specific for martensite avoiding a sharp decrease in ductility and toughness of steel. Due to RA, the quenched steel is able to strain under load; moreover, austenite greatly contributes to the tensile strength through the strain hardening. The degree of strain hardening can be much advanced if austenite is prone to strain-induced martensite transformation. With regard to Q & P-treated and nanobainitic steels, there is a general opinion [112] that the metastability of retained austenite should be limited since its rapid transformation into martensite at initial strain can lead to early steel embrittlement. It is considered that "blocky" retained austenite demonstrates a high tendency to SIMT and completely transforms into martensite at the beginning of tensile testing, while "filmy" austenite remains stable to higher strain degrees. The latter behaviour is facilitated by both carbon enrichment of filmy austenite (chemical stabilization) and the presence of neighboring strong phase (like martensite or bainitic ferrite), which resist the volume expansion caused by the shear $\gamma \rightarrow a'$ transformation.

The degree of RA stability to SIMT in Q & P-treated 55Si3Mn2CrVMoNb steel was evaluated under various schemes of deformation, such as (a) bulk deformation under uniaxial tensile (standard tensile tests) and (b) surface deformation under abrasion. The studies were performed on specimens treated according to three different Q & P treatment modes to provide different strength levels: (a) maximum strength (*UTS*~2300–2400 MPa) ($Q_{160^\circ C}$/ $P_{200^\circ C}$(90 min)), (b) average strength (~2000 MPa) ($Q_{160^\circ C}$/$P_{250^\circ C}$(90 min)), (c) low strength with high ductility (TEL = 23%) ($Q_{200^\circ C}$/ $P_{300^\circ C}$)(100 min)). These modes were designated as # 1, # 2 and # 3, respectively. They differed not only in mechanical properties but also in RA volume fraction which was 13 vol.% for #1 and #2 and 25 vol.% for # 3. In addition, RA had a different carbon content (0.97 wt.% for #1 and 1.22–1.23 wt. for #2 and #3). Thus, the selected modes should differ in the stability of retained austenite to SIMT. As reference a quenched sample of the same steel was used (62 HRC).The austenite metastability during tests was evaluated by parameter M calculated as:

$$M = \frac{\Delta RA}{RA}, \tag{3.2}$$

where RA is austenite volume fraction before the test, vol.%, ΔRA is an alteration in austenite volume fraction after the tests, vol.%.

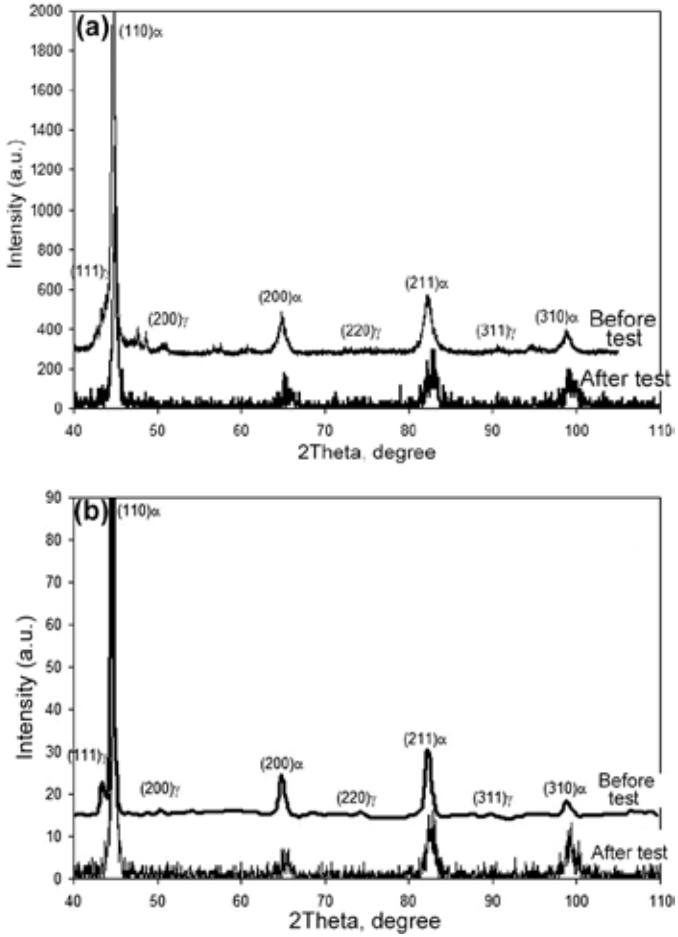

Figure 3.34. XRD patterns of 55Si3Mn2CrVMoNb steel before and after tensile testing (CuK$_a$-radiation) (a) $Q_{160^\circ C}/P_{200^\circ C}$(90 min), (b) $Q_{160^\circ C}/P_{250^\circ C}$(90 min), (c) $Q_{200^\circ C}/P_{300^\circ C}$(100 min)

After tensile testing, the RA volume fraction was XRD measured on the ruptured tip of the samples. After the wear test XRD measurement was performed on the worn surface. The corresponding XRD patterns before

and after the test are presented in Figure 3.34. It can be seen that, in all cases, the diffraction patterns of the fractured samples performed a sharp decrease in the austenite maxima intensity, especially of the peaks (200), (220), and (311), which were hardly identified on the diffraction patterns. The calculated amount of retained austenite was 2–3 vol.% for modes # 1 and #2, and slightly higher (4 vol.%) – for mode # 3 (Table 3.6). Given the very weak austenite peaks, these differences in austenite content were considered experimental errors. Based on the parameter M, it was stated that, regardless of RA volume fraction and carbon content, retained austenite in a great extent (by 77–85%) transformed to martensite under tensile strain which precedes the tensile fracture.

Taking into account that the austenite in the studied samples had different morphology ("blocky" and "filmy"), it was concluded that even "filmy" RA which had high carbon content (1.23 wt.%) almost completely transformed to martensite during the sample fracture. Therefore one can speculate that the TRIP effect took place contributing to steel properties under tensile testing.

Table 3.6. Change in RA volume fraction in 55Si3Mn2CrVMoNb steel after tensile strain and abrasive wear

Mode #	**The amount of retained austenite, vol.%**		**DRA, vol.%**	**RA metastability (parameter M)**
	Before tests	**After tests**		
Tensile test (CuK_a-radiation)				
1	13	3	10	77.0
2	21	2	19	90.5
3	25	4	21	84.0
Wear by "mild" abrasive (SiO_2) (FeK_a-radiation)				
1	13	11	2	13.3
2	28	26	2	7.1
3	24	23	1	4.2
Wear by "hard" abrasive (Al_2O_3) (FeK-radiation)				
1	13	8	5	38.4
2	28	20	8	28.5
3	24	22	2	8.3

Quite an opposite tendency of austenite for SIMT was indicated regarding the abrasive wear tests. In this case, the steel surface was deformed

by the abrasive particles. Two abrasive types were used for tests differing in hardness: "hard" alumina (Al_2O_3) and "mild" silica (SiO_2). Depending on the abrasive hardness the wear process proceeded through different mechanisms such as (a) ploughing (micro-cutting or plastic deformation) with deep scratches formation (in contact with a "hard" abrasive agent) and (b) multi-cycle low-stress contact fatigue (in contact with a "mild" abrasive agent) [184].

According to [185], the form of abrasive wear is determined by the ratio of the hardness of the metal surface ($H_м$) and the abrasive (H_a). If $H_м : H_a < 0.5$ the wear form is mechanic (micro-cutting or plastic ploughing) accompanied by higher weight loss. If $H_м : H_a \geq 0.5$ the wear form is contact fatigue characterized by a sharp decrease in weight loss. Given the samples' hardness (57 HRC (694HV) for regime #1, 52 HRC (583 HV) for regime #2 and 49 HRC (534 HV) for regime #3, the $H_м : H_a$ ratio values were as follows:

(a) the case of wear by SiO_2 (1100 HV) abrasive: 0.63 for regime #1, 0.53 for regime # 2, 0.48 for regime # 3;

(b) the case of wear by Al_2O_3 (2000 HV) abrasive: 0.35 for #1, 0.29 for # 2, 0.27 for # 3.

For alumina tests, the $H_м : H_a$ values are less than 0.5, therefore wear should pass through the mechanical form. For silica tests $H_м : H_a$ values are ≥ 0.5, i.e. wear should pass through the contact fatigue mechanism with preferential oxide scales formation/detachment (which is a mechano-chemical form of abrasive wear [185]).

The hard (Al_2O_3) abrasive test showed (Fig. 3.35) that Q&P treatment according to modes # 1 and # 2 provided almost the same weight loss (~ 0.060 g) despite the difference in hardness (52 HRC and 57 HRC, respectively). Mode # 3 provided a slightly lower (by 2–3%) weight loss despite this mode being characterized by a lower hardness (49 HRC).

Analysis of the XRD patterns showed that during the wear test with Al_2O_3 abrasive, austenite performed a certain tendency for SIMT, although it was lower than under tensile strain (Table 3.7). The highest tendency for SIMT showed the sample treated by mode # 1 when 38% of initial RA transformed into martensite during wear. The highest stability to SIMT was ascribed to mode # 3 when transformation covered only 8.3% of initial austenite. In this case, there was no correlation between the austenite metastability and weight loss.

During the wear test using "mild" (SiO_2) abrasive Q&P-treated steel performed higher stability to SIMT as compared with Al_2O_3– testing.

Mode # 1 performed the highest austenite metastability, although the M parameter was only 15% (Table 3.6).

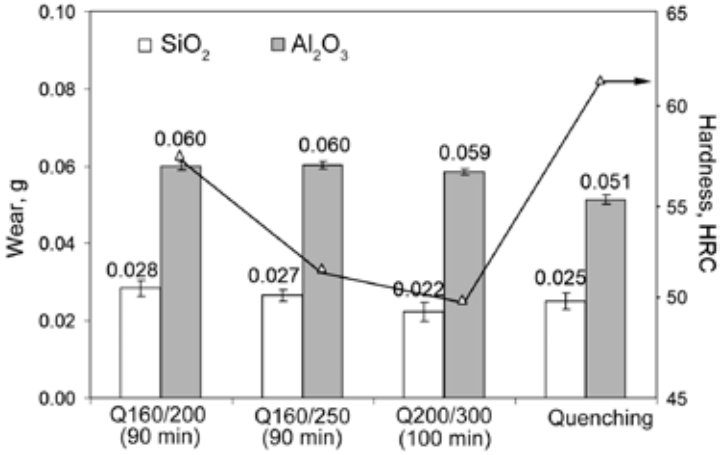

Figure 3.35. Weight loss of Q&P-treated 55Si3Mn2CrVMoNb steel after abrasive testing wear

For other modes, the austenite metastability to SIMT was much lower (M ~ 4–7%). In terms of SiO_2 – wear, the Q&P treatment modes were ranked as follows: #1 (0.0283 g) → #3 (0.0223 g) → #2 (0.0265 g), i.e. the weight loss values were directly proportional to the austenite metastability to SIMT (meaning that SIMT caused a decrease in wear resistance). Meanwhile, the most wear-resistant mode #3 (49 HRC) has exceeded by 11% a much harder (62 HRC) quenched reference sample.

The results obtained showed that RA in Q&P-treated 55Si3Mn2CrVMoNb steel exhibits a different tendency for SIMT depending on the character of strain. Maximum metastability of austenite showed at uniaxial tensile when the deformation strengthening reached the highest value before the bulk fracture. Under Al_2O_3 abrasive wear, SIMT also took place, but it didn't progress as intensively as for tensile strain. It can be assumed that the corundum particles wore the surface not only by plastic deformation (with scratches formation), but also by micro-cutting with a brittle detachment of metal microchips due to the high hardness and sharpness of Al_2O_3 particles. That is, the wear was not always proceeded through intensive strain, therefore austenite largely remained untransformed.

Under SiO_2 abrasive wear, the surface deformation probably didn't reach the critical for SIMT value due to low quartz hardness preventing its deep

penetration to the surface. In this case, the wear occurred in a mechano-chemical form, at lower contact stress within the elastic range. As a result, the surface was destroyed via a multi-cycle fatigue mechanism. This was confirmed by a lower (by an order of magnitude) value of weight loss as compared to corundum (~ 0.008 g/hour for quartz and ~ 0.06 g/hour for corundum). Under SiO_2 conditions, retained austenite showed high stability to SIMT.

It should be noted that under the Al_2O_3 test, all three Q & P modes had approximately the same wear behaviour, despite the different SIMT kinetics. This was associated with Al_2O_3 hardness, which was high enough to intensively destruct the various microstructures regardless of the degree of surface hardening due to SIMT. Under the SiO_2 test, the difference in wear resistance between different Q & P modes was more noticeable. In this case, the microstructure features and SIMT affected wear resistance to a greater extent. In the used wear conditions, the highest wear resistance was attributed to the case of ~ 25 vol.% RA which was rather stable to SIMT (mode # 3).

Bearing in mind that SiO_2 wear proceeded through the contact fatigue mechanism, it was presumed that metastable austenite (mode #1) accelerated the nucleation of fatigue microcracks owing to micro-stress appeared under the volumetric changes caused by SIMT. With that, the growth of the microcracks was facilitated by hard deformation martensite which appeared instead of ductile austenite in course of SIMT. In the case of mode # 3, stable austenite remained untransformed in the structure, ensuring the presence of ductile and tough austenite layers between the martensitic (bainitic) laths inhibiting the fatigue microcracks growth. Importantly, such a structure provided higher wear resistance relative to the quenched state. Summing up, Q & P treatment benefits not only high mechanical properties but also high tribological behaviour of steel.

3.6 Q & P-treated medium-carbon low alloyed steels as candidates in third generation AHSS

In Figure 3.36, a the correlation of tensile strength and ductility for Q & P-treated steels of 60Si2CrV and 55Si3Mn2CrVMoNb grades are presented. Each point refers to a specific Q & P mode. The upper limit of the scatter of experimental points performs the highest values of the PSE index for different strength levels (these values correspond to the maximum ductility values which can be obtained under Q & P treatment). As seen, with increasing UTS the maximum achievable elongation decreases

from 23% (at 1535 MPa) to 9% (at 2370 MPa). The top of the PSE values (35.6–36.5 GPa · %) correspond to UTS of 1400–1900 MPa. In the range of UTS=1900–2100 MPa, the maximum PSE value is 35.0 GPa · %, and in the range of UTS = 2100–2200 MPa, PSE does not exceed 22 GPa · %.

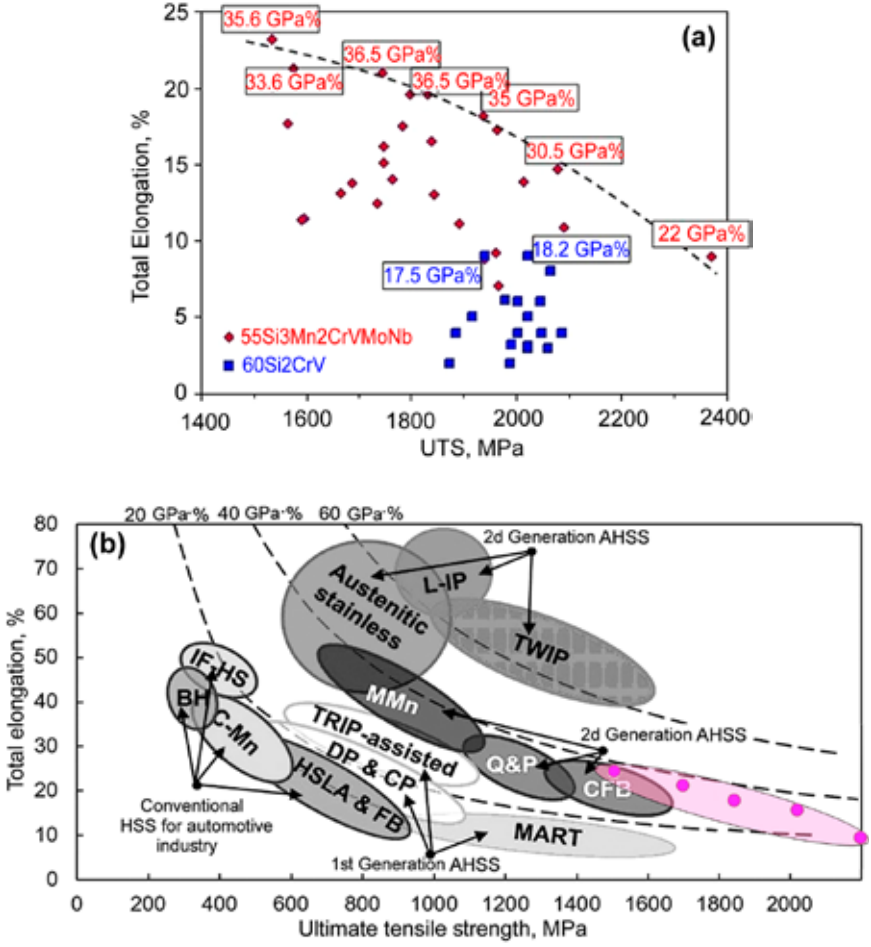

Figure 3.36. (a) "Strength/Ductility" correlation for Q & P-treated 60Si2CrV and 55Si3Mn2CrVMoNb steels, (b) comparison of 55Si3Mn2CrVMoNb steels mechanical properties (red points) with modern high-strength steels

These values represent the high mechanical properties level assured by Q & P treatment, which puts the 55Si3Mn2CrVMoNb steel abreast with the more expensive Cr-Ni high-strength steels (30CrMnSiNi2, 40CrMnSiNi3W, High-Tough, etc.) or Mo-V steels (40Cr5Mo2SiV, HST120 etc.) [4]. The Q & P-treated 60Si2CrV steel performs a reduced (relative to 55Si3Mn2CrVMoNb) complex of properties: the maximum PSE value does not exceed 18.2 GPa · %. However, Q & P-treated 60Si2CrV steel overperforms the same steel subjected to conventional (Q+T) heat treatment. Therefore, one can conclude that Q & P treatment benefits the mechanical properties of the steels belonging to different alloying systems.

Experimental points for Q & P treated 55Si3Mn2CrVMoNb steel, corresponding to the best "Strength/Ductility" combinations, are shown in the diagram in (Fig. 3.36, b) in a pink colour. Apparently, the points distribution falls within the target diagram's area which refers to third generation AHSS. Thus, the development of 55Si3Mn2CrVMoNb steel and its Q & P treatment modes can be considered as a solution to the relevant problem of developing high-strength, cost-saving alloyed steels meeting the requirements of third-generation AHSS.

Chapter 4. Improvement of 0.7–0.8 wt.% C steel performance characteristics using Q&P heat treatment

As shown in the previous chapters, Q&P heat treatment provides a multi-phase heterogeneous structure with high retained austenite content in steels, which improves the mechanical properties combination in the low-alloyed steels. However, in addition to mechanical properties, steel products must have higher performance characteristics regarding the conditions of their use. Such characteristics include, in particular, wear resistance and impact resistance, which is relevant, for example, for grinding balls and linings of drum mills [186]. This chapter is dedicated to investigating the effect of Q&P treatment on some performance characteristics of steels having a carbon content of 0.7–0.8 wt.%.

4.1 Effect of Q&P treatment on abrasive wear resistance of 0.75 wt.% C low-alloyed steel

The effect of Q&P treatment on the wear resistance of steel remains (with a few exceptions [187–189]) poorly illuminated in the research literature, while Q&P technology is promising for wear resistance in a view of obtaining metastable austenite. As shown in [190–193] SIMT occurring under the wear significantly increases the wear resistance of steels and cast irons. In hypereutectoid steels, the required amount of metastable austenite is quite easily achieved by conventional quenching which dissolves carbides thus decreasing M_S point. In steels with a carbon content of less than 0.8 wt.% the obtaining of a significant amount of RA requires additional costly alloying, and in this sense, the Q&P treatment looks perspective for being applied for these class of steels [194–196].

The steel 75CrMn2Si was fabricated in laboratory conditions using a high-frequency furnace (steel chemical composition was given in Table 2.1). The 20 kg ingot was forged and then rolled into a strip 15 mm thick and annealed at 850 °C. The kinetics of austenite transformation was investigated by a magnetometric method while the M_S point was determined by the dilatometric method. The samples of 25x10x10 (mm) size were made for the wear abrasive test. Before the test they were subjected to the Q&P

treatment according to the following schedule: (a) austenitization at 850 °C for 15 min, (b) quenching in boiling water (100 °C) for 10 s, (c) partitioning in a salt bath of a (K_2NO_3+$NaNO_2$) mixture, (d) final cooling in water (20 °C). Wear tests were carried out according to the procedure described in Chapter 2.

The M_S temperature of 75CrMn2Si steel was found as 175 °C. Figure 4.1 presents its TTT-diagram which performs only the pearlite area; below 500 °C, austenite transformation was not detected during the holding of 40 min meaning a sharp inhibition of bainitic transformation [197]. The temperature of the quenching (100 °C) was selected significantly lower M_s in order to obtain a sufficient amount of martensite. According to the Koistenen-Marburger equation, the volume fraction of martensite was 59.3 vol.%. The temperature and duration of holding at the partitioning stage was selected in order to obtain the various combinations of martensite, RA and lower bainite volume fractions. The partitioning was carried out at 250 °C, 300 °C and 350 °C for 1 min, 5 min, 10 min, 20 min, and 30 min.

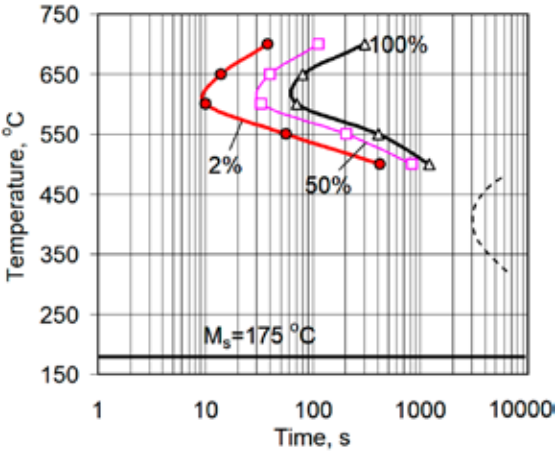

Figure 4.1. TTT-diagram for 75CrMn2Si steel

The effect of partitioning parameters on hardness of Q&P-treated samples was studied in comparison with fully quenched sample (Figure 4.3). The quenched sample had hardness of 63 HRC, but after 1 min of holding at each temperature, its hardness decreases substantially with further slow leveling after 10 min holding. In Q&P samples, after a rather sharp decrease in the first 10 min, the hardness gradually decreased during entire holding (up to 30 min). For any temperature and holding du-

ration, the quenched specimens performed higher hardness than Q & P specimens; a particularly large difference in hardness was noticed for 350 °C. With holding temperature hardness decreased both for the quenched and for the Q & P-treated specimens.

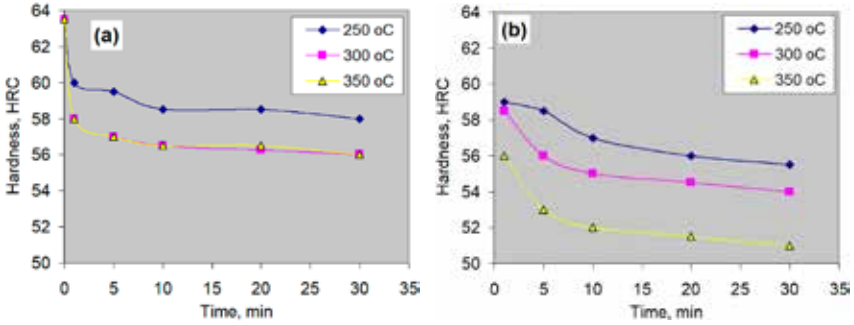

Figure 4.2. Effect of holding duration on hardness of 75CrMn2Si steel: (a) quenched samples and (b) Q & P-treated samples

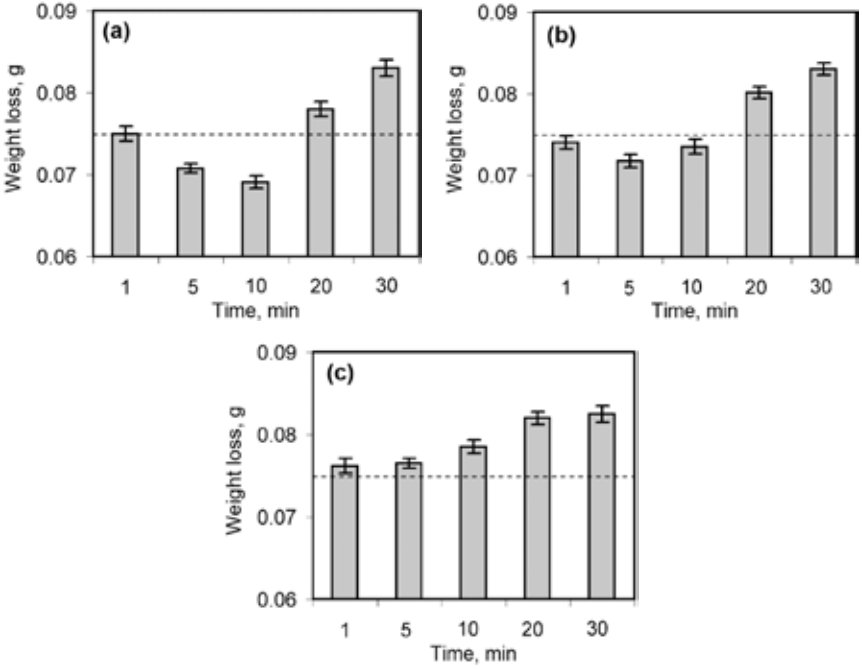

Figure 4.3. Effect of holding duration under partitioning on weight loss of Q & P-treated 75CrMn2Si steel

The results of the abrasive wear test are presented in Figure 4.3. Steel 75CrMn2Si fully quenched and tempered at 200 °C was used as a reference; its weight loss was 0.0765 g. A similar weight loss (0.075 g) was obtained after Q & P with partitioning at 250 °C for 1 min; with increasing the holding time to 5 min and 10 min, the weight loss gradually decreased to 0.071 g and 0.069 g, respectively, despite the progressive decrease in hardness (Fig. 4.3, a). With duration increase to 20 min and 30 min, the weight loss sharply increased to 0.078 g and 0.083 g, respectively, exceeding the weight loss of the reference sample.

A similar wear behaviour with holding duration was also recorded for Q & P samples partitioned at 300 °C (in this case the minimum weight loss (0.072 g) referred to 5 min holding). With regard to the samples treated at 350 °C, at a holding time of 5–30 min, their weight loss exceeded that of the reference sample. At maximum duration (30 min), all Q & P samples came to the same (maximal) weight loss (0.082–0.083 g) regardless of partitioning temperature. Thus, the best wear performance of Q & P-treated 75CrMn2Si steel was attributed to partitioning at 250 °C for 10 min.

For most of the samples, the microstructure consisted of fine-needle martensite with needles 4–8 μm long (Fig. 4.4); some isolated areas of retained austenite were evenly distributed between the martensitic needles. With the increase in partitioning duration, martensite was more intensively etched because of its decomposition with the dispersed carbides release. Samples Q & P-treated at 250 °C retained a martensite-austenite structure regardless of the holding duration (Fig. 4.4, a). With increasing temperature and duration of partitioning, the RA amount visually decreased, and the needle pattern of martensite became less pronounced (Fig. 4.4, b). At 350 °C, austenite was fairly well revealed in the structure only after 1 min of holding; at longer holding the structure lost its needle-like pattern (Fig. 4.4, c).

According to the data in Fig. 4.5, after 5 min holding at 250 °C, the RA volume fraction was 15 vol.%, and after holding of 10 min, its amount increased by 2 times exceeding RA amount in the reference sample (11 vol.%). With further holding, the RA volume fraction decreased to 22 vol.% with the simultaneous appearance on the XRD pattern of the weak peaks (121) and (211) characteristic of cementite carbide. The latter indicated a partial release of carbon during the decomposition of austenite, which corresponded to a decrease in RA amount.

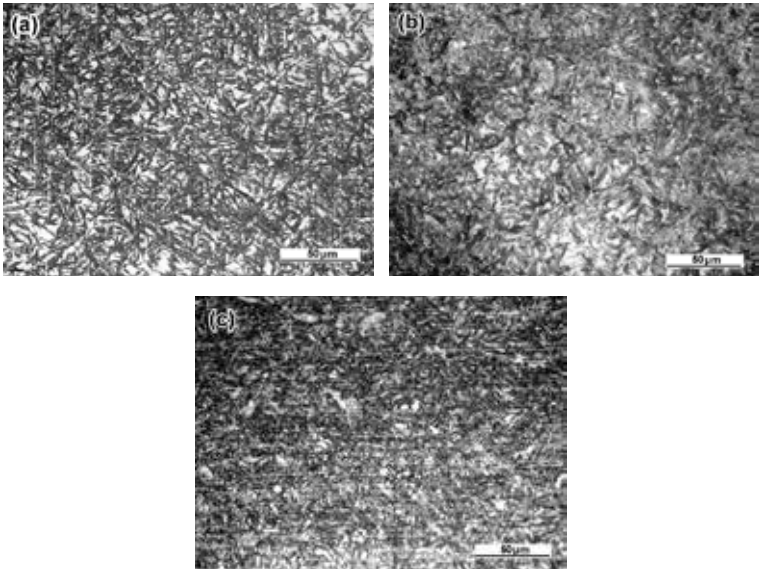

Figure 4.4. Microstructure of 75CrMn2Si steel after Q&P treatment with 30 min partitioning at (a) 250 °C, (b) 300 °C, and (c) 350 °C

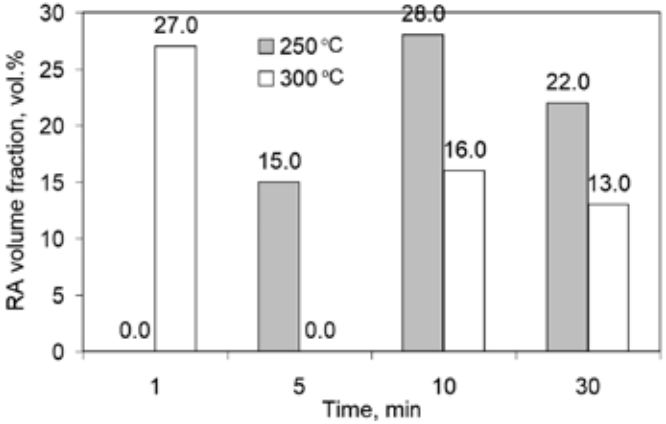

Figure 4.5. Variation in RA volume fraction depending on partitioning duration

Activation of carbon diffusion mobility by increasing partitioning temperature resulted in a sharp acceleration of carbon partitioning. This was followed by an increase in RA amount up to 28 vol.% after 1 min holding at 300 °C. With further holding, the RA amount gradually decreased to 13

vol.% (30 min). In this case, the cementite reflexes were present on XRD patterns regardless of the holding duration; the early appearance of cementite carbide was associated with the carbides precipitation from both austenite (decomposition) and martensite (tempering). Thus, under Q&P treatment the following processes took place in 75CrMn2Si steel: (a) carbon partitioning from martensite to austenite with its C-enrichment, (b) martensite tempering with cementite precipitation, (c) austenite decomposition via bainite mechanism (γFe → αFe + Fe_3C), (d) the partial transformation of austenite into "fresh" martensite upon final cooling. At higher temperature and prolonged partitioning, a complete austenite transformation is possible; in this case, the process "d" is absent. Thus, in Q&P-treated 75CrMn2Si steel, there may be a different combination of structural constituents, namely: (a) tempered martensite, RA, "fresh" martensite, b) tempered martensite, RA, bainite, "fresh" martensite; c) tempered martensite, bainite.

In the case of partitioning at 250 °C, the microstructure formation refers to the variant "a". According to Fig. 4.2 a, Q&P samples had lower hardness compared to the reference. With holding duration a difference in hardness between the Q&P sample and quenched sample gradually increased from 1.0 HRC (1 min) to 2.5 HRC (30 min). This was due to low carbon diffusion from martensite to austenite at 250 °C, and the austenite gradually stabilized as the holding duration increased. Obviously, at this temperature austenite decomposition (bainite transformation) progressed slowly, which was confirmed by the microstructural study.

At 300 °C, carbon diffusion and austenite C-enrichment were accelerated sharply. Already after 1 min holding, the RA volume fraction reached about 30 vol.%; however, the Q&P sample hardness slightly exceeded that of the quenched sample. In this case, the martensite of the quenched sample decomposed fast with the carbides release (which caused a sharp decrease in its tetragonality and a drop in hardness from 63.5 HRC to 58.0 HRC). At the same time in the Q&P sample carbon partitioned from martensite to austenite without carbide precipitation thus preventing fast loosing of martensite lattice tetragonality. With holding duration increase, the hardness of the Q&P sample became lower than that of the quenched sample being caused by a gradual "austenite → bainite" transformation, followed by a decrease in the "fresh" martensite amount. Therefore, the microstructure formed at 300 °C referred to variant "b". During holding at 350 °C, the mentioned above processes progressed so fast that after 30 min holding the austenite was fully transformed into

bainite which provided a hardness decrease. In this case, the microstructure referred to variant "c".

The decrease in RA amount during holding at 300–350 °C pointed to the fact that the presence of martensite accelerates the bainitic transformation. According to TTT-diagram, bainite transformation in 75CrMn2Si steel at 300–450 °C was not detected during the holding for 40 min. However, with Q&P treatment, bainite transformation was almost completed after 30 min of holding at 350 °C. The reason for such a sharp acceleration of transformation was the presence in Q&P samples of 59.3% martensite which (through the strain) facilitated the nucleation of the α-phase in austenite. According to Bhadeshia [198], the quenching-induced stresses (except the hydrostatic compressive ones), significantly accelerate bainitic transformation in steels. As shown in recent studies [162], another possible reason of the acceleration of bainitic transformation is an emerging of aFe nuclei on the "Martensite-Austenite" interphase boundary.

The alteration of microstructure under Q&P treatment influenced the abrasive wear resistance of 75CrMn2Si steel (Fig. 4.3). The decrease in weight loss relative to the reference was atributted to the initial stages of partitioning at 250–300 °C. The highest wear resistance referred to partitioning at 250 °C for 10 min. This behaviour is explained by formation of higher amount of retained austenite which transforms into martensite during the wear process. Despite the fact that under partitioning at 250 °C the austenite retained in the structure irrespective the holding duration, the weight loss of steel altered along the curve with a minimum corresponding to 10 min holding. The going down of this curve was related to the increase in the metastable austenite amount, while going up was caused by austenite stabilization to SIMPT due to its carbon saturation [196]. The austenite transformation to bainite, which occurred at 300 °C and 350 °C, led to a sharp decrease in steel wear resistance.

The presented results showed that Q&P treatment at the optimum mode allowed to increase the abrasion resistance of 75CrMn2Si steel by 8%. It was due to the formation of a multi-phase structure, consisting of different hardness phases. The combination of tempered martensite, "fresh" martensite, and ductile austenite enhanced the resistance to brittle fracture which is beneficial for steel mechanical properties and operational behavior.

4.2 Improving the exploitation performance of steel grinding balls through Q & P-based heat treatment

Grinding balls are widely applied in processing operations in mining, metallurgical, energy, cement, and building industries [199]. The grinding balls are loaded into the drum mill to grind up the various mineral raw materials (ore, clinker, coal, crushed stone, etc.) to prepare them for further processing. Since the minerals, as a rule, have increased hardness and abrasiveness, the balls undergo intensive wear during the operation. The largest volume of consumption is accounted for a large-diameter ball (100––120 mm), the specific consumption of which at the mining and processing enterprises of Ukraine reaches 1.5 kg per ton of processed material [200, 201]. The wear of the balls requires permanent loading of fresh balls into the mill which is very costly. Therefore, the balls are required to have much higher exploitation durability to reduce operational costs. This task is very relevant, especially for the mining and metallurgical industries enterprises.

It is known that there is a direct relationship between the balls' hardness and their operational durability, so the grinding balls' quality is usually evaluated by their hardness level. Standard of Ukraine DSTU8538 : 2015 regulates the production of rolled (forged) steel balls ranging them into five groups of quality. As the group number increases, the minimum values of surface and bulk hardness of the balls increase as well. To increase hardness the balls are subjected to thermal hardening which means the heat treatment using rolling (forged) heat [202]. Just after the rolling (forging) the balls are quenched in the water while the quenching is interrupted to retain some heat inside the balls. Due to this heat, the balls undergo tempering (self-tempering) being collected in the bunker [203]. Depending on the ball diameter, its chemical composition, and thermal hardening mode, the ball gain different surface hardness and different hardness gradient in its bulk. The balls of 100 mm and 120 mm in diameter should have a surface hardness of at least of 52 HRC and 50 HRC, respectively, to comply with the requirements of the 3rd Group of DSTU8538:2015.

The aforementioned high wear rate of grinding balls at Ukrainian mining and processing enterprises is explained by their low bulk hardness, which is a consequence of the uneven hardness gradient in the ball's cross-section. When the balls of 100–120 mm diameter are produced of steel of chemical composition 0.68–0.80 wt.% C, 0.80–1.25 wt.% Mn, 0.17–0.50 wt.% Si, then the depth of the hardened (quenched) layer does not exceed

10 mm while the bulk hardness is only 45–47 HRC [204, 205]. For such balls, the hardness gradient in cross-section is shown in Figure 4.6.

The bulk hardness of the balls can be increased by the complex alloying of steel by Mn, Cr, and Mo [206–208]. This increases the austenite stability in both the pearlite and bainite transformation areas thus ensuring the increase in quenching depth in the balls. Cr and Mo are quite costly elements; therefore their content in steel should be minimal [209]. In view of the foregoing, for the production of an experimental batch of 100 mm diameter balls with increased quenching depth, the experimental 75CrMn steel was proposed with the following chemical composition: 0.72–0.78 wt.% C, 0.25–– 0.35 wt.% Si, 0.85–0.95 wt.% Mn, 0.55–0.65 wt.% Cr, 0.05–0.10 wt.% Mo.

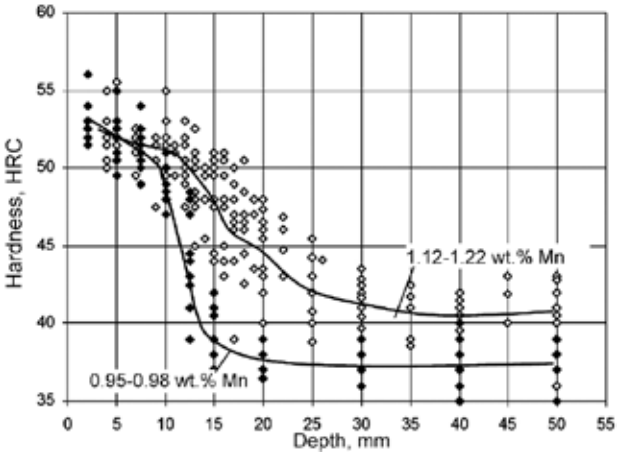

Figure 4.6. The hardness gradient in grinding steel balls made of C–Mn steel with different manganese content

The production of grinding balls with high bulk hardness is faced with the problem of the hardening cracks emerging in the balls. It is known that water quenching causes significant residual stresses in the steel products leading to cracks and distortion. In order to prevent the quenching cracks in the balls, water quenching is stopped when some heat remains in the bulk. After equalizing the temperature within the ball it acquires an averaged (equalized) temperature (T_{eq}) of 200–250 °C. With this temperature, the balls are kept in the storage bunker for self-tempering to release the stresses and prevent cracking [210]. The large diameter balls (with a diameter of ≥ 60 mm) made of Mn-Cr steel are prone to quenching cracks because of the formation of martensite structure in the entire cross-section

including a center [211, 212]. The probability of crack formation increases with the ball's diameter. In though-hardened balls of < 60 mm diameter, cracks do not appear. In larger diameter balls, in the case of the above-mentioned thermal hardening mode, the surface cracks occur immediately upon completion of self-tempering. Cracked balls are not allowed to use in mills as they intensively spall and break thus reducing the mill's operational performance.

The reason for the appearance of the cracks in the through-hardened balls is the unfavorable distribution of residual stresses, namely compressive stresses in the ball's center, and tensile stresses on the surface. This stress situation occurs due to the time lag between the austenite transformation in surface layers and in the bulk. When using the conventional mode of thermal strengthening (T_{eq} = 220–240 °C), under the quenching stage the martensitic transformation proceeds only in the surface layers to a depth of 10–15 mm while austenite remains untransformed in the ball's inner bulk. Under self-tempering, this austenite transforms to bainite or martensite increasing the volume in the central layers. This leads to deformation of the surface layers providing in there high tensile stress. The relaxation of these stresses is not possible since the ball temperature decreases significantly to this moment. These stresses cause the superficial cracks either after the ball's extraction from the bunker or during its storage in the warehouse (the incubation period of cracks formation may extend for several weeks [210]).

Based on the above, preventing cracks in the through-hardened balls is possible by lowering the amount of overcooled austenite in the balls before the onset of self-tempering. This approach requires longer quenching as compared with the standard mode thus the temperature in each ball's layers must fall below the M_S. The full elimination of austenite in the ball bulk can be achieved by cooling in water to room temperature, however, this can cause high quenching stresses with immediate cracking. Therefore a specific "austenite/martensite" volume ratio should be obtained in the balls' internal to the moment of quenching interruption to equalize the stresses inside the ball. Taking the lower austenite's specific volume compared to martensite, this will reduce the tensile stress level on the ball surface thus preventing the rapid appearance of the cracks. For stress relaxation and insurance of cracking absence, the quenched balls should be tempered eventually.

The formulated considerations for the thermal hardening of the through-hardened balls are essentially in line with the Q & P principle since

the temperature in each ball's layers must decrease below the M_S leading to martensite transformation in the entire volume of the ball. Obtaining an austenite-martensitic structure at the quenching stage and subsequent partitioning may result in an increase in the retained austenite amount in the ball center, which will further reduce the residual tensile stresses level on the surface. The successful application of Q & P heat treatment for 80 mm diameter high-Cr cast-iron balls is described in [213], but the use of the Q & P principle regarding the heat treatment of the steel grinding balls remained unexplored being of scientific and practical interest.

The above propositions were tested in manufacturing conditions during the production of the through-hardened 100 mm diameter grinding balls made of 75CrMn steel (the chemical composition of steel melt was 0.72 wt.% C, 0.37 wt.% Si, 0.89 wt.% Mn, 0.60 wt.% Cr, 0.14 wt.% Mo, 0.020 wt.% S; 0.020 wt.% P [214, 215]). The round billet was heated to 950–1000 °C and subjected to cross-helical rolling to form the ball shape. The rolled balls were cooled in the air for 160–190 s to 790–815 °C, afterwards, they were quenched in water (20–22 °C) in a drum-type device [216] according to various modes (Table 4.1).

Table 4.1. Effect of heat treatment mode on the surface hardness and tendency to crack (tempering duration of 10 hours)

Mode number	Quenching duration, s	Equalizes temperature (T_{eq}), °C	Cracks after air cooling	Tempering temperature (T_{temp}) °C	Hardness/ cracks after tempering
1	250	20	yes	–	61/yes
2	150	110–120	yes	170	58/yes
				200	57/no
				250	55/no
				300	52.5/no
3	135	125–135	no	200	57.5/no
				250	55.5/no
4	115	150–170	no	200	57.5/no
				250	55/no
5	80	220–240	yes	250	55/yes

The modes differed in cooling duration in order to change the T_{eq} temperature. Mode # 1 corresponded to the complete cooling of the balls in water, modes # 2, #3, and #4 ensured that T_{eq} (110–170 °C) is below

M_S (227 °C for 75CrMn steel), and mode # 5 ensured that $T_{eq} \sim M_S$. Thus, modes # 2–#4 met the Q & P principle, while mode # 5 corresponded to the standard thermal strengthening technology applied for the balls of the 3rd group. The T_{eq} temperature (measured with an optical pyrometer) was taken to be the maximal surface temperature that the quenched ball acquires after the heat redistribution in its volume 1.5 min after its removal from water. After quenching the balls were quickly (within 5–10 min) transferred to an electric furnace to be tempered at 170–300 °C for 2––10 hours. Some quenched balls were cooled in calm air without tempering. After heat treatment, the balls were visually inspected for hardening cracks presence. The microstructure and cross-sectional hardness gradient were investigated on the sample cut through the ball center. The balls impact resistance was evaluated on the installation according to the method described in section 2. The bulk hardness was calculated according to equation (4.1) [217]:

$$H_{Bulk} = 0.289 \cdot H_{surf} + 0.436 \times H_{0.25R} + 0.203 \cdot \\ \cdot H_{0.5R} + 0.063 \cdot H_{0.75R} + 0.009 \cdot H_{centre}, \quad (4.1)$$

where H_{surf} $H_{0.25R}$, $H_{0.5R}$, $H_{0.75R}$, H_{centre} are the hardness values measured on the surface and at a distance of 0.25R, 0.5R, 0.75R and in the centre of the ball (R is a ball's radius).

It was found that in the balls, cooled in water to room temperature (T_{eq} = 20 °C, mode # 1), cracks appeared within 2–5 min after quenching, i.e., on the way to a furnace for tempering (cracks are shown in Fig. 4.7, a). In the case of T_{eq} = 110 – 120 °C, the air-cooled balls (no tempering) were cracked when their temperature reduced to 65–70 °C. Tempering at 170 °C decreased their stress level but did not prevent cracks: 2–4 hours-tempered balls cracked 1 day after tempering, and 10 hours-tempered balls cracked 2 days hours tempering. Increasing the tempering temperature to 200––300 °C completely prevented cracking even with a minimum heating duration; cracks did not appear on such balls even a month after tempering.

In the case of modes # 3 and #4, cracks did not appear in the balls either when cooled in the air (without tempering) or after tempering at 200–250 °C. In the case of mode # 5 cracks appeared both after air cooling and after tempering at 250 °C (Fig. 4.7, b).

The surface hardness of the tempered balls varied in the range of 57.0––57.5 HRC (200 °C), 54.5–55.5 HRC (250 °C), 52.5 HRC (300 °C). The balls treated according to modes #2–#4 and tempered at 200–300 °C,

withstood impact tests at 8 impacts without cracks or breakage; some of them were successfully tested at 16–24 impacts, that is, with a 2–3-fold excess of standard impact amounts (Fig. 4.8, a). The ball of mode # 2 (tempering at 170 °C, 10 hours) with a surface crack was broken on the 7 th impact. The balls, which were processed according to modes # 1 and # 5 (having cracks on the surface), were broken on the 2th– 4th impact (Fig. 4.8, b).

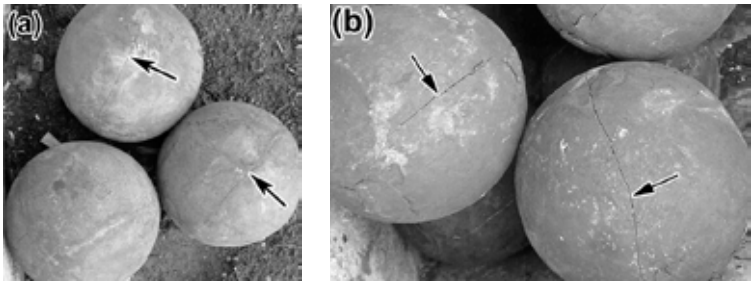

Figure 4.7. Cracks on the balls' surface processed according to the modes: (a) # 1, (b) # 5 (250 °C tempering)

Regardless of the heat treatment mode all inspected balls had even hardness distribution at the cross-section while the maximum gradient between the surface layers and the center was not higher 1.5 HRC after tempering at 200–250 °C and not higher 4 HRC after tempering at 300 °C (Table 4.2). Non-tempered balls had a hardness of 60–62 HRC through all cross-section. The balls' bulk hardness decreased from 56.9 HRC to 49.6 HRC as the tempering temperature increased from 170 °C to 300 °C.

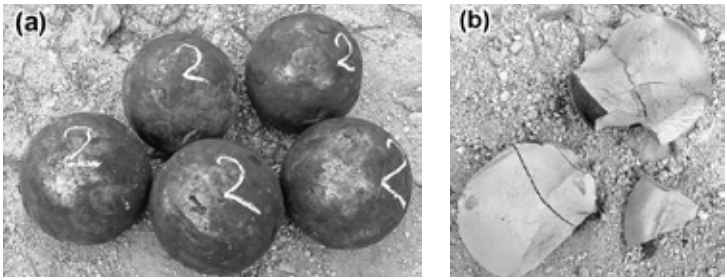

Figure 4.8. Balls after impact tests: (a) processing the mode # 3 (T_{temp}=200 °C), (b) processing the mode # 5 (T_{temp}=250 °C) (had a surface crack before the impact test)

The macrostructure of the balls was studied after deep hot etching with 50 vol.% aqueous HCl reagent. As follows from Fig. 4.9, the balls

had a dense structure with minor point liquation. Flakes and other defects of metallurgical origin were not found in the balls. Grinding-etching cracks (Fig. 4.9, a-c) were present on the samples of the balls treated according to modes # 1, # 5, and # 3 (T_{temp}=200 °C tempering), in the latter case the number of the cracks was minimal. Cracks were not detected on the samples of the balls treated according to mode # 4 (T_{temp}=200 °C tempering).

Table 4.2. Cross-section hardness distribution and bulk hardness (H_{Bulk}) of balls (tempering for 10 hour) (HRC)

T_{eq}, °C	$T_{temp.}$, °C	Distance from the surface, mm									H_{Bulk}
		5	10	15	20	25	30	35	40	50	
110–120	–	62	62	61	62	60	60	60	60	60	61.0
	170	58	57	57	57	56	57	57	57	56	56.9
	200	57	57	57	56	56	56	55	57	56	56.4
	250	56	56	55	55	54	54	55	55	54	54.9
	300	52	50	49	48	48	47	48	47	47	49.6
125–135	–	62	62	62	62	61	61	62	61	61	61.6
	200	57	56	57	57	56	57	57	57	57	56.7
	250	54	54	54	54	54	54	54	54	53	54.0
150–175	–	60	60	61	60	59	60	60	59	60	59.8
	200	56	56	57	57	56	56	57	56	56	56.2
	250	55	55	55	55	55	55	54	55	55	54.7
220–240	250	54	55	55	54	54	54	54	53	53	54.2

The metallography study showed (Figs. 4.11 and 4.12) that the balls heat-treated by modes #2, #3 and #4 had a heterogeneous structure with alternation of dark and light zones (this structure was found at the depth of more than 10 mm from the surface). The dark zones were formed by tempered martensite, while light areas had a needle-like structure well identified on the austenite background.

The microhardness of the tempered martensite and the martensite-austenite areas were 482–535 and 566–598 HV respectively (Table 4.3). The higher microhardness of the latter was due to the presence of "fresh" martensite formed after tempering completion.

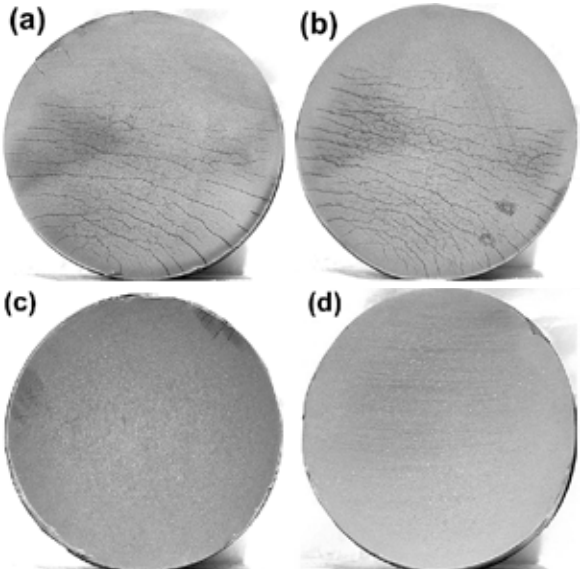

Figure 4.9. Macrostructure of 100 mm diameter balls after heat treatment by the modes (a) # 1, (b) # 5 (T_{temp}=200 °C), (c) # 3 (T_{temp}=200 °C), (d) # 4 (T_{temp}=200 °C)

Table 4.3. Microhardness (HV_{50}) of microstructural components in balls with different hardness levels

Cross-sectional hardness of the ball, HRC	Microstructure	
	Tempered martensite	Martensite + austenite
50–52	482.2 ± 20	566.0 ± 17
54–55	519.2 ± 13	598.4 ± 24
56–57	535.3 ± 22	596.2 ± 24

The presence of retained austenite in different layers of the ball, detected visually in the microstructural study, was confirmed by X-ray diffraction. XRD study revealed that in the ball processed by mode #3 (T_{temp} = = 200 °C) the volume fraction of retained austenite was 8 vol.% at a depth of 5 mm, 25 vol.% at a depth of half of, 30 vol.% in the ball center.

The presented results showed that modes #2–#4 (except the tempering at 170 °C) ensured high hardness in the balls' cross-section without the cracks' absence. The bulk hardness was 54.0–56.7 HRC (T_{temp} = 200– – 250 °C), which is almost by 10 HRC higher compared to standard balls.

The experimental balls had a high impact resistance, which was beneficial for their operation in heavy-duty mills.

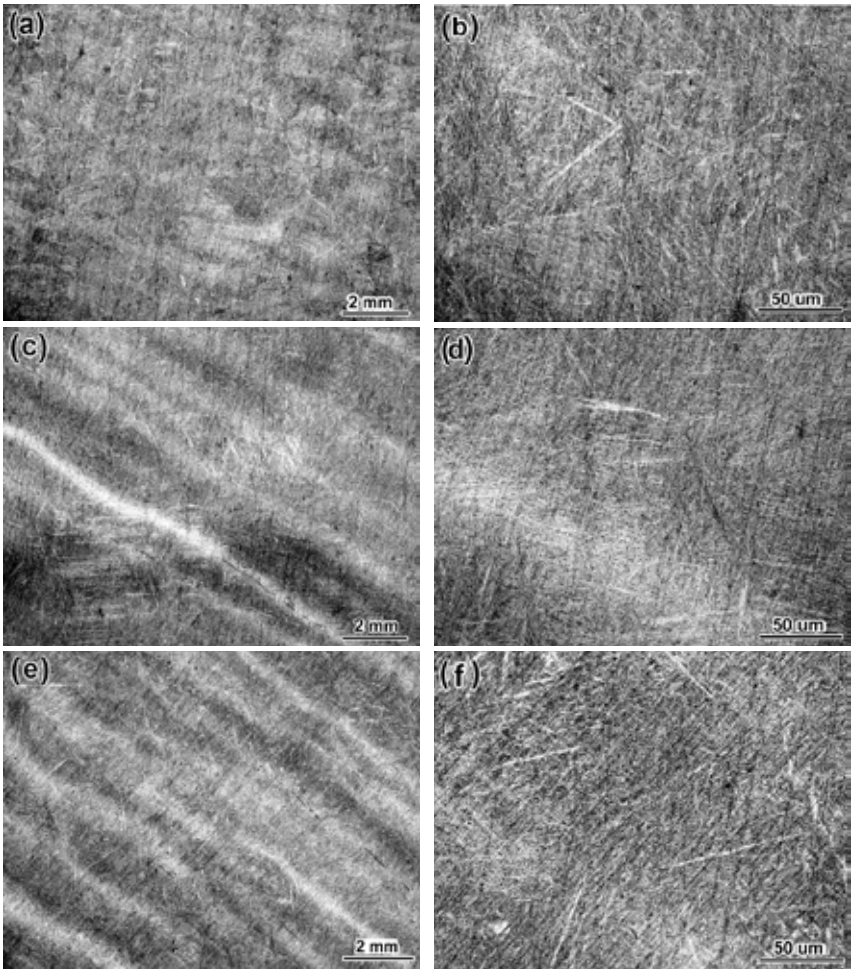

Figure 4.10. Microstructure of a ball treated according to the mode # 2 (T_{temp}=170 °C, 10 hour) at a depth of (a, b) 5 mm, (c, d) half of radius, (e, f) in the center

The absence of the quenching cracks in the balls treated according to modes #2–#4 was due to the optimum microstructure distribution within the balls before the quenching interruption, which was predominantly martensite in the surface layers and austenite-martensite in the central lay-

ers. To determine the austenite/martensite ratio on the ball's cross-section during the quenching, computer simulation was applied [218, 219].

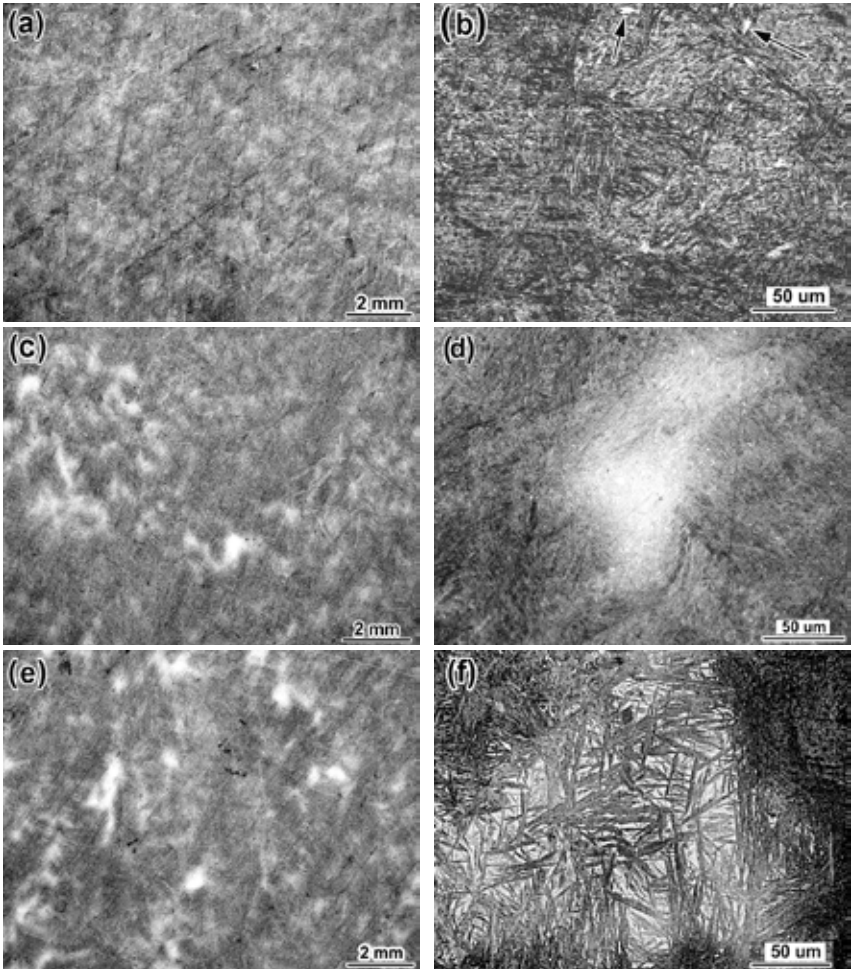

Figure 4.11. Microstructure of a ball heat-treated according to the mode # 3 (T_{temp} = 200 °C, 10 hour) at a depth of (a, b) 5 mm, (c, d) half of radius, (e, f) in the center

The quenching process simulation (Fig. 4.12) revealed that upon the heat-treatment according to the standard technology, the martensite transformation takes place only to a depth of ≤15 mm while only to the depth of 5 mm the martensite amount was of 60–70 vol.%. Thus, in the case of

thermo-hardening according to standard technology, the balls had an austenitic structure in its bulk to the moment of quenching interruption.

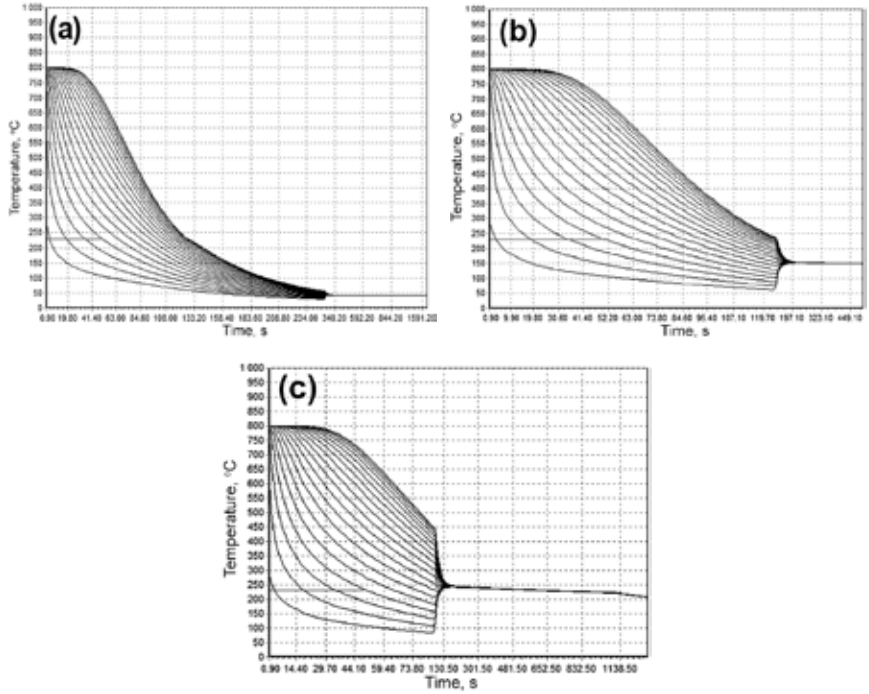

Figure 4.12. The computer simulation of temperature distribution in the 100 mm ball (75CrMn steel) heat-treated according to the modes (a) # 1, (b) # 4, (c) # 5

This state referred to compressive stress on the ball surface and a tensile stress in its center (Fig. 4.13, a). During the tempering process, the austenite is partially transformed into bainite in the central layers; the remaining austenite is transformed into martensite during cooling after tempering followed by the specific volume growth in the central layers. This causes a change in the stress character which turns to tensile stresses on the ball surface.

In the case of mode #4, the martensite transformation extends to a depth of up to ~ 40 mm from the surface, i.e. it covers most of the ball bulk. This results in a balanced stress state, which is characterized either by the absence of tensile stresses on the surface or by their low level not causing cracks (Fig. 4.13, b). Therefore, under modes with T_{eq} = 130–170 °C, the

balls were not cracked not only after tempering but also when cooled in air, i.e. without tempering.

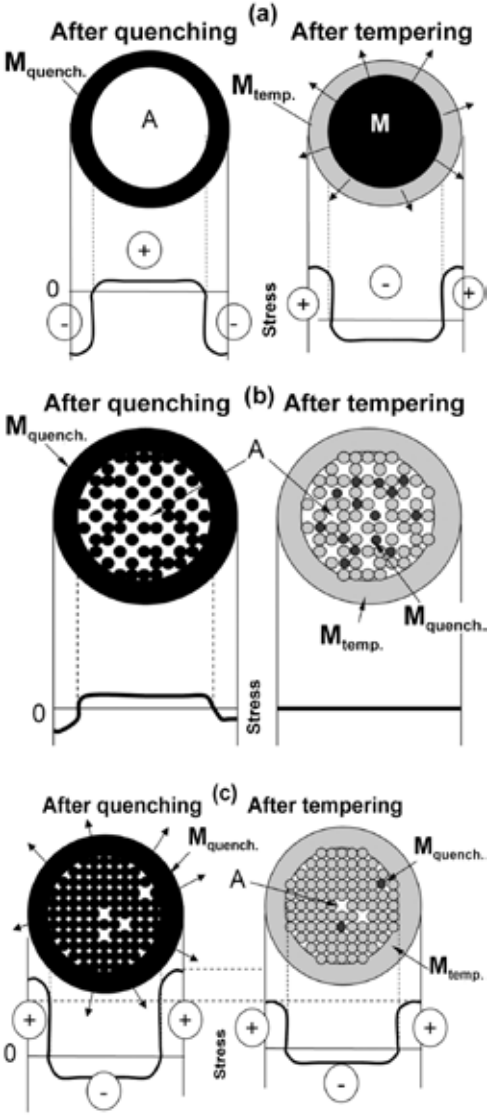

Figure 4.13. Scheme of microstructural components and stresses distribution after quenching and tempering by the modes (a) # 5, (b) # 4, (c) #2

Increasing the quenching duration (which causes a decrease in T_{eq} to 110–120 °C) leads to an increase in the martensite fraction in the central layers of the ball. Its content varies from 85 vol.% on the surface to 45 vol.% in the center of the ball. The appearance of a large amount of martensite in the center leads to high tensile stresses on the surface (Fig. 4.13, c), causing the ball cracking for cooling both in air and after tempering at 170 °C. That means that at T_{temp} = 170 °C the stress relaxation is not sufficient to prevent cracking. If the ball is cooled in water for 250 s, a mostly martensitic (≥ 85 vol.%) structure is formed throughout the ball's section. As a result, the high tensile stresses occur on the surface exceeding the steel's tensile strength followed by cracking just after the quenching completion (Fig. 4.13, c).

Thus, the heat treatment according to the parameters within modes #2–#4 guarantees the cracks' absence in the tempered balls.

It can be assumed that at the tempering stage some part of austenite in the central layers transformed into lower bainite. In addition, there was a carbon redistribution from martensite to austenite with the enrichment of the latter. This assumption is supported by the XRD study results which showed that the carbon content of retained austenite in the ball center was 1.12%, which is 1.55 times higher than the average carbon content in the steel. Carbon enrichment stabilized austenite to bainitic transformation, resulting in austenite partial transformation into martensite after tempering, and partial retaining in the structure in a considerable amount (25–30 vol.%). This formed the "light" needle areas in the structure shown in Fig. 4.11–4.13. Since austenite has a much lower specific volume (compared to martensite), increasing the RA amount in the bulk reduced the tensile stresses on the surface, preventing cracks formation. In the surface layers up to a depth of 10 mm, the RA amount was much lower (5–10 vol.%), because under the quenching the temperature reached there a minimum level leading to the development of martensite transformation.

The optimal parameters of heat treatment of 100 mm diameter balls made from 75CrMn steel were determined as follows: (a) post-rolling cooling in the air for 160–190 s to reach a temperature of 790–820 °C, (b) the water quenching for 125–135 s to achieve T_{eq} = 140–170 °C, (c) tempering at 200–250 °C for at least 1 hour. This mode provided in the balls: (a) even hardness of 54–58 HRC within a cross-section with a minimum hardness gradient of less than 2 HRC, (b) high impact resistance, and (c) the absence of cracks on the balls.

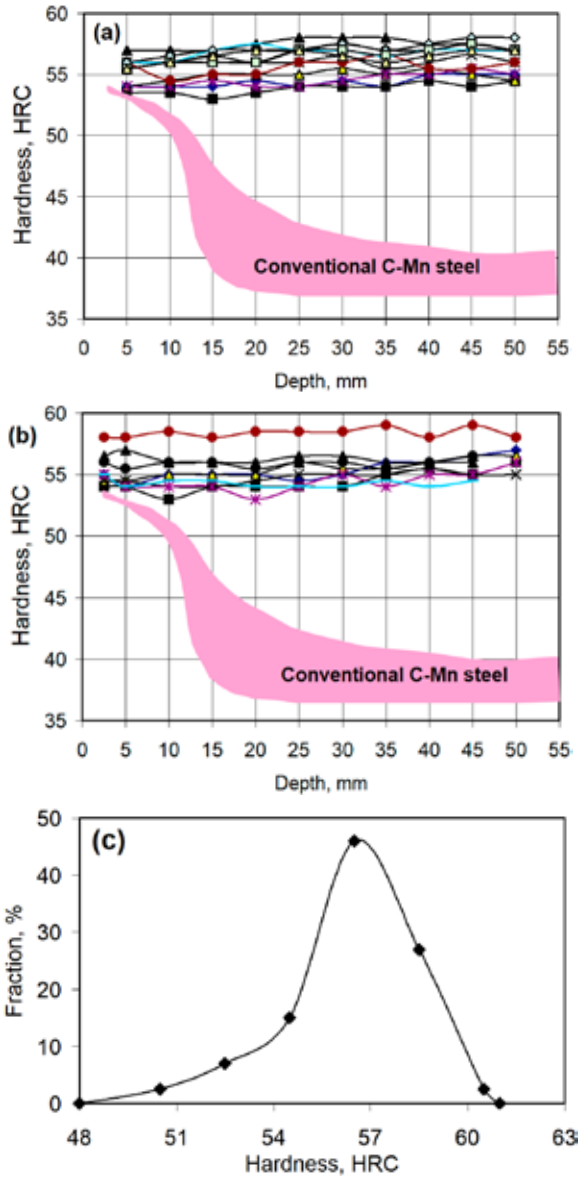

Figure 4.14. The hardness of the 100 mm diameter balls (75CrMn steel) from a pilot batch: (a, b) hardness profiles in the balls of different controlled groups, (c) generalized distribution of bulk hardness values among the pilot batch

Pilot-industrial testing of the above technology of 100 mm diameter balls heat treatment with a cross-sectional hardening was carried out in the conditions of the rail rolling workshop of "Azovstal Iron and Steel Works" [220]. Since the workshop was not equipped with a furnace for tempering, it was proposed to use for this purpose a storage bunker partially (by 30–50 vol.%) filled with the just-rolled conventional balls, the temperature of which approximately corresponded to the tempering temperature (220–250 °C). The proposed technology envisaged the following steps: (a) preparation of the bunker for tempering of the experimental balls (filling it by 30–50 vol.% (50–60 t) with conventionally produced balls with a T_{eq} of 220–250 °C), (b) laying the dividing steel grid above the conventional balls, (c) filling the bunker by 75CrMn steel balls treated with a T_{eq} of 140–170 °C (in the amount of ~50 t), (d) tempering the balls in the sealed bunker for 48 hours. Upon finishing the heat treatment, the 75CrMn steel balls were reloaded into a separate bunker for quality control and testing. According to the adopted scheme, the tempering of 75CrMn steel balls was provided due to the heat irradiated by the hot "bed" of conventional balls.

The above technological scheme was used to manufacture 635 t of 100 mm diameter balls made of 75CrMn steel. The equalized temperature of the balls varied in the range of 149–178 °C with an average value of 159.4 °C. After two days of tempering (after removing the lid) the temperature of the balls in the center of the bunker was 200–230 °C while the temperature of the balls lying along the bunker's walls was only 160–170 °C. The temperature distribution resulted in some difference in the balls' hardness: it was 53.5––55.0 HRC in the bunker's center and 56–59 HRC – next to the bunker's walls.

The hardness profiles on the experimental balls' cross-section are presented in Fig. 4.14. It is seen that the uniform hardness was recorded throughout the cross-section varying in the range of 53.5–58.0 HRC. Accordingly, the ball bulk hardness varied from 50.6 to 60.1 HRC with an average value of 55.2 ± 0.6 HRC. For the most part (48%) of the balls had a bulk hardness of 57 HRC (Fig. 4.14, c). At the same time the bulk hardness of the conventional balls was only 45–47 HRC. All the controlled balls (30 pcs) have passed the impact test without breackage (Fig. 4.15).

The periodic inspection carried out during the month after heat treatment showed that the experimental balls were free of cracks. The manufactured batch of 75CrMn steel balls was shipped to consumers (the mining and processing enterprises of Ukraine). Thus, the performed study has shown that the use of the Q & P principle allowed to increase the balk

hardness by 10 HRC in the large diameter balls while preventing cracks and maintaining a high impact resistance.

Figure 4.15. The view of 100 mm diameter balls made of 75CrMn steel after the impact test

References

1. Qian L., Zhou Q., Zhang F., Meng J., Zhang M., Tian Y. Microstructure and mechanical properties of a low carbon carbide-free bainitic steel co-alloyed with Al and Si. *Materials & Design*. 2012; 39: 264–268.
2. Nie Y. H., Fu W. T., Hui W. J., Dong H., Weng Y. Q. Very high cycle fatigue behaviour of 2000 MPa ultra-high-strength spring steel with bainite–martensite duplex microstructure. *Fatigue & Fracture of Engineering Materials & Structures*. 2009; 32(3): 189–196.
3. Gao G., Zhang H., Gui X., Luo P., Tan Z., Bai B. Enhanced ductility and toughness in an ultrahigh-strength Mn-Si-Cr-C steel: The great potential of ultrafine filmy retained austenite. *Acta Materialia*. 2014; 76: 425–433.
4. Gol'dshtejn M.I., Grachev S. V., Veksler Ju. G. *Special'nye stali*. – Moscow: MISIS; 1999. (in Russian).
5. Fonstein N. *Advanced high strength sheet steels: physical metallurgy, design, processing, and properties*. – Berlin: Springer; 2015.
6. Senuma T. Physical metallurgy of modern high strength steel sheets. *ISIJ International*. 2001; 41(6): 520–532.
7. Kuziak R., Kawalla R., Waengler S. Advanced high strength steels for automotive industry. *Archives of Civil and Mechanical Engineering*. 2008; 8(2): 103–117.
8. Das D., Chattopadhyay P. P. Influence of martensite morphology on the work-hardening behavior of high strength ferrite-martensite dual-phase steel. *Journal of Materials Science*. 2009; 44(11): 2957–2965.
9. Sarwar M., Priestner R. Influence of ferrite-martensite microstructural morphology on tensile properties of dual-phase steel. *Journal of Materials Science*. 1996; 31(8): 2091–2095.
10. Hong S. C., Lee K. S. Influence of deformation induced ferrite transformation on grain refinement of dual phase steel. *Materials Science and Engineering: A*. 2002; 323(1–2): 148–159.
11. AHSS data utilization. URL: https://www.autosteel.org/research/ahss-data-utilization
12. Karelova A., Krempaszky C., Werner E., Tsipouridis P., Hebesberger T., Pichler A. Hole expansion of dual-phase and complex-phase AHS Steels – effect of edge conditions. *Steel Research International*. 2009; 80(1): 71–77.

13. Venezuela J., Liu Q., Zhang M., Zhou Q., Atrens A. The influence of hydrogen on the mechanical and fracture properties of some martensitic advanced high strength steels studied using the linearly increasing stress test. *Corrosion Science*. 2015; 99: 98–117.
14. Zaefferer S., Ohlert J., Bleck W. A study of microstructure, transformation mechanisms and correlation between microstructure and mechanical properties of a low alloyed TRIP steel. *Acta Materialia*. 2004; 52(9): 2765–2778.
15. Bogachev I. N. *Cavitation destruction and cavitation-resistant alloys*. – Moscow: Metallurgija; 1972. (in Russian).
16. Zackay V. F., Parker E. R., Fahr D., Busch R. The enhancement of ductility in high-strength steels. *ASM Transactions Quarterly*. 1967; 60(2): 252–259.
17. Malinov L. S., Malinov V. L. Saving-alloyed alloys with martensite transformation and strengthening technologies. – Kharkiv: NNC HFTI; 2007 (in Russian).
18. Chejljah A. P. Saving-alloyed metastable alloys and strengthening technologies. Mariupol: PSTU; 2009. (in Russian).
19. Filippov M. A., Litvinov V. S., Nemirovskij Ju. R. *Steels with metastable austenite*. – Moscow: Metallurgija; 1988. (in Russian).
20. Popov V. S., Brykov N. N., Dmitrichenko N. S. *Durability of the equipment of the refractory manufacturing*. – Moscow: Metallurgija; 1978. (in Russian).
21. Bogachev I. N., Mintz R. I. *Cavitation destruction of low-carbon alloys*. – Moscow: Mashgiz; 1959. (in Russian).
22. Bleck W., Guo X., Ma Y. The TRIP effect and its application in cold formable sheet steels. *Steel Research International*. 2019, 88: 1700218.
23. Socrate S. *Mechanics of microvoid nucleation and growth in high-strength metastable austenitic steels*. – Massachusetts: Massachusetts institute of technology; 1995.
24. Tan X., Xu Y., Yang X., Wu D. Microstructure-properties relationship in a one-step quenched and partitioned steel. *Materials Science and Engineering: A*. 2014; 589: 101–111.
25. Matlock D. K., Speer J. G., De Moor E., Gibbs P. J. Recent developments in advanced high strength sheet steels for automotive applications: an overview. *Jestech*. 2012; 15(1):1–12.
26. Malinov L. S., Chejljah A. P., Malinova E. L. Structure and proprties of saving-alloyed manganese steels. *Metally*. 1993; 1: 106–111. (in Russian).

27. Malinov L. S., Chejljah A. P., Sokolov K. N. Effect of deformation martensite on properties of Fe-Cr-Mn steels. *Metally*. 1988; 2: 78–84. (in Russian).
28. Malinov L. S., Chejljah A. P., Harlanova E. Ja. Effect of intercritical quenching on amount and stability of retained austenite in the structural steels. *Metallovedenie i Termicheskaja Obrabotka Metallov*. 1989; 12: 12–15. (in Russian).
29. Malinov L. S., Burova D. V. Effect of intercritical quenching on high-temperature tempering on structure and properties of steels 40CrNi and 40CrNi2MA. *Visnik Priazovs'kogo Derzhavnogo Tehnichnogo Universitetu*. 2013; 26: 93–99. (in Russian).
30. Malinov L. S. Increasing the properties of the steels and high0strength cast iron by multi-phase structure including baunute and metastable austenite. Metally i Lit'e Ukrainy. 2004; 7: 8–10. (in Russian).
31. Malinov L. S., Burova D. V., Malysheva I. E. The methods of the increasing the properties of steel 10Mn2VB to ensute its new applications and energy saving. *New Materials and Technologies in Metallurgy and Machine Building*. 2017; 2: 71–75. (in Russian).
32. Mak-Mak N.E., Rjabikina M. A., Chejljah A. P. Effect of carburizing and quenching from different temperatures on wear resistance and the roughness of the worn surface of strictural steel. *Problemi Tertja ta Znoshuvannja*. 2015; 4 (69): 75–81. (in Russian).
33. Chejljah A. P., Karavaeva N. E. Effect of high-temperature heat treatment on structure and properties of carburized steel 20Mn. *Naukovi Notatki*. 2015; 50: 238–243. (in Russian).
34. Pla-Ferrando R., Sanchez-Caballero S., Reig M. J., Pla R., Sellés M. A., Seguí V. J. Advanced high strength steel (AHSS) TWIP: A door to the future in metal forming. *AIP Conference Proceedings*. 2012; 1431 (1): 65–73.
35. Sohn S. S., Choi K., Kwak J. H., Kim N. J., Lee S. Novel ferrite–austenite duplex lightweight steel with 77% ductility by transformation induced plasticity and twinning induced plasticity mechanisms. *Acta Materialia*. 2014; 78: 181–189.
36. Gavrilyuk V. G., Berns H. High-strength austenitic stainless steel. *Metal Science and Heat Treatment*. 2007; 49(11–12): 566–568.
37. Cai M., Li Z., Chao Q., Hodgson P. D. A novel Mo and Nb microalloyed medium Mn TRIP steel with maximal ultimate strength and moderate ductility. *Metallurgical and Materials Transactions A*. 2014; 45(12): 5624–5634.

38. Lee S., Lee S. J., Kumar S., Lee K., De Cooman B. C. Localized deformation in multiphase, ultra-fine-grained 6 pct Mn transformation-induced plasticity steel. *Metallurgical and Materials Transactions A*. 2011; 42(12): 3638–3651.
39. Heo Y., Song Y. Y., Park S. J. Influence of silicon in low density Fe-C–Mn-Al Steel. *Metallurgical and Materials Transactions A*. 2012; 43(6): 1731–1735.
40. Morales-Rivas L., Garcia-Mateo C., Sourmail T., Kuntz M., Rementeria R., Caballero F. G. Ductility of nanostructured bainite. *Metals*. 2016; 6(12): 302–1735.
41. Garcia-Mateo C., Caballero F. G., Sourmail T., Kuntz M., Cornide J., Smanio V., Elvira R. Tensile behaviour of a nanocrystalline bainitic steel containing 3 wt% silicon. *Materials Science and Engineering: A*. 2012; 549: 185–192.
42. Avishan B., Garcia-Mateo C., Morales-Rivas L., Yazdani S., Caballero F. G. Strengthening and mechanical stability mechanisms in nanostructured bainite. *Journal of Materials Science*. 2013; 48(18): 6121–6132.
43. Speer J., Matlock D. K., De Cooman B. C., Schroth J. G. Carbon partitioning into austenite after martensite transformation. *Acta Materialia*. 2003; 51(9): 2611–2622.
44. Speer J. G., Edmonds D. V., Rizzo F. C., Matlock D. K. Partitioning of carbon from supersaturated plates of ferrite, with application to steel processing and fundamentals of the bainite transformation. *Current Opinion in Solid State and Materials Science*. 2004; 8(3): 219–237.
45. Edmonds D. V., He K., Rizzo F. C., De Cooman B. C., Matlock D. K., Speer J. G. Quenching and partitioning martensite – A novel steel heat treatment. *Materials Science and Engineering: A*. 2006; 438: 25–34.
46. Lee S., Lee K., De Cooman B. C. Observation of the TWIP+TRIP plasticity-enhancement mechanism in Al-added 6 wt pct medium Mn steel. *Metallurgical and Materials Transactions A*. 2015; 46(6): 2356–2363.
47. Lee S., De Cooman B. C. On the selection of the optimal intercritical annealing temperature for medium Mn TRIP steel. *Metallurgical and Materials Transactions A*. 2013; 44(11): 5018–5024.
48. Caballero F. G., Bhadeshia H. K.D.H., Mawella K. J.A., Jones D. G., Brown P. Very strong low temperature bainite. *Material Science and Technology*. 2002; 18: 279–284.

49. Tsuji N., Maki T. Enhanced structural refinement by combining phase transformation and plastic deformation in steels. *Scripta Materialia*. 2009; 60(12): 1044–1049.
50. Jurchenko A. N., Simonov Ju. N. The microstructural features, mechanical properties and heat treatment of bainite steels. *Vestnik Permskogo Nacional'nogo Issledovatel'skogo Politehnicheskogo Universiteta. Mashinostroenie, Materialovedenie*. 2016; 18(3): 160–181 (in Russian).
51. Raabe D., Ponge D., Dmitrieva O., Sander B. Nanoprecipitate-hardened 1.5 GPa steels with unexpected high ductility. *Scripta Materialia*. 2009; 60: 1141–1144.
52. Han Y., Xiu W., Liu C., Wu H. Isothermal transformation of a commercial super-bainitic steel: Part I microstructural characterization and hardness. *Journal of Materials Engineering and Performance*. 2017; 26(2): 472–477.
53. Timokhina I. B., Beladi H., Xiong X. Y., Adachi Y., Hodgson P. D. Nanoscale microstructural characterization of a nanobainitic steel. *Acta Materialia*. 2011; 59: 5511–5522.
54. Caballero F. G., Bhadeshia H. K.D.H. Very strong bainite. *Current Opinion in Solid State & Materials Science*. 2004; 8: 251–257.
55. Yang J., Wang T. S., Zhang B., Zhang F. C. Microstructure and mechanical properties of high-carbon Si-Al-rich steel by low-temperature austempering. *Materials & Design*. 2012; 35: 170–174.
56. Bhadeshia H. K.D.H. Nanostructured bainite. *Proceedings of the Royal Society of London A: Mathematical, Physical and Engineering Sciences*. 2010; 466: 3–18.
57. Garcia-Mateo C., Caballero F. G., Bhadeshia H. K.D.H. Acceleration of low temperature bainite. *ISIJ International*. 2003; 43: 1821–1825.
58. Caballero F. G., Miller M. K., Babu S. S., Garcia-Mateo C. Atomic scale observations of bainite transformation in a high carbon high silicon steel. *Acta Materialia*. 2007; 55: 381–390.
59. Bhadeshia H. K.D.H., Lord M., Svensson L. E. Silicon–rich bainitic steel welds. *Transactions of JWRI*. 2003; 32(1): 91–96.
60. Wang T. S., Yang J., Shang C. J., Li X. Y., Zhang B., Zhang F. C. Microstructures and impact toughness of low-alloy high-carbon steel austempered at low temperature. *Scripta Materialia*. 2009; 61: 434–437.
61. Sourmail T., Caballero F. G., García-Mateo C., Smanio V., Ziegler C., Kuntz M., Elvira R., Leiro A., Vuorinen E., Teeri T. Evaluation of potential of high Si high C steel nanostructured bainite for wear

and fatigue applications. *Materials Science and Technology*. 2013; 29: 1166–1173.
62. Garcia-Mateo C., Caballero F. G. Ultra-high-strength bainitic steels. *ISIJ International*. 2005; 45: 1736–1740.
63. Yoozbashi M. N., Yazdani S., Wang T. S. Design of a new nanostructured, high-Si bainitic steel with lower cost production. *Materials & Design*. 2011; 32: 3248–3253.
64. Caballero F. G., Miller M. K., Garcia-Mateo C. Carbon supersaturation of ferrite in a nanocrystalline bainitic steel. *Acta Materialia*. 2010; 58: 2338–2343.
65. Narayanaswamy B., Hodgson P., Timokhina I., Beladi H. The impact of retained austenite characteristics on the two-body abrasive wear behavior of ultrahigh strength bainitic steels. *Metallurgical and Materials Transactions A*. 2016; 47(10): 4883–4895.
66. Bhadeshia H. K.D.H. *Bainite in Steels*. 2nd ed. London: Maney Publishing; 2001.
67. Caballero F. G., Miller M. K., Garcia-Mateo C., Cornide J. New experimental evidence of the diffusionless transformation nature of bainite. *Journal of Alloys and Compounds*. 2013; 577: 626–630.
68. Wang Y., Zhang K., Guo Z., Chen N., Rong Y. A new effect of retained austenite on ductility enhancement in high strength bainitic steel. *Materials Science and Engineering: A*. 2012; 552: 288–294.
69. Huang H., Sherif M. Y., Rivera-Diaz-Castillo P.E.J. Combinatorial optimization of carbide-free bainitic nanostructures. *Acta Materialia*. 2013; 61: 1639–1647.
70. Han Y., Wu H., Liu C., Liu Y. Microstructures and mechanical characteristics of a medium carbon super-bainitic steel after isothermal transformation. *Journal of Materials Engineering and Performance*. 2014; 23: 4230–4236.
71. Tkachenko F. K. K voprosu o vlijanii kremnija na grafitizaciju promyshlennogo belogo chuguna. *Izvestija Vuzov. Chernaja Metallurgija*. 1959; 10: 131–138. (in Russian).
72. Kurdjumov G. V., Utevskij L. M., Jentin R. I. *Prevrashhenija v zheleze i stali*. Moscow: Nauka; 1977. (in Russian).
73. De Meyer M., Vanderschueren D., De Coon B. C. The influence of the substitution of Si by Al on the properties of cold rolled C-Mn-Si TRIP steels. *ISIJ International*. 1999; 39: 813–822.

74. Hojo T., Sugimoto K. I., Mukai Y., Ikeda, S. Effects of aluminum on delayed fracture properties of ultra-high strength low alloy TRIP-aided steels. *ISIJ International*. 2008; 48: 824–829.
75. Speer J. G., De Moor E., Findley K. O., Matlock D. K., De Cooman B. C., Edmonds D. V. Analysis of microstructure evolution in quenching and partitioning automotive sheet steel. *Metallurgical and Materials Transactions A*. 2011; 42: 3591–3601.
76. Cornide J., Garcia-Mateo C., Capdevila C., Caballero F. G. An assessment of the contributing factors to the nanoscale structural refinement of advanced bainitic steels. *Journal of Alloys and Compounds*. 2013; 577: 43–47.
77. Caballero F. G., Bhadeshia H. K.D.H., Mawella K. J.A., Jones D. G., Brown P. Design of novel high strength bainitic steels: Part 1. *Materials Science and Technology*. 2001; 17(5): 512–516.
78. Caballero F. G., Bhadeshia H. K.D.H., Mawella K. J.A., Jones D. G., Brown P. Design of novel high strength bainitic steels: Part 2. *Materials Science and Technology*. 2001; 17(5): 517–522.
79. Garcia-Mateo C., Caballero F. G., Bhadeshia H. K.D.H. Development of hard bainite. *ISIJ international*. 2003; 43(8): 1238–1243.
80. Sourmail T., Smanio V. Influence of cobalt on bainite formation kinetics in 1 Pct C steel. *Metallurgical and Materials Transactions A*. 2013; 44(5): 1975–1978.
81. Shipway P., Bhadeshia H. The effect of small stresses on the kinetics of the bainite transformation. *Materials Science and Engineering: A*. 1995; 201: 143–149.
82. Matsuzaki A., Bhadeshia H., Harada H. Stress affected bainitic transformation in a Fe-C-Si-Mn alloy. *Acta Metallurgica et Materialia*. 1994; 42: 1081–1090.
83. Hu H., Zurob H. S., Xu G., Embury D., Purdy G. R. New insights to the effects of ausforming on the bainitic transformation. *Materials Science and Engineering: A*. 2015; 626: 34–40.
84. He J., Zhao A., Huang Y., Zhi C., Zhao F. Acceleration of bainite transformation at low temperature by warm rolling process. *Materials Today*. 2015; 2: 289–294.
85. Freiwillig R., Kudrman J., Chraska P. Bainite transformation in deformed austenite. *Metallurgical Transactions A*. 1976; 7(8): 1091–1097.
86. Shirzadi A. A., Abreu H., Pocock L., Klobčuar D., Withers P. J., Bhadeshia H. K.D.H. Bainite orientation in plastically deformed austenite. *International Journal of Materials Research*. 2009; 100: 40–45.

87. Yang J., Huang C., Hsieh W. Mechanical stabilization of austenite against bainitic reaction in Fe-Mn-Si-C bainitic steel. *Materials Transactions, JIM*. 1996; 37: 579–585.
88. Larn R., Yang J. The effect of compressive deformation of austenite on the bainitic ferrite transformation in Fe-Mn-Si-C steels. *Materials Science and Engineering: A*. 2000; 278: 278–291.
89. Santofimia M. J., Zhao L., Sietsma J. Microstructural evolution of a low carbon steel during application of quenching and partitioning heat treatments after partial austenitization. *Metallurgical and Materials Transactions A*. 2009; 40: 46–57.
90. Clarke A. J., Speer J. G., Matlock D. K., Rizzo F. C., Edmonds D. V., Santofimia M. J. Influence of carbon partitioning kinetics on final austenite fraction during quenching and partitioning. *Scripta Materialia*. 2009; 61(2): 149–152.
91. Matlock D. K., Brautigam V. E., Speer J. G. Application of the quenching and partitioning (Q & P) process to a medium-carbon, high-Si microalloyed bar steel. *Materials Science Forum*. 2003; 426: 1089–1094.
92. Misra R. D.K., Zheng H., Wu K. M., Karjalainen L. P. Niobium-containing quenching and partitioning processed ultrahigh strength martensite–austenite dual phase steels. *Materials Science and Engineering: A*. 2013; 579: 188–193.
93. Clarke A. J., Miller M. K., Field R. D., Coughlin D. R., Gibbs P. J., Clarke K. D., Alexander D. J., Powers K. A., Papin P. A., Krauss G. Atomic and nanoscale chemical and structural changes in quenched and tempered 4340 steel. *Acta Materialia*. 2014; 77: 17–27.
94. Toji Y., Matsuda H., Herbig M., Choi P. P., Raabe, D. Atomic-scale analysis of carbon partitioning between martensite and austenite by atom probe tomography and correlative transmission electron microscopy. *Acta Materialia*. 2014; 65: 215–228.
95. Seo E. J., Cho L., DeCooman B. C. Application of quenching and partitioning processing to medium Mn steel. *Metallurgical and Materials Transactions A*. 2015; 46(1):27–31.
96. Zhang J., Ding H., Wang C., Zhao J., Ding T. Work hardening behaviors of a low carbon Nb-microalloyed Si-Mn quenching-partitioning steel with different cooling styles after partitioning. *Materials Science and Engineering: A*. 2013; 585: 132–138.

97. Speer J. G., Assunção F. C.R., Matlock D. K., Edmonds D. V. The "quenching and partitioning" process: background and recent progress. *Materials Research*. 2005; 8(4): 417–423.
98. Seo E. J., Cho L., De Cooman B. C. Kinetics of the partitioning of carbon and substitutional alloying elements during quenching and partitioning (Q&P) processing of medium Mn steel. *Acta Materialia*. 2016; 107: 354–365.
99. Sun J., Yu H. Microstructure development and mechanical properties of quenching and partitioning (Q&P) steel and an incorporation of hot-dipping galvanization during Q&P process. *Materials Science & Engineering A*. 2013; 586: 100–107.
100. Sadovskij V. D., Fokina E. A. Retained austenite in quenched steel. Moscow: Nauka; 1986. (in Russian).
101. Malinov L. S., Konop-Ljashko V. I. Vlijanie starenija na razvitie martensitnogo prevrashhenija pri deformacii v metastabil'nyh austenitnyh staljah. *Izv. AN SSSR. Metally*. 1982; 3: 130–133. (in Russian).
102. Malinov L. S., Chejljah A. P. Effect of manganese and heat treatment on structure and properties of Fe – 0.1% C – 14% Cr steeld. *Izvestija vuzov. Chernaja Metallurgija*. 1983; 6: 83–87. (in Russian).
103. Li H. Y., Lu X. W., Li W. J., Jin X. J. Microstructure and mechanical properties of an ultrahigh-strength 40SiMnNiCr steel during the one-step quenching and partitioning process. *Metallurgical and Materials Transactions A*. 2010; 41(5): 1284–1300.
104. Han X., Zhong Y., Xin P., Cui Z., Chen J. Research on one-step quenching and partitioning treatment and its application in hot stamping process. *Journal of Engineering Manufacture*. 2017; 231(11): 1972–1982.
105. Ghazvinloo H. R., Honarbakhsh-Raouf A., Rashid A. R.K. Mechanical properties of a high Si and Mn steel heat treated by one-step quenching and partitioning. *Metallurgist*. 2015; 59(1–2): 90–96.
106. Maheswari N., Chowdhury S. G., Kumar K. H., Sankaran S. Influence of alloying elements on the microstructure evolution and mechanical properties in quenched and partitioned steels. *Materials Science & Engineering A*. 2014; 600: 12–20.
107. Zhou S., Zhang K., Wang Y., Gu J. F., Rong Y. H. High strength-elongation product of Nb-microalloyed low-carbon steel by a novel quenching-partitioning-tempering process. *Materials Science & Engineering A*. 2011; 528: 8006–8012.

108. Zhang J., Ding H., Misra R. D.K., Wang C. Enhanced stability of retained austenite and consequent work hardening rate through pre-quenching prior to quenching and partitioning in a Q-P microalloyed steel. *Materials Science & Engineering A*. 2014; 611: 252–256.
109. Seo E. J., Cho L., Estrin Y., De Cooman B. C. Microstructure-mechanical properties relationships for quenching and partitioning (Q&P) processed steel. *Acta Materialia*. 2016; 113: 124–139.
110. Zhong N., Wang X. D., Wang L., Rong Y. H. Enhancement of the mechanical properties of a Nb-microalloyed advanced high-strength steel treated by quenching-partitioning-tempering process. *Materials Science & Engineering A*. 2009; 506: 111–116.
111. Nayak S. S., Anumolu R., Misra R. D.K., Kim K. H., Lee D. L. Microstructure-hardness relationship in quenched and partitioned medium-carbon and high-carbon steels containing silicon. *Materials Science & Engineering A*. 2008; 498:442–456.
112. Shi J., Sun X., Wang M., Hui W., Dong H., Cao W. Enhanced work-hardening behavior and mechanical properties in ultrafine-grained steels with large-fractioned metastable austenite. *Scripta Materialia*. 2010; 63(8): 815–818.
113. Timokhina I. B., Hodgson P. D., Pereloma E. V. Effect of microstructure on the stability of retained austenite in transformation-induced-plasticity steels. *Metallurgical and Materials Transactions A*. 2004; 35A: 2331–2341.
114. Lee S., Lee S. J., De Cooman B. C. Austenite stability of ultrafine-grained transformation-induced plasticity steel with Mn partitioning. *Scripta Materialia*. 2011; 65(3): 225–228.
115. Xiong X. C., Chen B., Huang M. X., Wang J. F., Wang L. The effect of morphology on the stability of retained austenite in a quenched and partitioned steel. *Scripta Materialia*. 2013; 68(5): 321–324.
116. Sakuma Y., Matlock D. K., Krauss G. Intercritically annealed and isothermally transformed 0.15 pct C steels containing 1.2 pct Si-1.5 pct Mn and 4 pct Ni: Part II. Effect of testing temperature on stress-strain behavior and deformation-induced austenite transformation. *Metallurgical Transactions A*. 1992; 23: 1233–1241.
117. Clarke A. J., Speer J. G., Miller M. K., Hackenberg R. E., Edmonds D. V., Matlock D. K., Rizzo F. C., Clarke K. D., De Moor E. Carbon partitioning to austenite from martensite or bainite during the

quench and partition (Q&P) process: A critical assessment. *Acta Materialia*. 2008; 56: 16–22.
118. Jimenez-Melero E., Van Dijk N. H., Zhao L., Sietsma J., Offerman S. E., Wright J. P., Van der Zwaag S. Characterization of individual retained austenite grains and their stability in low-alloyed TRIP steels. *Acta Materialia*. 2007; 55(20): 6713–6723.
119. Jirková H., Mašek B., Wagner M. F.X., Langmajerová D., Kučerová L., Treml R., Kiener D. Influence of metastable retained austenite on macro and micromechanical properties of steel processed by the Q&P process. *Journal of Alloys and Compounds*. 2014; 615: 163–168.
120. Sugimoto K. I., Misu M., Kobayashi M., Shirasawa H. Effects of second phase morphology on retained austenite morphology and tensile properties in a TRIP-aided dual-phase steel sheet. *ISIJ international*. 1993; 33(7): 775–782.
121. Samek L., De Moor E., Penning J., De Cooman B. C. Influence of alloying elements on the kinetics of strain-induced martensitic nucleation in low-alloy, multiphase high-strength steels. *Metallurgical and Materials Transactions A*. 2006; 37 (1): 109–124.
122. Chejljah A. P. The ways to develop metastable states in the Fe-based alloys. *New Materials and Technologies in Metallurgy and Machine Building*. 2002; 2: 31–34 (in Russian).
123. Santofimia M. J., Nguyen-Minh T., Zhao L., Petrov R., Sabirov I., Sietsma J. New low carbon Q&P steels containing film-like intercritical ferrite. *Materials Science and Engineering: A*. 2010; 527: 6429–6439.
124. Santofimia M. J., Zhao L., Petrov R., Kwakernaak C., Sloof W. G., Sietsma J. Microstructural development during the quenching and partitioning process in a newly designed low-carbon steel. *Acta Materialia*. 2011; 59: 6059–6068.
125. Kim D. H., Speer J. G., Kim H. S., De Cooman B. C. Observation of an isothermal transformation during quenching and partitioning processing. *Metallurgical and Materials Transactions A*. 2009; 40(9): 2048–2060.
126. Seo E. J., Cho L., De Cooman B. C. Application of quenching and partitioning (Q&P) processing to press hardening steel. *Metallurgical and Materials Transactions A*. 2014; 45: 4022–4037.
127. Ericsson C. E., Bhat M. S., Parker E. R., Zackay V. F. Isothermal studies of bainitic and martensitic transformations in some low alloy steels. *Metallurgical Transactions A*. 1976; 7: 1800–1803.

128. Oka M., Okamoto H. Swing back in kinetics near Ms in hypereutectoid steels. *Metallurgical Transactions A*. 1988; 19: 447–452.
129. Vetters H., Dong J., Bomas H., Hoffmann F., Zoch H. W. Microstructure and fatigue strength of the roller-bearing steel 100Cr6 (SAE52100) after two-step bainitisation and combined bainitic-martensitic heat treatment. *International Journal of Materials Research*. 2006; 97: 1432–1440.
130. Kawata H., Hayashi K., Sugiura N., Yoshinaga N., Takahashi M. Effect of martensite in initial structure on bainite transformation. *Materials Science Forum*. 2010; 638–642: 3307–3312.
131. Kaletin Ju.M., Ryzhkov A. G., Kaletin A. Ju. Effect of silicon and aluminium of the proprties of structural Cr-Ni steels with bainite structure. *Izvestija Vuzov. Chernaja Metallurgija*. 1989; 6: 96–99. (in Russian).
132. Kaletin Ju.M., Ryzhkov A. G., Kaletin A. Ju. The alloying and heat treatment fo steels with bainite structure. *Metallovedenie i Termicheskaja Obrabotka Metallov*. 1987; 10: 13–16. (in Russian).
133. Mašek B., Jirková H., Hauserova D., Kučerová L., Klauberová D. The effect of Mn and Si on the properties of advanced high strength steels processed by quenching and partitioning. *Materials Science Forum*. 2010; 654: 94–97.
134. Allten A. G., Payson P. The effect of silicon on the tempering of martensite. *Transactions of the American Society of Metals*. 1953; 45: 498–532.
135. Owen W. S. The effect of silicon on the kinetics of tempering. *Transactions of the American Society of Metals*. 1954; 46: 812–829.
136. Yi H. L., Chen P., Hou Z. Y., Hong N., Cai H. L., Xu Y. B., Wu D., Wang G. D. A novel design: Partitioning achieved by quenching and tempering (Q–T & P) in an aluminum-added low-density steel. *Scripta Materialia*. 2013; 68: 370–374.
137. De Moor E., Speer J. G., Matlock D. K., Kwak J. H., Lee S. B. Effect of carbon and manganese on the quenching and partitioning response of CMnSi steels. *ISIJ international*. 2011; 51(1): 137–144.
138. Hsu T. Y. Quenching–partitioning–tempering process for ultra-high strength steel. *International Heat Treatment and Surface Engineering*. 2008; 2 (2): 64–67.

139. Hsu T. Y., Jin X. J., Rong Y. H. Strengthening and toughening mechanisms of quenching–partitioning–tempering (Q-P-T) steels. *Journal of Alloys and Compounds*. 2013; 577: 568–571.
140. Wang X. D., Guo Z. H., Rong Y. H. Mechanism exploration of an ultrahigh strength steel by quenching-partitioning-tempering process. *Materials Science and Engineering A*. 2011; 529: 35–40.
141. Li Q., Huang X., Huang W. Microstructure and mechanical properties of a medium-carbon bainitic steel by a novel quenching and dynamic partitioning (Q-DP) process. *Materials Science and Engineering A*. 2016; 662: 129–135.
142. Gui X., Gao G., Guo H., Zhao F., Tan Z., Bai B. Effect of bainitic transformation during BQ&P process on the mechanical properties in an ultrahigh strength Mn-Si-Cr-C steel. *Materials Science and Engineering: A*. 2017; 684: 598–605.
143. Chejljakh A. P., Malinov L. S. The effect of the stepped quenching on structure and properties of Cr-Mn steels. *Izvestia AN SSSR. Metally*. 1990; 5: 92–97 (in Russian).
144. Huang X., Liu W., Huang Y., Chen H., Huang W. Effect of a quenching–long partitioning treatment on the microstructure and mechanical properties of a 0.2 C% bainitic steel. *Journal of Materials Processing Technology*. 2015; 222: 181–187.
145. Billur E., Dykeman J., Altan T. Three generations of advanced high strength steels for automotive applications. *Stamping Journal*. 2014; Mar/Apr: 12–13.
146. Efremenko V. G., Zurnadzhi V. I. The prospectives of using Q&P technology of heat treatment for the improvement of the complex of mechanical properties of steel. *Vestnik PGTU*. 2015; 31: 35–41. (in Russian).
147. Efremenko V. G., Chabak Ju. G., Zurnadzhi V. I. The prospectives of using "Q-P-T" technology for increasing wear resistance of steel components. Proceedings of the conference "The problems of exploitation duration of the materials, coatings and structures"; October 14, 2014; – Vinnitsa, Ukraine. (in Russian).
148. Hlestov V. M., Dorozhko G. K. *The transformation of deformed austenite in steel.* Mariupol: PSTU; 2002. (in Russian).
149. Van Dijk N. H., Butt A. M., Zhao L., Sietsma J., Offerman S. E., Wright J. P., Van der Zwaag S. Thermal stability of retained austenite

in TRIP steels studied by synchrotron X-ray diffraction during cooling. *Acta Materialia*. 2005; 53(20): 5439–5447.
150. Zhou M., Xu G., Wang L., He B. Effects of austenitization temperature and compressive stress during bainitic transformation on the stability of retained austenite. *Transactions of the Indian Institute of Metals*. 2017; 70 (6): 1447–1453.
151. Lenkovs'kyi T. M. Fatigue crack-growth resistance of thermally hardened 65G steel under transverse shear. *Materials Science*. 2016; 53(2): 200–206.
152. Delagnes D., Lamesle P., Mathon M. H., Mebarki N., Levaillant C. Influence of silicon content on the precipitation of secondary carbides and fatigue properties of a 5% Cr tempered martensitic steel. *Materials Science and Engineering: A*. 2005; 394(1–2): 435–444.
153. Speich G. R., Leslie W. C. Tempering of steel. *Metallurgical Transactions*. 1972; 3(5): 1043–1054.
154. Ray S. K. TEM investigation of carbide precipitation in low carbon steels containing silicon. *Transactions of the Japan Institute of Metals*. 1983; 24(2): 81–87.
155. Mesquita R. A., Barbosa C. A., Morales E. V., Kestenbach H. J. Effect of silicon on carbide precipitation after tempering of H11 hot work steels. *Metallurgical and Materials Transactions A*. 2011; 42(2): 461–472.
156. Michal G. M., Slane J. A. The kinetics of carbide precipitation in silicon-aluminum steels. *Metallurgical and Materials Transactions A*. 1986; 17(8): 1287–1294.
157. Bag A., Ray K. K., Dwarakadasa E. S. Influence of martensite content and morphology on tensile and impact properties of high-martensite dual-phase steels. *Metallurgical and Materials Transactions A*. 1999; 30(5): 1293–1202.
158. Zurnadzhy V. I., Yefremenko V. H., Zaichuk N. P., Havrylova V. H., Dzherenova A. V. Kinetics of athermal martensite transformation in steel 60Si2CrA and 55Si3Mn2CrMoVNb. *Naukovi Notatky*. 2018; 61: 60–65 (in Ukrainian).
159. Zurnadzhy V. I. Kinetics of athermal martensite transformation in steel 60Si2CrA. Proceedings of the conference: "Promissing technologies based on novel physic-metallurgy research and computer simulation"; April 20–21, 2017; – Kyiv, Ukraine (in Ukrainian).
160. Zurnadzhi V. I. The definition of martensite start temperature in steels 60Si2CrA and 55Si3Mn2CrMoVNb by analytic-experimental meth-

od. Proceedings of the conference: "Promissing technologies based on novel physic-metallurgy research and computer simulation"; April 19–20, 2018; – Kyiv, Ukraine (in Russian).
161. Gorni A. A. *Steel forming and heat treating handbook*. São Vicente: Brazil; 2011.
162. Popov A. A., Popova L. *E. TTT and CCT diagrams of the decomposition of overcooled austenite. The termist's handbook*. – Moskow: Metallurgija; 1961. (in Russian).
163. Navarro-Lopez A., Sietsma J., Santofimia M. J. Effect of prior athermal martensite on the isothermal transformation kinetics below Ms in a low-C High-Si steel. *Metallurgical and Materials Transactions A*. 2016; 47: 1028–1039.
164. De Knijf D., Petrov R., Föjer C., Kestens L. A. Effect of fresh martensite on the stability of retained austenite in quenching and partitioning steel. *Materials Science & Engineering A*. 2014; 615: 107–115.
165. Zurnadzhi V. I., Efremenko V. G., Brykov M. N., Dzherenova A. V. Effect of martensite on the kinetics of bainite transformation in steels 60Si2CrVA i 55Si3Mn2CrMoVNb. *New Materials and Technologies in Metallurgy and Machine Building*. 2017; 2: 23–27. (in Russian).
166. Zurnadzhy V., Zaichuk N., Sergeev A., Chabak Y., Efremenko V. Optimal Parameters of Q&P Heat Treatment for High-Si Steels Found by Modeling Based on "Constrained Paraequilibrium" Concept. In: Ivanov V. et al. (eds) Advances in Design, Simulation and Manufacturing II. DSMIE2019. *Lecture Notes in Mechanical Engineering*. Springer, 2020. P. 487–496.
167. Zurnadzhi V. I., Efremenko V. G., Brykov M. N., Gavrilova V. G., Tsvetkova E. V. Volumetrical changes at heating in steel 60Si2CrV subjected to Q&P treatment. *Izvestiya. Ferrous Metallurgy*. 2019; 62(1): 42–48.
168. Guljaev A. P. *Metal Science. Textbook*. 6th ed. – Moscow: Metallurgija; 1986. (in Russian).
169. Zurnadzhy V. I., Efremenko V. G., Gavrilova V. G., Kussa R. O., Efremenko A. V., Kudin V. V., Pomazkov M. V. Formation of a Heterophase Structure in Low-Alloyed Steel by Means of Application of Innovative Technology of Heat Treatment by 'Quenching and Partitioning', *Metallofizika i Noveishie Tekhnologii*. 2018; 40(12): 1603–1624.
170. Zurnadzhi V. I., Efremenko V. G., Cvetkova E. V., Dzherenova A. V., Kussa R. A. Creating the composite structure in low-alloy steel by

Q&P heat treatment. Proceedings of the conference: "Materialy for Extremal Expoitation-7"; December 2, 2017; – Kyiv, Ukraine (in Russian).
171. Zurnadzhi V. I., Efremenko V. G., Gavrilova V. G., Grigor'eva M. A. The development of high-strength state in a steel by Q&P heat treatment. Proceedings of the conference: "University Science-2018; May 24, 2018; – Mariupol, Ukraine (in Russian).
172. Belyakov L. N., Petrakov A. F., Pokrovskaya N. G., Shal'kevich A. B. New high-strength steels. *Metal Science and Heat Treatment*. 1998; 39(8): 334–337.
173. Koval A. D., Efremenko V. G., Brykov M. N., Andrushchenko M. I., Kulikovskii R. A., Efremenko A. V. Principles of development of grinding media with increased wear resistance. Part 2. Optimization of steel composition to suit conditions of operation of grinding media. *Journal of Friction and Wear*. 2012; 33(2): 153–159.
174. Stormvinter A., Hedstrjm P., Borgenstam A. Investigation of lath and plate martensite in a carbon steel. *Solid State Phenomena*. 2011; 172: 61–66.
175. He Y., Rao Q., Tan Y. Investigation on the morphology of martensite in carbon steels. *Journal of Central South University of Technology*. 1996; 3: 122–134.
176. Jacques P., Girault E., Catlin T., Geerlofs N., Kop T., Van Der Zwaag S., Delannay F. Bainite transformation of low carbon Mn-Si TRIP-assisted multiphase steels: influence of silicon content on cementite precipitation and austenite retention. *Materials Science and Engineering: A*. 1999; 273: 475–479.
177. Garcia-Mateo C., Sourmail T., Caballero F. G., Smanio V., Kuntz M., Ziegler C., Leiro A., Vuorinen E., Elvira R., Teeri T. Nanostructured steel industrialization: plausible reality. *Materials Science and Technology*. 2014; 30(9): 1071–1078.
178. Zhao J., Li J., Ji H., Wang, T. Effect of austenitising temperature on mechanical properties of nanostructured bainitic steel. *Materials (Basel)*. 2017; 10(8): 874–884.
179. Zurnadzhi V. I., Efremenko V. G., Matvienko V. N., Brykov M. N., Tsvetkova E. V., Ksenita M. A. Phase-structure state and the mechanical properties of steel 60Si2CrA after Q&P+T treatment. *Visnyk Pryazovskoho Derzhavnoho Tekhnichnoho Universytetu*. 2017; 35: 40–50. (in Russian).

180. Van Slycken J., Verleysen P., Degrieck J., Samek L., De Cooman B. C. High-strain-rate behavior of low-alloy multiphase aluminum- and silicon-based transformation-induced plasticity steels. *Metallurgical and Materials Transactions A*. 2006; 37: 1527–1539.
181. Malinov L. S., Malysheva I. E., Malinova D. V. Egfect of the heat treatment with the heating to the interctitical interval on the proprties of steels 60Si2A i 60Si2CrVA. *Metallurgicheskaja i Gornorudnaja Promyshlennost'*. 2012; 1: 55–58. (in Russian).
182. Malinov L. S., Burova D. V. The increasing the propeties of moddle-carbon low-alloy steel by the austempering from interctitical annealing for creating a multi-phase structure. *New Materials and Technologies in Metallurgy and Machine Building*. 2013; 2: 64–69. (in Russian).
183. Garcia-Mateo C., Caballero F. G., Bhadeshia H. K. Mechanical properties of low-temperature bainite. *Materials Science Forum*. 2005; 500: 495–502.
184. Burova D. V. *The improvement of the properties of low-alloy structural steels with different carbon content by the heat treatment with heating in the intercritical range*. Thesis for PhD degree. – Mariupol: PSTU; 2016 (in Russian).
185. Tenenbaum M. M. *The abrasive wear resistance*. – Moscow: Mashinostroenie; 1976. (in Russian).
186. Kostetzkij B. I. *Friction, lubrication and wear in machines*. – Kyiv: Tekhnika; 1970. (in Russian).
187. Venkataraman K. S., Narayanan K. S. Energetics collision between grinding media in ball mills and mechanochemical effects. *Powder Technology*. 1998; 96(3): 190–201.
188. Wang C., Li X., Chang Y., Han S., Dong H. Comparison of three-body impact abrasive wear behaviors for quenching-partitioning-tempering and quenching-tempering 20Si2Ni3 steels. *Wear*. 2016; 362–363: 121–128.
189. Liu S. G., Dong S. S., Yang F., Li L., Hu B., Xiao F. H., Chen Q., Liu H. S. Application of quenching-partitioning-tempering process and modification to a newly designed ultrahigh carbon steel. *Materials & Design*. 2014; 56: 37–43.
190. Efremenko V. G., Zurnadzhi V. I., Chabak Y. G., Tsvetkova O. V., Dzherenova A. V. Application of the Q&P Treatment for increasing the wear resistance of low-alloy steel with 0.75% C. *Materials Science*. 2017; 53 (1): 67–75.

191. Colaço R., Vilar R. On the influence of retained austenite in the abrasive wear behavior of a laser surface melted tool steel. *Wear.* 2005; 258 (1–4): 225–231.
192. Efremenko V. G., Shimizu K., Cheiliakh A. P., Pastukhova T. V., Chabak Y. G., Kusumoto K. Abrasive resistance of metastable V-Cr-Mn-Ni spheroidal carbide cast irons using the factorial design method. *International Journal of Minerals, Metallurgy, and Materials.* 2016; 23: 645–657.
193. Hesse O., Merker J., Brykov M., Efremenko V. Zur Festigkeit niedriglegierter Stäble mit erhöhtem Kohlenstoffgehalt gegen abrasiven Verschleiß. *Tribologie und Schmierungstechnik.* 2013; 60(6): 37–43 (in German).
194. Malinov L. S., Kharlashkin V. A. Effect of cementation and heat treatment of steel 10Г12 on metastable austenite in the structure, abrasive and impact wear resistance. *Metallurgical and Mining Industry.* 2011; 3(2): 58–62.
195. Efremenko V. G., Chabak Ju. G., Zurnadzhi V. I. Temperature-Time intervals of phase transformations in steel 75CrMn2Si. Proceedings of the conference: "University Sicence-2015"; May 19–20, 2015; Mariupol, Ukraine. (in Russian).
196. Zurnadzhi V. I., Efremenko V. G., Cvetkova E. V. Effect of the Q&P obratreatment on microstructure of low-alloyed steel 75CrMn2S. Proceedings of the conference: "Problems and Prospects of Railway Transport Development"; May 19–20, 2016; Dnipro, Ukraine. (in Russian).
197. Zurnadzhi V. I., Chabak Ju.G., Efremenko V. G. The effect of time-temperature parameters of Q&P treatment on the abrasive wear resistance of steel 75CrMn2Si. Proceedings of the conference: "Materials for the extremal exploitation-6"; December 1–2, 2016; – Kyiv, Ukraine (in Russian).
198. Popova L. E., Popov A. A. *The diagrams of the sustenite transformation in steels and b-Ti-based alloys.* – Moscow: Metallurgija; 1991. (in Russian).
199. Bhadeshia H. K.D.H. Effect of stress & strain on formation of bainite in steel. *Hot Workability of Steels and Light Alloys–Composites.* 1996; 543–556.
200. Najzabekov A. B., Muhametkaliev B. S., Arbuz A. S., Lezhnev S. N. Decreasing of the consumption of steel grinding balls by improvement of

the technology of their manufactoring. *Vesti Vysshih Uchebnyh Zavedenij Chernozem'ja*. 2016; 4 (46): 78–86. (in Russian).
201. Prohorenko E. M., Klepikov V. F., Litvinenko V. V., Hajmovich P. A., Shul'gin N.A., Morozov A. I. Diagnostika processov iznosa materialov v sharovyh barabannyh mel'nikah. *Vostochno-Evropejskij zhurnal peredovyh tehnologij*. 2015; 1/5(73): 14–20. (in Russian).
202. Zaec V. N. The evaluation of working conditions of grinding balls made of eutectoid steel in mill drum. *Visnyk KhNTUSH im. P. Vasylenka.* 2015; 158: 288–293. (in Russian).
203. Efremenko V. G., Tkachenko F. K., Kuz'min S.O., Rtishhev A. B., Zinchenko Ju.A., Ganoshenko I. V., Trufanova O. I. The effectiveness of using gribding balls on improved quality in the conditions of "Central'nyj GOK". *Metallurgicheskaja i Gornorudnaja Promyshlennost'*. 2009; 1: 90–93. (in Russian).
204. Zelikovich A. Ja., Tokmakov A. M. The improvement of the quality of heat tretamnet of grinding balls. *Stal'*. 1994; 2: 64–65. (in Russian).
205. Efremenko V. G., Popov E. S., Kuz'Min S.O., Trufanova O. I., Efremenko A. V. Introduction of three-stage thermal hardening technology for large diameter grinding balls. *Metallurgist*. 2014; 9–10(57): 849–857.
206. Efremenko V. G., Ganoshenko I. V., Tkachenko F. K., Zhurba V. A., Trufanova O. I. Improving the hardness of OAO Azovstal metallurgical combine steel balls for crushing mills. *Steel in Translation*. 2008; 2 (38): 176–178.
207. Moema J. S., Papo M. J., Slabbert G. A., Zimba J. Grinding media quality assurance for the comminution of gold ores. Paper presented at: World Gold Conference; 2009; The Southern African Institute of Mining and Metallurgy, South Africa.
208. Blickensderfer R., Tylszak J. H. Evaluation of commercial US grinding balls by laboratory impact and abrasion tests. *Mining, Metallurgy & Exploration*. 1989; 6(2): 60–66.
209. Tkachenko F. K., Kuz'min S.O., Efremenko V. G., Kazankov V. G. Kinetics of the transformation of austenite in railway steels M74 and 75CrMnSiMo under continiuos cooling. *Bulletin of Dnipropetrovsk National University of Railway Transport*. 2009; 29: 198–201. (in Russian).
210. Glazkov A. J., Klimenko A. N., Baguzin V. I. Manufactoring grinding balls abroad. *Chernaja Metallurgija*. 1979; 9: 19–21. (in Russian).

211. Tkachenko F. K., Efremenko V. G., Tikhonyuk S. L., Degtyarev S. I., Vorona, N. N. Effect of heat treatment on the properties of highly hardenable rolled milling balls. *Metal Science and Heat Treatment*. 2001; 8: 26–29. (in Russian).
212. Camurri C., Carrasco C., Colàs R. Improving the working life of steel grinding balls by optimizing their hardness and tenacity. *Materials Science Forum*. 2014; 783: 2260–2265.
213. Guljaeva T. P., Sedovolosaja T. P., Danilov A. P. The quality of grainding balls made of alloyed steel grades. *Izvestija vuzov. Chernaja Metallurgija*. 1995; 6: 75. (in Russian).
214. Jia X., Zuo X., Liu Y., Chen N., Rong Y. High wear resistance of white cast iron treated by novel process: principle and mechanism. *Metallurgical and Materials Transactions A*. 2015; 12(46): 5514–5525.
215. Zurnadzhi V. I., Efremenko V. G., Dunaev E. V., Lekatu A., Kussa R. A. Increasing volume hsrdness of steel gribnding balls using Q-n-P heat treatment. *Science and Transport Progress. Bulletin of Dnipropetrovsk National University of Railway Transport*. 2018; 2(74): 103–113. (in Russian).
216. Efremenko V. G., Zurnadzhi V. I., Matvienko V. N. The application of a Q&P heat treatment for improving quality of steel grinding balls. Proceedings of the conference "Problems and Prospects of Railway Transport Development"; May 17–18, 2018; Dnipro, Ukraine. (in Russian).
217. Efremenko V. G. Thermal hardening of grinding balls to gain the required hardness. *Metallurgicheskaja i Gornorudnaja Promyshlennost'*. 2002; 4: 51–54. (in Russian).
218. Rolled grinding balls. Standard of Ukraine DSTU8538:2015.
219. Efremenko V. G. Thedevelopment of the scientific basement of the manufacturing and hardening of steel grinding balls of increased quality. Thesis for the Doctor of Science degree Mariupol': PSTU; 2005 (in Russian).
220. Efremenko V. G., Tkachenko F. K., Efremenko A. V. Computer simulation of the structural transformation in steel balls by interupred quanching. *Teorija i Praktika Metallurgii*. 2003; 5–6: 119–123. (in Russian).
221. The mode of the heat treatment of steel grinding balls. Patent of Ukraine No 127190. Authors: Efremenko V. G., Zurnadzhy V. I., Dunaiev Ye.V., Karmazin A. V., Chabak Yu.G., Trufanova O. I., July 25, 2018. (in Ukrainian).